STUDY ON THE FEASIBILITY OF NITROGEN HUFF-N-PUFF IN HEAVY OIL RESERVOIRS

A Thesis

Submitted to the Faculty of Graduate Studies and Research

In Partial Fulfillment of the Requirement

For the Degree of

Master of Applied Science

in

Petroleum Systems Engineering

University of Regina

By

Binyang Zou

Regina, Saskatchewan

April, 2019

UNIVERSITY OF REGINA

FACULTY OF GRADUATE STUDIES AND RESEARCH

SUPERVISORY AND EXAMINING COMMITTEE

Binyang Zou, candidate for the degree of Master of Applied Science in Petroleum Systems Engineering**,** has presented a thesis titled, ***Study on The Feasibility of Nitrogen Huff-N-Puff in Heavy Oil Reservoirs,*** in an oral examination held on April 8, 2019. The following committee members have found the thesis acceptable in form and content, and that the candidate demonstrated satisfactory knowledge of the subject material.

External Examiner:	Dr. Liming Dai, Industrial Systems Engineering
Supervisor:	Dr. Fanhua Zeng, Petroleum Systems Engineering
Committee Member:	Dr. Farshid Torabi, Petroleum Systems Engineering
Committee Member:	Dr. Saman Azadbakht, Petroleum Systems Engineering
Chair of Defense:	Dr. Andrei Volodin, Department of Mathematics & Statistics

ABSTRACT

For heavy reservoirs, conventional oil recovery methods are polymer flooding and Steam-assisted Gravity Drainage (SAGD). Such methods are affected by various factors including reservoir thickness, formation heterogeneity, heat loss, and cost, especially in heavy oil reservoirs with depths ranging from 1000 to 2000 m. In these relatively deep reservoirs, the temperature is generally around 40 to 50℃. Their crude oil has a viscosity in the tens of thousands of centipoises at surface conditions, but only a few hundred centipoises at high temperature in the reservoirs. At this reservoir condition, there is sufficient mobility of crude oil making it possible for nitrogen (N_2) Huff-n-Puff to be applied. Therefore, this study is to confirm the ability of nitrogen to form foamy oil and the feasibility of nitrogen Huff-n-Puff in relatively deep heavy oil reservoirs.

This study includes three types of tests. The first category is the PVT tests to measure N_2 solubility in heavy oil. The temperature is set from 50 to 80 ℃ with an incremental increase of 5 ℃, and each temperature has four pressure setting of 3 to 8 MPa. It was found that nitrogen has a lower solubility than carbon dioxide and methane. The solubility of nitrogen in the oil sample at 50℃ and 7 MPa is 7.6 m^3/m^3.

The second category is the pressure depletion tests conducted in a 1-D cylindrical model to observe the foamy oil flow. These tests were conducted consistently at four

different pressure decline rates. It confirmed the possibility of foamy oil formed by nitrogen and summarized the variation of the flow pattern.

The last is the Huff-n-Puff tests conducted in a 2-D planar model to confirm N_2 feasibility. It can be concluded that the highest recovery factor of 35.73 % occurs when the pressure decline rate is 16KPa/min. and N_2 Huff-n-Puff has a strong potential to recover hydrocarbon in deep heavy oil reservoirs effectively.

This research is the first study to apply nitrogen to heavy oil reservoirs. Confirmation of the technology's feasibility will significantly reduce the cost of exploiting heavy oil reservoir.

ACKNOWLEDGMENTS

First of all, I would like to express my greatest and most sincere gratitude to my supervisor, Dr. Fanhua (Bill) Zeng, for his patience, guidance, and encouragement throughout my graduate studies at the University of Regina. This work would not have been possible without the support of Dr. Zeng.

Secondly, I would like to express my special appreciation to all the thesis committee members Dr. Farshid Torabi, Dr. Saman Azadbakht, and Dr. Liming Dai for their valuable comments, questions ,and suggestions.

Lastly, I would like to thank all members of Dr. Zeng's research group for their guidance, help, and support. Thanks to Mr. Xiang Zhou, Mr. Kewei Zhang, Mr. Mingyi Wu, Mr. Zhongwei Du, Mrs. Shanshan Yao, Mr. Xiaolong Peng, Mrs. Xinqian Lu, Mr. Jun Yang, Mr. Lilong Yang, Mr. Di Pu, Mr. Zixi Guo, Mr. Chen Shen, Mr. Haoran Hu, and Ms. Xiao Hu for their advice during this research discussion. I am grateful to all of those with whom I have had the pleasure to work with during my graduate study.

DEDICATION

To

My beloved parents, Xiaoming Zou and Xi Wang,

and my girlfriend, Xiao Hu.

Table of Contents

ABSTRACT i

ACKNOWLEDGMENTS iii

DEDICATION iv

LIST OF FIGURES x

List of Tables xiii

NOMENCLATURE xv

CHAPTER 1 INTRODUCTION 1

1.1 Background 1

1.2 Problem Statement 5

1.3 Research Objectives 7

1.4 Thesis outline 7

CHAPTER 2 LITERATURE REVIEW 9

2.1 Heavy oil 9

2.2 Foamy Oil Flow 10

2.2 Characteristics of Nitrogen in Oil Reservoirs 12

2.3 Application of Nitrogen in Oil Reservoirs 17

CHAPTER 3 PROPERTIES OF NITROGEN AND OIL SAMPLE 23

3.1 Overview 23

3.2 Experimental Material and Apparatuses 23

3.2.1 Oil Sample 23

3.2.2 DBR Pressure-Volume-Temperature (PVT) System.....26

3.3 Experimental Procedure.....29

3.3.1 PVT Cell Cleaning.....29

3.3.2 Oil and Gas Injection 29

3.3.3 Measurement.....30

3.4 Results and Discussions.....31

3.5 Chapter Summary 39

CHAPTER 4 PRESSURE DEPLETION TESTS IN 1-D SAND-PACK 40

4.1 Overview.....40

4.2 Experimental Material and Apparatuses 41

4.2.1 Oil Sample 41

4.2.2 1-D Cylindrical Sand-pack Model.....41

4.3 Experimental Procedure.....44

4.3.1 Sand-pack Model Preparation.....44

4.3.2 Experimental System Setup 47

4.3.3 Leaking Tests 49

4.3.4 Pore Volume Measurement 50

4.3.5 Absolute Permeability Measurement 53

4.3.6 Live Oil Preparation 57

4.3.7 Live Oil Saturation and Initial Oil/Water Saturation Measurements ... 59

4.3.8 Live Oil Viscosity Measurement 62

4.3.9 Pressure Depletion Tests 62

4.4 Results and Discussion 63

4.4.1 Overview 63

4.4.2 Oil/Gas Production 66

4.4.3 Pressure Analysis 80

4.4.4 Comparison with Other Solvent 92

4.5 Chapter Summary 96

CHAPTER 5 HUFF-N-PUFF TESTS IN 2-D SAND-PACK 98

5.1 Overview 98

5.2 Experimental Material and Apparatuses 99

5.2.1 Oil sample 99

5.2.2 2-D Planar Sand-pack Model 100

5.3 Experimental Procedure 103

5.3.1 Sand-pack Model Preparation 103

5.3.2 Sand Packing 106

5.3.3 Experimental System Setup 108

5.3.4 Leaking Tests 111

5.3.5 Pore Volume Measurement 112

5.3.6 Absolute Permeability Measurement 115

5.3.7 Oil Saturation and Initial Oil/Water Saturation Measurements 119

5.3.8 Single-Well Huff-n-Puff Tests 123

5.3.9 2-Well Huff-n-Puff Tests 124

5.4 Results and Discussions 124

5.4.1 Overview 124

5.4.2 Oil/Gas Production 126

5.4.3 Production Phase Analysis 136

5.4.4 Residual Oil Saturation Profile 140

5.4.5 Solvent chamber growth 144

5.5 Chapter Summary 151

CHAPTER 6 CONCLUSIONS AND RECOMMENDATIONS 153

6.1 Conclusion 153

6.2 Recommendation 155

Reference 157

LIST OF FIGURES

Figure 3.1 Viscosity of the Dead Oil Sample.....25

Figure 3.2 DBR PVT System Schematic Plan.....27

Figure 3.3 DBR PVT System.....28

Figure 3.4 Solubility of Nitrogen at 7 MPa 33

Figure 3.5 Solubility of Nitrogen at 55 ℃.....36

Figure 4.1 1-D Cylindrical Sand-pack Model.....42

Figure 4.2 Distribution of Inlet/Outlet Port and Pressure Points.....46

Figure 4.3 Illustration of the Experimental Device System.....48

Figure 4.4 Permeability Measurement.....55

Figure 4.5 Live Oil Rotary.....58

Figure 4.6 Cumulative Oil Production.....65

Figure 4.7 Cumulative oil production, Oil/Gas Production Rate, and the Inner Pressure Curves with Pressure Decline Rater of 2 kPa/min 69

Figure 4.8 Cumulative oil production, Oil/Gas Production Rate, and the Inner Pressure Curves with Pressure Decline Rater of 8 kPa/min 72

Figure 4.9 Cumulative oil production, Oil/Gas Production Rate, and the Inner Pressure Curves with Pressure Decline Rater of 16 kPa/min 75

Figure 4.10 Cumulative oil production, Oil/Gas Production Rate, and the Inner Pressure Curves with Pressure Decline Rater of 32 kPa/min 77

Figure 4.11 The Distribution of Pressure Points 81

Figure 4.12 Pressure Difference in the Test with Pressure Decline Rate of 2 kPa/min 85

Figure 4.13 Pressure Difference in the Test with Pressure Decline Rate of 8 kPa/min 87

Figure 4.14 Pressure Difference in the Test with Pressure Decline Rate of 16 and 32 kPa/min 89

Figure 4.15 Production Curves for Other Solvents 93

Figure 5.1 2-D Planar Sand-pack Model 102

Figure 5.2 Distribution of Inlet ports, Outlet ports, and Thermocouples 105

Figure 5.3 Vibrator on the 2-D Model 107

Figure 5.4 The Illustration of the Experimental Device System 110

Figure 5.5 Permeability Measurement 117

Figure 5.6 Oil Saturation Process 120

Figure 5.7 Cumulative Oil Production with Pressure Decline Rate of 2 kPa/min 127

Figure 5.8 Pressure Depletion Curve and the Oil Production Curve of the First Cycle 128

Figure 5.9 Cumulative Oil Production with Pressure Decline Rate of 8 kPa/min 130

Figure 5.10 Pressure Depletion Curve and the Oil Production Curve of the First Cycle 131

Figure 5.11 Pressure Depletion Curve and the Oil Production Curve in the 7th Cycle and in the Pressure Depletion Test..... 133

Figure 5.12 Cumulative Oil Production with Pressure Decline Rate of 16 and 32 kPa/min 135

Figure 5.13 Residual Oil Distribution..... 141

Figure 5.14 Residual Oil Distribution in Propane-based and Mixture Solvent CSI 143

Figure 5.15 Solvent Chambers in the Test with Pressure Decline Rate of 2 kPa/min 145

Figure 5.16 Solvent Chambers in the Test with Pressure Decline Rate of 16 kPa/min 147

Figure 5.17 The Shape of the Simulated Gas Chambers 148

Figure 5.18 Solvent Chambers in Propane-based CSI..... 150

List of Tables

Table 3.1 Viscosity of the Dead Oil Sample 24

Table 3.2 Solubility of Nitrogen at 7 MPa 32

Table 3.3 Solubility of Nitrogen at 55 ℃ 35

Table 3.4 Solubility Comparison 38

Table 4.1 The Parameters of the Dead Oil and the 1-D Cylindrical Sand-pack Model 43

Table 4.2 Porosity Measurement 52

Table 4.3 Permeability Measurement 54

Table 4.4 Permeability of the Sand-pack Model 56

Table 4.5 Parameters of the 1-D Cylindrical Sand-pack Model 61

Table 4.6 Oil/Gas Recovery Factor 64

Table 4.7 Oil Recovery Factor of Each Experiment. 79

Table 4.8 Nitrogen Release Rate at Each Stage 91

Table 4.9 Oil Recovery of Other Solvents 95

Table 5.1 Porosity Measurement 114

Table 5.2 Permeability Measurement 116

Table 5.3 Permeability of the 2-D Sand-Pack Model 118

Table 5.4 Parameters of the 2-D Planar Sand-pack Model 122

Table 5.5 Oil Recovery Factor of the Tests. 125

Table 5.6 Oil Production Characteristics of Phase 1 and Phase 2 in Previous Studies.....137

NOMENCLATURE

Notations

A	cross section area of the sandpack, cm^2
A, B	coefficients
C_t	total compressibility, 1/kPa
D	diameter of the sandpack, cm
K	absolute permeability of the sandpack, D
L	length of the sandpack, cm
Q	flow rate, cm^3/min
R_{SO}	solution gas oil ratio, Sm^3/m^3
S_g	gas saturation, %
S_O	oil saturation, %
S_w	water saturation, %
V	volume of the nitrogen storage vessel, cm^3
V_g	gas volume, m^3
V_o	oil volume, m^3
V_w	water volume, m^3
X	length of the 2-D sand-pack, cm
Y	Width of the 2-D sand-pack, cm
Z	Thickness of the 2-D sand-pack, cm

Greek Symbols

σ	interfacial tension of gas-liquid phase
ρ_g	gas density, kg/m^3
ρ_o	oil density, kg/m^3
ρ_w	water density, kg/m^3
Φ	porosity of the sandpack, %
μ	viscosity of the flush fluid, mPa·s

Subscripts

P	pressure
T	temperature
t	total

Abbreviations

CHOP	Cold Heavy Oil Production
CHOPS	Cold Heavy Oil Production with Sands
CMG	Computer Modeling Group
CSI	Cyclic Solvent Injection
CHSI	Cyclic Hot Solvent Injection
CSS	Cyclic Steam Stimulation DLA

GOR	Gas Oil Ratio IN
OOIP	Original Oil in Place
PV	Pore Volume
PVT	Pressure-Volume-Temperature
SAGD	Steam Assisted Gravity Drainage
SARA	Saturates, Aromatics, Resins, and Asphaltenes
SRC	Saskatchewan Research Council
VAPEX	Vapor Extraction

CHAPTER 1 INTRODUCTION

1.1 Background

Petroleum, although a nonrenewable energy source, will remain as the primary source of energy worldwide (Nelson, Sheehy, O'Donnell, & Heisler, 2016). As oil demand continues to increase, the oil consumption is estimated to grow accordingly in the next five years or more before reaching its peak value (expected international energy agency). Unlike the increasing demand for oil, the scarcity of conventional oil reservoirs makes it a challenge to meet the demand. Fortunately, unconventional oil reservoirs account for 70% of total oil reserves worldwide (Jin et al., 2017). Therefore, exploitation of unconventional oil reservoirs in the current oil industry has become the main focus to increase oil production (Crandall & Wise, 1984; X. Wang, Peng, Zhang, Du, & Zeng, 2018; Y. long Zhao, Xie, Peng, & Zhang, 2016).

Unconventional oil reservoirs are reservoirs with a wide variety of sources, which include oil sands, extra heavy oil, gas to liquids, tight oil, oil shale, and other liquids(X. Wang et al., 2018). Among them, the recoverable reserves of tight oil and heavy oil are 47.0 % and 29.7 %, respectively. Tight oil and heavy oil are considered as the momentous resources for meeting the rapidly growing oil demand (Jiang, 2013).

Although heavy oil resources are available worldwide, the most resourceful deposit is the Athabasca Oil Sands in Alberta, Canada. Canada, the country with the most abundant oil reserves, has about 49 percent of the world's heavy oil resources. The heavy oil and bitumen

reservoirs are mainly distributed in Alberta and Saskatchewan with an estimated OOIP of around 2.5 trillion barrels (Bayestehparvin, Ali, & Abedi, 2016; Firoozabadi, 2001; Yuan & Jin, 2008; Zhou & Zeng, 2014).

Heavy oil generally consists of oil sand, extra heavy oil or bitumen, which are trapped in unconsolidated sandstones. These type of crude oil are extremely viscous, making extraction difficult. Due to the high viscosity, heavy oil and bitumen are unable to be pumped out by conventional production methods. As a result, the recovery methods for heavy oil reservoir at different production stages will be introduced in the following parts.

Primary Production

Primary production is the exploitation of crude oil by the pressure difference generated by gas, gravity drainage, or the combination of these two effects. This process is also known as 'nature lift.'

For heavy oil reservoir, one of the optimal methods of primary production is Cold Heavy Oil Production with Sand (CHOPS). In this method, continuous oil and sand are produced from the wellbore to form wormholes or voids, which improves the oil recovery factor of heavy oil reservoirs (J. J. J. Sheng, Maini, Hayes, & Tortike, 1999). Due to the sand production in the wellbore, in most cases, the CHOPS wells rely on the artificial lift to help produce oil and sand. In exceptional cases, when the depth of the reservoir is less than 300 meters, heavy oil can be produced by surface open-pit mining. This cold production method is widely applied in heavy oil reservoirs in Alberta and Saskatchewan. The advantage of this method is that the presence of wormholes can lead to a high production rate.

In general, the primary production recovery factor of conventional reservoirs is around 30 %, but that of unconventional reservoirs is only about 10 to 15 %. However, CHOPS consume too much initial pressure in the reservoir, so that some new wells began to use other EOR method to extract oil without going through the CHOPs process. Those EOR methods are commonly referred to as non-CHOPS methods and are briefly discussed below.

Post-CHOPS Production

Compared with conventional reservoirs, there is more residual oil in unconventional reservoirs after primary recovery. Nevertheless, due to the unique properties of heavy oil and the unconsolidated sandstones, the conventional displacement method of restoring reservoir pressure utilizing water, natural gas or carbon dioxide injection has no functional effect (B. B. Maini, Sarma, & George, 2010). In general, the main methods that are used in heavy oil post-CHOPS recovery involves both thermal and non-thermal approaches (Yazdani & Maini, 2006). Thermal methods mostly refer to steam injection, which is the most effective method to reduce heavy oil viscosity. Non-thermal methods include the application of polymers, chemicals, solvents or microbes to reduce the oil viscosity or to increases the water viscosity.

Thermal Methods

Thermal methods mainly include three steam injection technologies:

1. Cyclic Steam Stimulation (CSS) injects steam through a single well. The high pressure and high-temperature steam are injected to rupture the formation, heat the surrounding heavy oil, and reduce oil viscosity. The injection process can last for a few months. Steam injection is followed by the soaking process. There is no common

understanding of soaking time, which usually ranges from days to weeks. During the soaking period, heavy oil absorbs the heat and then the oil is pumped out through the same well. This process is repeated until the cost outweighs the income. The oil recovery factor of CSS is generally around 20 %. At the end of CSS, continuous steam injection method will usually be used to carry on the production of oil.

2. Continuous Steam Injection (steam flooding), needs at least two wells. One is a steam injection well, and the others are oil production wells. High-temperature and high-pressure steam is injected into the formation to raise the temperature of the crude oil, which will lower the viscosity and mobilize the oil to be produced. Since steam flooding requires a large contact area with oil, it is often applied after CSS. Compared with CSS, steam flooding has a lower thermal efficiency but has a higher recovery factor. The oil recovery factor of steam flooding is generally around 50 %.
3. Steam-assisted Gravity Drainage (SAGD), is a specific type of steam flooding method that involves two stacked horizontal wells. High-temperature steam is continuously injected into the upper wellbore, causing the heating oil to drain into the lower wellbore. Compared with steam flooding, SAGD is supported by gravity drainage and has higher oil recovery efficiency.

Based on the many successful pilot tests and filed applications, thermal methods have become the most common technologies for enhancing heavy oil recovery (Boyle, Gittins, & Chakrabarty, 2003; Yazdani & Maini, 2006; L. Zhao, Anderson, & O' Rourke, 2005; L. Zhao et al., 2010).

Non-thermal Methods

The most common non-thermal recovery approaches in heavy oil reservoirs are chemical flooding and solvent-based methods. Chemical flooding is a generic term describing an injection process using a particular type of chemical solution. These include polymers, micellar, alkaline and soapy materials, which are all used to improve the sweep efficiency of water flooding or reduce the surface tension. Chemical flooding is usually applied in heavy oil reservoirs with oil viscosity less than 1,000 cP.

In the last 50 years, Vapor Extraction (VAPEX) or the Cyclic Solvent Injection (CSI) is considered as the solvent-based method in heavy oil reservoirs. VAPEX, similar to the SAGD concept, uses solvent vapor to reduce the viscosity of heavy oils. The injected solvent vapor expands and dilutes the heavy oil under high pressure. The diluted heavy oil will then flow by gravity to the lower wellbore. CSI is similar to CCS. The solvent is soluble in heavy oil to reduce its viscosity. In Jia's study (Jia, 2014), foamy oil flow is also one of the dominant mechanism in the VAPEX and CSI processes(Du, Zeng, Peng, & Chan, 2018). It has been reported that solvent-based method only consumes about 3 % energy of that in steam-based methods (Das, 1998). However, its main cost comes from the consumption of solvents.

1.2 Problem Statement

Thermal recovery is currently the preferred method to exploit heavy oil reservoirs. However, for deep heavy oil reservoirs, due to the length of the wellbore being long, the heat loss becomes tremendous (Jia, Zeng, & Gu, 2015; Knorr & Imran, 2012; Yazdani & Maini,

2006), causing a considerable amount of heating required. For steam-based methods, they are inevitably accompanied by carbon dioxide emissions. Since environmental issues become more prominent, the cost of carbon dioxide treatment continues to increase. Moreover, the international oil price is very low as of 2019. Under various factors, steam-based methods become uneconomical (Huang, Zhou, Yang, Liao, & Zeng, 2017). For such reservoirs, the solvent-based method is more reasonable, and cyclic solvent injection is more efficient than continuous solvent injection methods (K. Zhang, 2018).

In general, when the reservoir is relatively deep, the formation temperature is relatively high. The advantage of this reservoir condition is that even if the crude oil viscosity underground is high, the crude oil can maintain sufficient mobility under such high temperature. This makes it unnecessary to use expensive hydrocarbon gases in the CSI method. Nitrogen, on the other hand, can meet the demand and further reduce costs. Research on nitrogen Huff-n-Puff process for heavy oil reservoirs has not been found in present published studies. In other words, the potential influence of nitrogen Huff-n-Puff process has not been throughly studied yet.

Worldwide, relatively deep heavy oil fields are concentrated in formations from 1,000 to 2,000 m deep.(Freitag, 2014). According to the relationship between formation temperature and depth(Sadykova, 2014), The temperature of the 1000 to 2000 m deep formation is generally 40 to 60℃. This study explores the feasibility of nitrogen Huff-n-Puff in deep heavy oil reservoirs, thus a heavy oil reservoir at a depth of 1500 m and 50℃ is used as the

research object. However, due to the limitation of the pressure capacity of the experimental equipment, the highest pressure used in this study is 7 MPa.

1.3 Research Objectives

The main objective of this thesis is the nitrogen Huff-n-Puff process methodology study, and the scope of this study is listed as follows:

1. To confirm nitrogen's ability to form foamy oil flow.
2. To determine the feasibility of nitrogen Huff-n-Puff process in heavy oil reservoirs.

In this work, experimental studies including PVT tests, 1-D sand-pack, and 2-D sand-pack tests. In PVT tests, the experiments are conducted in a mercury-free DBR Pressure-Volume-Temperature (PVT) system to measure the solubility of nitrogen, after which the viscosity of the heavy oil-nitrogen live oil is measured in a 1-D cylindrical sand-pack model with Darcy's Equation. In the 1-D cylindrical sand-pack tests, pressure depletion tests are conducted on the heavy oil-nitrogen systems to determine the oil production curves under different constant pressure decline rates. The feasibility of nitrogen Huff-n-Puff process is lastly verified in the 2-D model of the Huff-n-Puff tests.

1.4 Thesis outline

This thesis is composed of five chapters. The first chapter is about the status quo of heavy oil exploitation and a brief introduction of this research. The second chapter is a survey of foamy oil in heavy oil system and the theoretical knowledge involved in the Huff-n-Puff process. Chapter 3 is an explanation of the measurement of the basic parameters of nitrogen

involved in this study. It mainly includes the viscosity of dead oil and the solubility of nitrogen. In Chapter 4, four sets of experiments are conducted in a 1- D sand-pack model under different pressure decline rates to observe the phenomenon of foamy oil. Chapter 5 describes a group of tests that are conducted in a 2- D sand-pack model to verify the feasibility of nitrogen Huff-n-Puff process. In the last chapter, the significant conclusions of this study are summarized, and some recommendations are listed for future work.

CHAPTER 2 LITERATURE REVIEW

2.1 Heavy oil

Heavy oil refers to a high-viscosity crude oil of more than 50 mPa·s under the formation conditions or a degassed crude oil viscosity of 1,000-10,000 mPa·s at the reservoir temperature. In addition to the high viscosity, heavy oil also has a high density. Heavy oil contains fewer light components and higher asphalt content. The viscosity of the heavy oil changes with temperature. With a temperature increase of 8 to 9 ℃, the viscosity can be reduced by half. At the reservoir temperature, a degassed crude oil with a viscosity greater than 10,000 mPa·s is called extra heavy oil.

Intuitively comparing heavy oil and thin oil, we can see that thin oil flows like water, but heavy oil is difficult to flow. This is caused by the high viscosity of heavy oil that can go up as high as several million centipoises, like mud. The mobility of heavy oil is also very undesirable making the thick oil naturally difficult to extract from the reservoirs.

The precipitates (wax) produced during the production of oil wells are often solid or semi-solid, with a dark brown color. The composition is mainly paraffin, the colloids are mixed with the asphaltenes, and the sand particles are carried by the drilling fluid. These precipitates are what makes the viscosity of the crude oil so high. The rheological properties of the high waxy crude oil vary significantly with temperature, exhibiting different rheological properties at different temperatures. When the oil temperature is higher than the waxing point of the crude oil, the wax crystal is completely dissolved in the crude oil. The

dissolved paraffin can be regarded as a homogeneous medium having interaction between the paraffin wax and the petroleum solvent molecule. Its viscosity is a single-valued function of temperature and is characterized by the properties of Newtonian fluids. During the process of the oil temperature falling from the waxing point to the abnormal point, the wax crystals are continuously precipitated. The dispersed particle concentration of the system is increased, and an excellent dispersion system is formed with the viscosity characteristics remaining as a Newtonian fluid.

When the oil temperature is lower than the abnormal point, the wax precipitated in the crude oil causes a qualitative change in the physical structure (such as particle orientation, shape, and arrangement) inside the system. The crude oil viscosity is no longer a single-valued function of temperature but is also related to shear rate, manifested as pseudoplastic fluid properties. When the oil temperature drops below the de-flow point or the freezing point, the amount of wax crystals is greatly increased, and the concentration of dispersed particles in the system increases accordingly. The particles begin to interconnect with each other. At this time, the crude oil has thixotropic and yielding properties of the pseudoplastic fluid.

2.2 Foamy Oil Flow

During the primary production of some heavy oil reservoirs in Canada, Venezuela and China, abnormal development phenomena are shown: low production gas-oil ratio, high oil recovery rate and higher than expected primary recovery (Aghabarati, Dumitrescu, Lines, & Settari, 2008; B. Maini, 2007; Yarlong Wang, 1999). Hyperosmotic flow channels

(wormholes) and foamy oil phenomena are two mechanisms for explaining this anomalous phenomenon (Ingham et al., 2011; Izquierdo, Kamp, & Vallejos, 2000; Sun, Zhang, Cui, Duan, & Zhao, 2014). Between the two, researchers generally believe that the latter is the main cause. The foamy oil phenomenon was first discovered in a Canadian heavy oil reservoir and is characterized by the presence of oil in a continuous phase and the presence of bubbles in a dispersed phase (J. J. J. Sheng et al., 1999). The foamy oil phenomenon usually occurs when the reservoir pressure is lower than the bubble point pressure, the dissolved gas separates from the oil phase, and together forms dispersed small bubbles in the oil phase (Mastmann, Moustakis, & Bennion, 2001). Since the phenomenon of foamy oil has a significant effect on oil recovery and crude oil flow characteristics, it is of great significance to study the structural characteristics of these special reservoirs. Stable oil/gas interface properties are important factors influencing the foamy oil phenomenon (J. J. Sheng, Maini, Hayes, & Tortike, 1997). Smith pointed out that asphaltenes as a medium for gas nucleation, are the leading cause of the phenomenon of foamy oil (Smith, 1988). Studies by Claridge and Tang et al. have also demonstrated this mechanism, while they point out that asphaltenes have a stabilizing oil/gas interface to stabilize foamy oil (Leung et al., 2006; Tang & Firoozabadi, 2006). However, Maini stated that asphaltenes have no effect on bubble nucleation and growth through experimental research (J. J. Sheng et al., 1997). Therefore, the effect of asphaltenes on the stability of foamy oils requires further investigation. In addition, Maini highlighted that the height of the oil column, the viscosity of the crude oil, and the porous medium all have an effect on the stability of the foamy oil (J. J. Sheng et al., 1997). At the

same time, Liu pointed out that at low reservoir temperature, higher initial solution gas/oil ratio, and smaller pore volume are beneficial to the stability of foamy oil (Liu, Wu, & Li, 2013).

2.2 Characteristics of Nitrogen in Oil Reservoirs

Nitrogen is an inert gas with low density, low viscosity, and low thermal conductivity. It also has low solubility in water and is difficult to react with formation fluids and rock minerals. It can avoid emulsification, sedimentation, blockage of the formation, and corrosion of the ground/underground equipment. Nitrogen does not support combustion, it is not explosive, and it is safe and reliable. Nitrogen has a large compression coefficient, strong expansion capacity, and high elastic energy. It is an ideal gas for lifting and driving oil flow. Nitrogen accounts for approximately 78% of the air's volume. Combing the use of advanced membrane separation nitrogen production technology (Falk-Pedersen & Dannstrom, 1997; Mansourizadeh & Ismail, 2009; R. Wang, Liu, Lin, & Chung, 2002; Zhu, Hrabanek, Gora, Kapteijn, & Moulijn, 2006) with inexhaustible air resources, it is possible to efficiently and quickly produce large amount of nitrogen with a purity of more than 95 % directly into the well. Therefore, when the cost is low, the source is widespread, and the construction is convenient, nitrogen has the potential to become the comprehensive and large-scale popularization of application technology.

Enhance formation energy

1. Large compression coefficient

The compression coefficient of nitrogen is much larger than that of CO_2 (three times more than CO_2.), natural gas and flue gas. Since nitrogen has a lower critical temperature, it's compression factor is less affected by temperature. Therefore, even under high-temperature gas injection conditions, the compression factor remains large. Because nitrogen has a large compression coefficient, it allows for easy expansion after depressurization, and large elasticity can become a powerful driving force for displacement and lifting of underground fluids. Therefore, nitrogen is also called energetic gas.

2. High volume coefficient

The volume coefficient of nitrogen is higher than that of similar gases such as flue gas, natural gas, and CO_2. Its volume coefficient is proportional to pressure and inversely proportional to temperature. The volume coefficient is defined as:

$$\mathrm{B} = \mathrm{C}(\frac{P}{TZ}) \tag{2.1}$$

where B is the volume coefficient; C is a constant; P is the pressure, MPa; T is the temperature, °C; Z is the compression coefficient.

The high volume coefficient of nitrogen means that with the same volume of gas injected, nitrogen can displace and lift more oil and gas.

3. Nitrogen column static head is low

$$\Delta \mathrm{X} = \int_1^2 \frac{\mathrm{do}}{\rho} \tag{2.2}$$

$$\rho = \frac{PM}{ZRT} \tag{2.3}$$

$$\Delta \mathrm{X} = \int_1^2 \frac{\mathrm{ZRT}}{PM} \tag{2.4}$$

where X is the volume coefficient; R is the universal gas constant; P is the pressure, MPa; T is the temperature, °C; Z is the compression coefficient. ρ is the density, kg/m^3; M is the energy, J.

The static pressure column is low due to the small density of nitrogen. According to the equation, when the wellhead pressure is 5 MPa, the nitrogen column with a depth of 1000 m is only 0.608 MPa. When nitrogen is used to drive and lift the wellbore fluid, the mixed fluid flow pressure gradient is small, and the energy consumption is small.

4. Low friction coefficient

Due to the low density of nitrogen, the viscosity coefficient is small, the flow performance is good, and the frictional resistance is small. Whether in underground porous media or wellbore lifting, the nitrogen flow resistance is small which leads to lesser energy consumption. Nitrogen also plays the role of increasing the energy of the formation.

5. Easy to form the foam

Nitrogen readily forms a foam with the wellbore or subsurface fluid. When a decent foaming agent is added, the generated nitrogen foam has a volume which can expand by 3 to 10 times the volume of the underground fluid. Moreover, due to the high viscosity of the foam, there is a stronger ability to displace fluids. The slippage loss is also less, which is more beneficial to the displacing and lifting of underground fluids.

Improve heat energy utilization

1. Thermal insulation

Nitrogen has a low thermal conductivity of only 0.0288 W/m•K, making it an ideal thermal insulation material. Nitrogen injection at the same time as steam injection can effectively prevent heat dissipation in the wellbore and the rock above and below the formation, significantly reduce heat loss and ensure the dryness of steam. Thereby improving the steam injection effect.

2. Expanding the heat source carrier

The volume of nitrogen is large, and nitrogen injection at the same time of steam injection can greatly increase the heat source carrier, thereby increasing the sweep volume of gas injection, and effectively improving the steam injection effect.

3. Prevent steam override

The difference between the density of steam and crude oil is enormous. When steam is injected, the steam overrides, causing steam to enter the upper oil layer. This override causes no heating to the middle and lower oil layers, which seriously affects the thermal recovery effect. The nitrogen vapor density is lower than that of the steam, which preferentially occupies the upper space, forcing the steam to descend and heat the middle and lower oil layers.

4. Alleviate steam fingering

Due to the difference in viscosity and mobility between steam and crude oil, steam fingering occurs during steam injection, which seriously disturbs the steam injection effect. Since nitrogen readily forms a viscous foam with the underground fluid, it can effectively alleviate and suppress the fingering of steam.

5. Improve the heating effect

The injected steam has low viscosity, good flow performance, and fast flow rate. When steam is hot, the gas-flow quickly passes through the oil layer and fails to thoroughly heat the oil layer, resulting in poor thermal recovery. If a nitrogen foam is used, the heat source carrier is enlarged, and the flow rate is moderated so that it flows slowly through the oil layer. In addition, nitrogen assisted drainage has a high drainage rate, in turn, helps avoid water accumulation at the bottom of the well. Since the water and the oil both have higher heat capacity, if a large amount of condensed water is accumulated underground, it will significantly reduce the dryness of the steam and seriously affect the thermal recovery effect.

Improve oil displacement efficiency

1. Improve formation conductivity

Nitrogen has a small molecular weight and a low viscosity coefficient of only 117.96 x 10^{-7} Pa·s at 25 °C. It has a strong penetrating ability making it easier to enter the pore throat of the formation. In addition, the high nitrogen injection rate and large flushing force can purify the wellbore and the formation, and dredge the pore throat passage. This significantly improves the conductivity of the formation, and at the same time displace the residual oil in the rock fracture.

2. Assist oil displacement

When nitrogen is added to some active substances, it can readily form foam with the formation water in the oil layer. This foam can then effectively reduce the oil-water interfacial tension and improve the wettability of the rock surface. In addition, when the foam flows

through the pore throat of the formation, the gas-flow is deformed, and the pressure gradient is increased, which can overcome the capillary pressure and displace the restrained oil.

3. Miscibility and extraction

Under suitable pressure and temperature conditions, nitrogen and crude oil can reach the mixed dynamic phase through multiple contacts, reduce the interfacial tension, and play the role of miscible flooding. At the front of the nitrogen-oil contact, extraction can occur to improve oil displacement effect.

4. Increase production pressure difference

Since the nitrogen density is low and the static pressure is small, when the oil flow is lifted, the oil-nitrogen mixed liquid column has a small pressure gradient. This small pressure gradient can effectively increase the production pressure difference.

2.3 Application of Nitrogen in Oil Reservoirs

In general, pure nitrogen is not widely used in heavy oil reservoirs. Rather, the common use of nitrogen is to aid in steam stimulation, called nitrogen assisted cyclic steam stimulation and nitrogen foam assisted steam flooding.

Nitrogen Assisted Cyclic Steam Stimulation

In the process of cyclic steam stimulation, the heating radius and heating area will increase gradually with the increase of the Huff-n-Puff cycles. However, when the number of Huff-n-Puff cycles increases to a certain extent, the heat from steam injection into the formation can only make up for the formation heat loss. Heating radius and heating area are

no longer expanded, resulting in a rapid decrease in the amount of single well oil production and oil/ gas ratio, and the economic benefits are worsened. At the same time, the oil layer undergoes a large number of cyclic steam stimulation and then depressurizes. Even if it is heated, it will be difficult to drain into the wellbore because there is not enough oil driving force. Due to the limited heating radius (usually about 30 m) and the override in the longitudinal direction of the steam, the mobility in the plane and in the longitudinal direction is unsatisfactory with a large amount of oil remaining in the formation. Therefore, in the context of cyclic steam stimulation, there are problems regarding how to enlarge the heating belt, increase the longitudinal and plane sweep efficiency, and provide sufficient oil displacement drive force to the oil layer. Injecting a certain amount of nitrogen into the heavy oil reservoir during the steam injection process provides an excellent way to solve these problems. The nitrogen assisted cyclic steam stimulation method is an improved technology for cyclic steam stimulation for the characteristics of high formation pressure in medium and deep heavy oil reservoirs. This technology is to inject nitrogen into the formation under high pressure. The injected gas is fully dissolved and highly compressed in the reservoir. The solution gas drive in the production stage and the gas expansion of the compressed gas drive extract the crude oil to the bottom of the well. The main effect of nitrogen assisted cyclic steam stimulation is to dissolve and reduce the viscosity of heavy oil and improve the mobility of crude oil in the formation. Injection of nitrogen into the reservoir is to increase the volume expansion rate of the crude oil and the pressure of the reservoir. The injection of nitrogen can bring the steam into the deep reservoir, expand the heating chamber, increase

the sweep volume and so on. For the nitrogen assisted cyclic steam stimulation technology, some research results have been initially obtained in both indoor and field experiments.

Svrcek measured the solubility of nitrogen in Athabasca asphalt at various pressures through laboratory experiments (Mehrotra & Svrcek, 1982). The experimental results show that the solubility of nitrogen in asphalt is only 3.28 mL/mL at 33.9 ℃ and 6 MPa. Due to the low solubility of nitrogen in crude oil, nitrogen has a small effect on the viscosity and expansion of crude oil (Merotra & Svrcek, 1982).

Dong optimized the amount of nitrogen injected, injection method, and injection speed during steam flooding through laboratory simulation experiments (Dong & Huang, 2002). The experimental results show that only 0.4 PV 0f nitrogen can increase oil recovery by 8.8 %, from 34.3 % to 43.1 %. The small slug injection method can obtain a better economic benefit, but the actual injected slug size needs to be determined by numerical simulation.

L.S.Monte-Mor pointed out that steam and a small amount of flue gas (about 10 %) can increase the displacement efficiency and energy utilization efficiency (Trevisan, Laboissiere, & Monte-Mor, 2013). The presence of gas can make the pressure of the leading edge more stable. Nitrogen in the flue gas can drive the heated crude oil out of the porous medium to improve oil recovery, but the recovery rate does not increase with the increase of the injected gas volume. The selection of the gas-water ratio needs to be further studied.

Du pointed out that injecting nitrogen and then injecting steam during the Huff-n-Puff process can allow nitrogen to enter the deeper formation and delay the breakthrough time of nitrogen during the production stage (Yang Wang, Du, Ge, Jiang, & Zhang, 2013). The strong

compressibility of nitrogen can keep the formation pressure at a high level, which is conducive to the recovery factor of crude oil.

In 1992, Gaosheng Oilfield added nitrogen as a drainage aid during the steam injection (6~12 m^3 liquid nitrogen injection per cycle) and had a significant improvement in assisting drainage. 13 wells were constructed, and 10 wells were effective at oil production(Yanbin et al., 2012).

In 2005, the Lukeixing Oilfield conducted a nitrogen injection test in one well. The highest pressure is at 33.0 MPa, and the highest injection rate is at 60 m^3/min. The injection volume of liquid nitrogen is 63 m^3, which is equivalent to nitrogen gas of 37824 m^3. After 7 days of soaking time, the wellhead pressure dropped from 32.0 MPa to 22.0 MPa. The pre-production of the well was 3.3 t/d, after the nitrogen injection test, the initial production of the well was 7.8 t/d, and the current stable production was 5.7 t/d. The test results show that the reservoir can achieve stable production, and the injected gas can reduce the viscosity of crude oil and increase production (Yanbin et al., 2012).

Nitrogen Foam Assisted Steam Flooding

There are two main reasons for restricting steam flooding recovery. First is the low steam sweep efficiency. Steam is prone to gravity override. In the case of gravity override, due to the small steam density, the steam is displaced along the top of the heavy oil layer, causing the crude oil in the lower part of the oil layer to remain in the formation without displacement (Doe & Doe, 1990). On the other hand, due to the difference in mobility ratio, steam fingering can easily occur, and the heterogeneity of the formation causes steam turbulence. The steam

first enters the relatively high permeability layer, and the low permeability layer is not injected with steam. Also, the oil-water interfacial tension is high, and the displacement efficiency is low.

Nitrogen foam has been proposed as a way to improve the thermal method recovery of heavy oil in the last century, and relevant indoor and field research has been carried out (Ding, Mehra, & Donnelly, 2007). Research shows that nitrogen foam profile control technology can effectively control steam turbulence, adjust the steam absorption profile of thermal recovery wells, increase the volume of steam, and improve the production of reservoirs. The principles are:

1. Displace the “top” reservoir by the difference in density between nitrogen and crude oil. Lowers the oil-water interface, and forces the residual oil to produce (Ransohoff & Radke, 2007).
2. When nitrogen foam is formed, the nitrogen mobility is reduced, the nitrogen turbulent flow channel is blocked, and the nitrogen sweep area is increased. When a foaming agent is added to the nitrogen gas, the extremely low residual oil saturation of the nitrogen gas in the belt facilitates foaming of the foaming agent (Muijs, Keijzer, & Wiersma, 1988). After the foams are formed, the nitrogen gas becomes a discontinuous phase, and the nitrogen flow rate is drastically lowered. On the microscopic surface, the foam liquid film blocks a large number of gas passages, and the liquid film passes through the pore throat causing deformation which generates

additional resistance. The nitrogen is forced to displace the crude oil to a portion with high oil saturation, thereby increasing the nitrogen sweep efficient.

3. Due to the difference in gravity between nitrogen and water, nitrogen enters the higher part of the reservoir in the vertical direction, forcing the water to move downwards and function as a pressure cone (Holden, 1998). For oil wells with side water or bottom water, nitrogen foam is injected to form a foam flow at the oil-water interface, so that the relative water permeability is lowered, the oil relative permeability is increased, and the water cone in bottom water is controlled (Sobocinski & Cornelius, 2007).
4. The foaming agent is one type of surfactant which can reduce the interfacial tension between oil and water, improve the wettability of rock surface, and improve the efficiency of oil displacement (Isaacs, Green, Jossy, & Maunder, 2007). In the oil layer with high oil saturation, the foaming agent is readily soluble in oil, it does not blister, it does not block pore channels, and it improves oil displacement efficiency (Chang, Grigg, & Recovery, 1996).

CHAPTER 3 PROPERTIES OF NITROGEN AND OIL SAMPLE

3.1 Overview

Nitrogen is known as a low-solubility gas in the heavy oil system. Limited studies have mentioned the solubility of nitrogen in heavy oil, or the effect of nitrogen on the viscosity of heavy oil after it is dissolved in heavy oil. In this section, the experiments are conducted in a mercury-free DBR Pressure-Volume-Temperature (PVT) system to measure the solubility of nitrogen.

3.2 Experimental Material and Apparatuses

3.2.1 Oil Sample

The oil sample used in these experiments is a conventional Canadian heavy oil with a density of 0.98 g/cm^3. This oil sample can be regarded as dead oil because it is exposed to room temperature and pressure for a long time. The viscosity of the dead oil is measured by a Brookfield viscometer at different temperatures. In the process of measuring viscosity, this dead oil is heated by a heating tape.

The measurement process is repeated three times with an error of less than 5%. Then, the average of these three measurements is taken to obtain the viscosity data for the dead oil sample. The results are shown in Table 3.1 and Figure 3.1.

Table 3.1 Viscosity of the Dead Oil Sample

Temperature, °C	Experimental Data	Trend Line
	Viscosity, cP	Viscosity, cP
19.2	6400	6408
25	4810	4100
29.7	2622	2855
30.1	2514	2769
39.5	1622	1342
40	1560	1292
40.4	1490	1253
41.5	1200	1151
43	870	1025
45	730	879
47.3	634	736
50	600	598
60	330	276

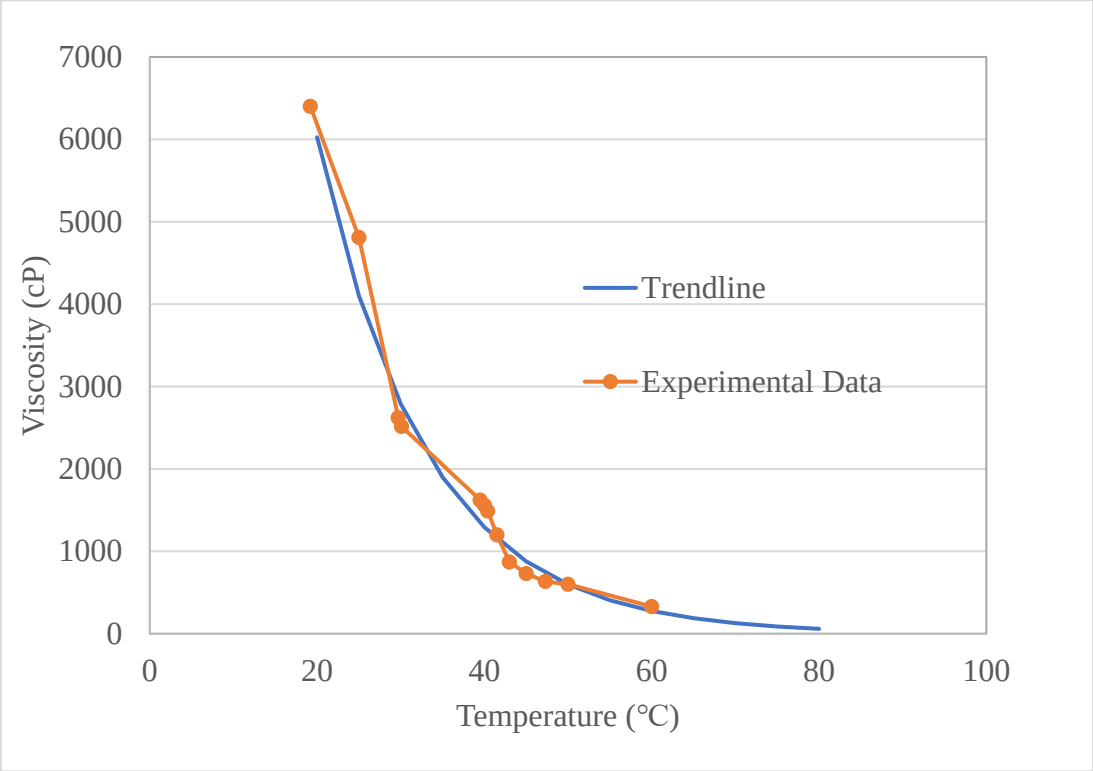

Figure 3.1 Viscosity of the Dead Oil Sample

3.2.2 DBR Pressure-Volume-Temperature (PVT) System.

The PVT tests are conducted in a mercury-free DBR Pressure-Volume-Temperature (PVT) system. This system is divided into three sections as shown in Figure 3.2.

1. Section A is the record and display system. It has a high definition camera (as shown in Figure 3.3.a), a camera lift controller (as shown in Figure 3.3.b), and a display screen (as shown in Figure 3.3.c).
2. Section B is the PVT cell and control system. It contains a visual PVT cell in an air bath (as shown in Figure 3.3.), a control panel (as shown in Figure 3.3.c) that regulates the temperature in the air bath, the magnetic stirrer in the PVT cell, and displays the pressure in the PVT cell.
3. Section C is the injection system. It contains two transfer cylinders with nitrogen and oil sample respectively, a vacuum pump, and a syringe pump.

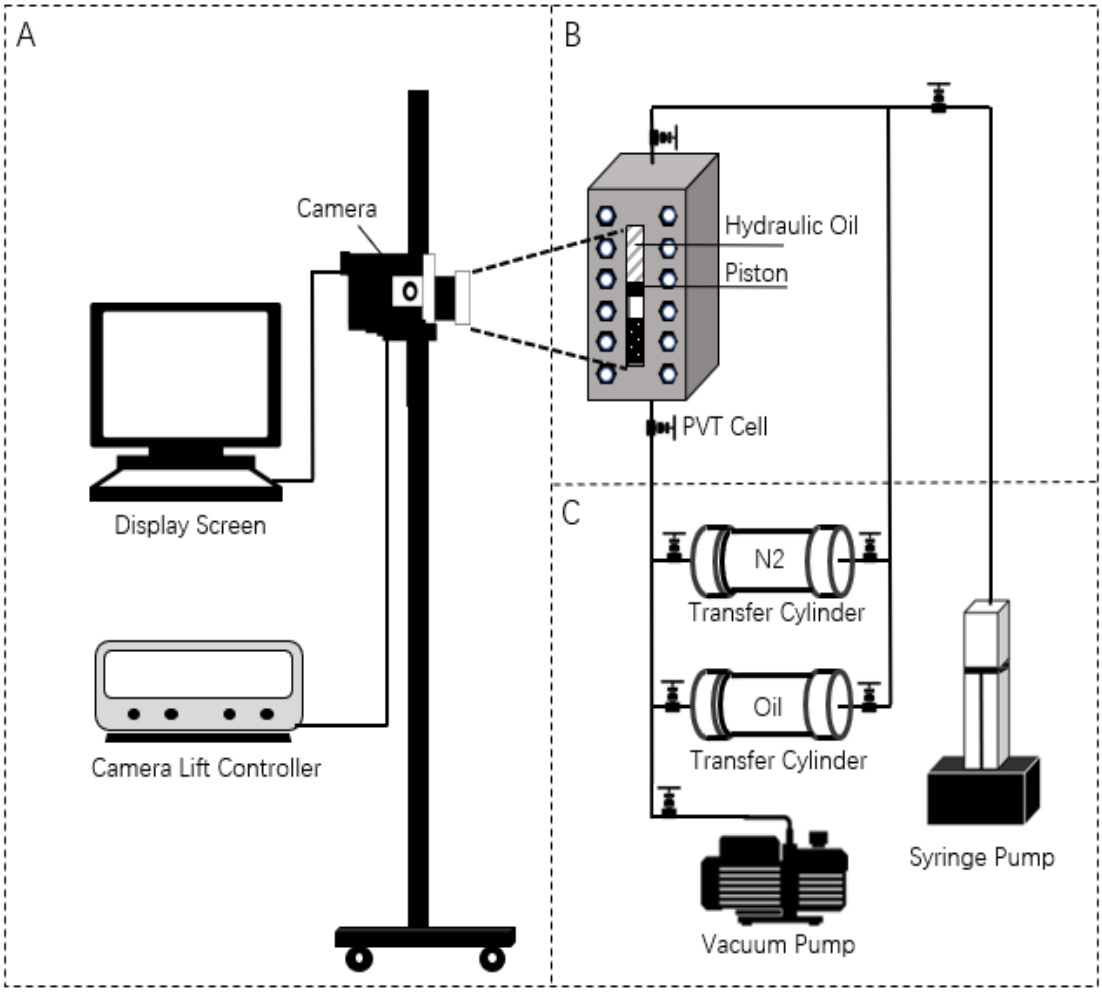

Figure 3.2 DBR PVT System Schematic Plan

(a)

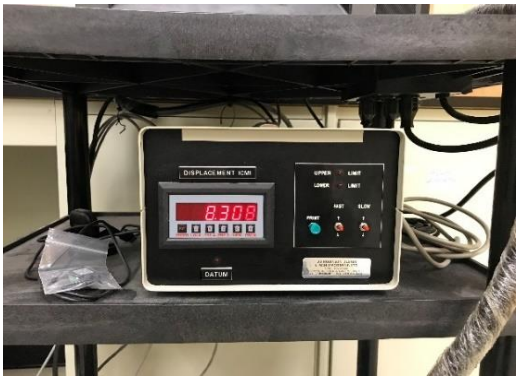

(b)

(c)

(d)

(e)

(f)

Figure 3.3 DBR PVT System

3.3 Experimental Procedure

3.3.1 PVT Cell Cleaning

In order to reduce the wear and ensure the sealing of the PVT cell, the frequency of disassembling the PVT cell should be reduced. Moreover, the cleaning process needs to be carried out under sealed conditions. To start the cleaning process, push the piston to the bottom of the PVT cell with a pump to drain out the residues. Next, inject toluene and kerosene into the cell to dissolve the remaining oil and asphaltenes, and push the piston to the bottom to drain the mixed liquid out. This process needs to be repeated several times to ensure that all residual oil and residual asphaltenes are discharged from the PVT cell.

Once the oil and asphaltenes are drained, inject ethanol to dissolve the remaining toluene and kerosene, then push the piston to the bottom to drain the mixed liquid out. This process also needs to be repeated several times to ensure that all toluene and kerosene are discharged from the PVT cell. Finally, connect the PVT cell to the vacuum pump and vacuum it for two hours to complete the cleaning process. At this stage, no more impurities existed in the PVT cell.

3.3.2 Oil and Gas Injection

To facilitate observation and reading during the measurement process, there should be enough oil sample injected into the PVT cell. The injection volume of the oil sample is set to 20 ml, and correspondingly, nitrogen volume is set to be 1,500 ml at room temperature and pressure.

First, open both valves above and below the PVT cell, push the piston to the bottom of the cell, and inject nitrogen from the bottom valve slowly until the piston rises 10 cm. Afterward, close the top valve, and continue to inject nitrogen until the pressure rises to 274 psi (1,792 kPa). Since the cross-sectional area inside the PVT cell is 7.92 cm^2, in this case, the volume of nitrogen is equal to 1,500 ml at room temperature and pressure. Lastly, inject the oil sample of 20ml into the PVT cell.

3.3.3 Measurement

Since the conditions of the later experiments are at 7 MPa and 50 ℃, a series of experiments are conducted to measure solubility at this pressure and temperature setting (Yadali Jamaloei, Dong, Yang, Yang, & Mahinpey, 2013). Increasing the pressure and temperature in the PVT cell to 7 MPa and 50℃ respectively, this state is maintained for 4 hours while keeping the magnetic stirrer on. The function of the magnetic stirrer is to evenly dissolve nitrogen into the oil sample. After 4 hours, record the changes in piston height, real-time temperature, and real-time pressure. With the recorded measurements, calculate the solubility at this condition. Next, repeat the above steps to calculate the solubility at different pressure and temperature conditions. When the pressure is maintained at 7 MPa, the temperature is set from 40 to 80 ℃ with 5 ℃ incremental increase. Then the temperature is maintained at 55℃, and the pressure is set from 7 to 1 MPa with 1 MPa incremental decrease.

3.4 Results and Discussions

The first set of data is measured when the pressure is stable at 7 MPa, and the temperature is varied from 40 to 80 ℃ with 5 ℃ incremental increase. The result is shown in Table 3.2 and Figure 3.4. From Figure 3.4, it can be seen that when the pressure is constant, the solubility of nitrogen decreases linearly with increasing temperature.

Table 3.2 Solubility of Nitrogen at 7 MPa

Pressure, kPa	Temperature, ℃	Experimental Data		Trend Line	
		Solubility, mol%	Solubility, cm^3/cm^3	Solubility, mol%	Solubility, cm^3/cm^3
7000	40.2	0.1220	8.34	0.1215	8.22
	44.9	0.1157	7.98	0.1158	7.90
	50.2	0.1036	7.23	0.1095	7.54
	55.4	0.1035	7.32	0.1032	7.18
	60.0	0.0967	6.92	0.0977	6.87
	64.9	0.0886	6.44	0.0918	6.54
	64.7	0.0871	6.32	0.0921	6.55
	70.0	0.0865	6.40	0.0857	6.19
	78.5	0.0754	5.78	0.0755	5.61
	80.5	0.0693	5.36	0.0731	5.47

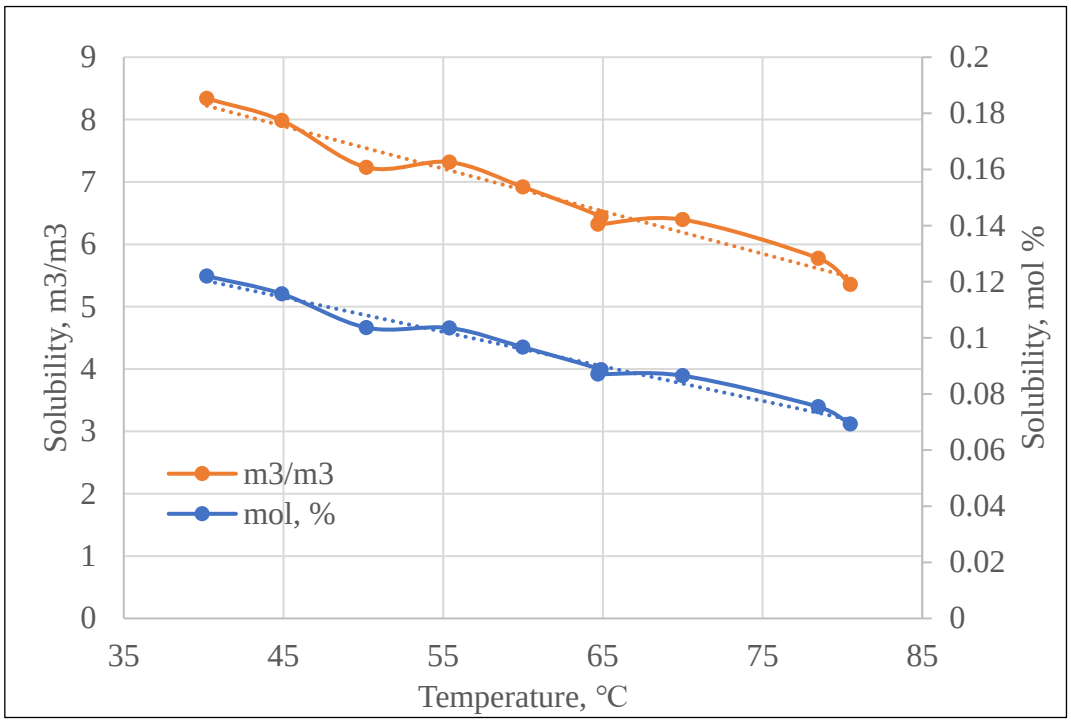

Figure 3.4 Solubility of Nitrogen at 7 MPa

For the second set of the experiments, the temperature is maintained at 55℃, and the pressure is set from 7 to 1 MPa with 1 MPa incremental decrease. The result is shown in Table 3.3 and Figure 3.5. It can be seen in Figure 3.5 that when the temperature is constant, the solubility of nitrogen increases linearly as well with increasing pressure. The experimental data only has a solubility at 6.6 MPa, which is about 6.7 cm^3/cm^3.

Table 3.3 Solubility of Nitrogen at 55 ℃

Temperature, ℃	Pressure, kPa	Experimental Data		Trendline	
		Solubility, mol%	Solubility, cm^3/cm^3	Solubility, mol%	Solubility, cm^3/cm^3
55.5	7164	0.1290	7.31	0.1048	7.61
	6212	0.1177	6.67	0.0953	6.85
	5206	0.1003	5.69	0.0853	6.04
	4144	0.0891	5.05	0.0746	5.19
	3137	0.0729	4.13	0.0646	4.39
	2096	0.0674	3.82	0.0542	3.56
	1172	0.0454	2.57	0.0449	2.82

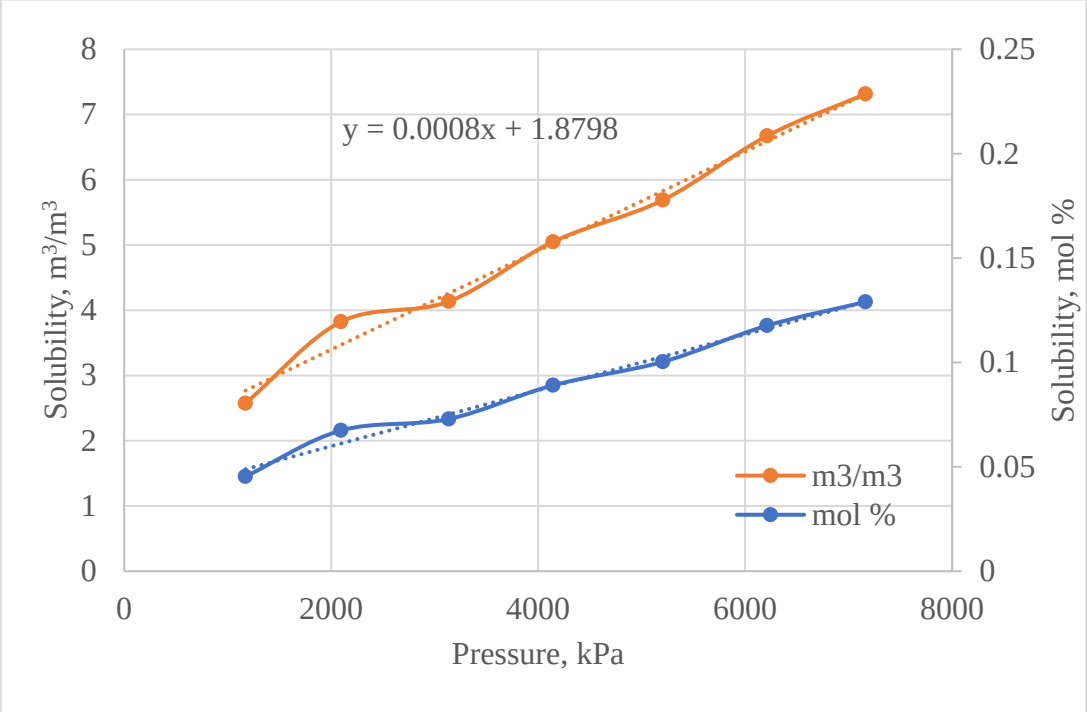

Figure 3.5 Solubility of Nitrogen at 55 ℃

Many researchers have measured the solubility of gases commonly used in CSI. Although the oil samples they used are different from the oil sample used in these experiments, they are also oil samples of heavy oil. Since the viscosity of the oil samples used is close to those that have been studied, the solubility measurement results can be utilized as a basis for comparison. The solubility results are displayed in Table 3.4 below.

Table 3.4 does not contain the solubility of propane and butane because the dew point pressure of these two gases is too low. The dew point pressure of propane at room temperature is 800 kPa, while that of butane is only 400 kPa. This means that the saturation pressure formed by propane and butane is capped at 800 kPa and 400 kPa, respectively. Since this is not within the range of comparison in these experiments, it also does not have the value of discussion.

From Table 3.4, the solubility of carbon dioxide is much higher than the solubility of methane and nitrogen. Although the solubility of nitrogen and methane differs slightly, the solubility of nitrogen is still only about one-half of that of methane. In summary, the solubility of nitrogen in heavy oil is less than that of carbon dioxide and methane.

Table 3.4 Solubility Comparison

Temperature, °C	Pressure, kPa	Solubility, m^3/m^3		
		CO_2 (Mehrotra & Svrcek, 1982)	CH4 (Mehrotra & Svrcek, 1982)	N_2
40	6	37.12		7.31
62	6	28.03		5.91
96.8	6	17.95		3.82
45	7		12.87	7.90
67	7		11.46	6.39
100	7		10.38	4.14

3.5 Chapter Summary

In this chapter, the experiments are conducted in a mercury-free DBR Pressure-Volume-Temperature (PVT) system to measure the solubility of nitrogen. These experiments demonstrated that the solubility of nitrogen is low and does not have the effect of viscosity reduction. Low solubility may result in insufficient gas drive force, but may also increase the stability of the foamy oil. The next chapter will study the phenomenon of foamy oil formed by N_2 and its application in Huff-n-Puff.

CHAPTER 4 PRESSURE DEPLETION TESTS IN 1-D SAND-PACK

4.1 Overview

Foamy oil is a very significant production mechanism in Huff-n-Puff, especially in Cyclic Solvent Injection. The objective of this chapter is to experimentally determine whether the oil saturated with nitrogen can form foamy oil during the pressure depletion process or not. Some researchers have previously observed the phenomenon of foamy oil by conducting pressure depletion tests in the 1-D cylindrical sand-pack model(Wu, 2018; Zhou, Yuan, Zeng, Zhang, & Jiang, 2017). They have demonstrated the method's reliability by studying foamy oil in a 1-D cylindrical sand-pack model and completed the research on carbon dioxide, methane, propane, and other solvents(Peng, 2016; Peng, Zeng, Du, & Yang, 2017). The same method is used to observe the phenomenon of foamy oil in this chapter. In order to compare the results with previous conventional CSI gases, the experiments of forming foamy oil with nitrogen use a 1-D cylindrical model of the same size(Du, Peng, & Zeng, 2018a). This study is aimed at high temperature deep heavy oil reservoirs and assumes a condition of 7 MPa and 50 ℃. The purpose of the study is to discuss the possibility of forming foamy oil under these conditions, so the temperature and viscosity of the crude oil are no longer changing. Another critical factor in forming foamy oil is the pressure decline rate. Thus the experiments in this chapter will be conducted consistently at four different pressure decline rates. Oil samples,

the viscosity of the oil, sand-pack properties are also set to be the same as the study by Wu et al.

4.2 Experimental Material and Apparatuses

4.2.1 Oil Sample

The oil sample used in this chapter is the same one in Chapter 3. This heavy oil sample is first settled to centrifuge at 3000 rpm for 90 minutes to make sure the dead oil sample is free of water. After the dehydration process, the viscosity of the dead oil is measured to be 4,810 cP at 25 °C, and 598 cP at 50 °C.

4.2.2 1-D Cylindrical Sand-pack Model

As shown in Figure 4.1, the experiments are conducted in a 1-D cylindrical sand-pack model. This model has a length of 95 cm and a diameter of 3.8 cm. There are six ports on the sand-pack. The inlet port and the outlet port are on the two sides of the sand-pack. The rest of the four ports are evenly distributed along the sand-pack to measure the pressure. These ports are 21.6 cm apart from each other, and they are all connected to the pressure transducers. The parameters of the dead oil and the 1-D cylindrical sand-pack model are shown in Table 4.1. Nitrogen gas sample is supplied by Praxair Canada Inc. The purity of nitrogen in the tank is higher than 99 %, and the pressure of nitrogen is higher than 14 MPa.

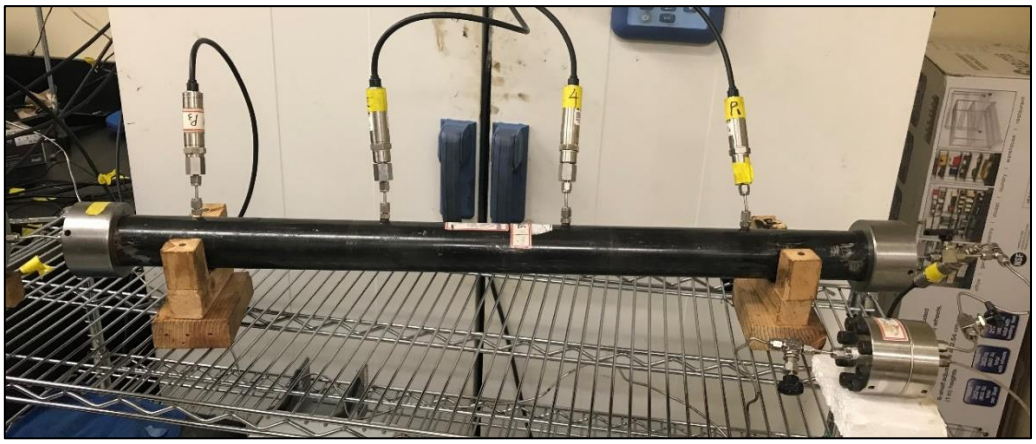

Figure 4.1 1-D Cylindrical Sand-pack Model

Table 4.1 The Parameters of the Dead Oil and the 1-D Cylindrical Sand-pack Model

Oil Density, g/ml	0.9816
Mole Weight, g/mol	389
Mole Volume, ml/mol	396.3
Viscosity@25℃, cP	4810
Viscosity@50℃, cP	598
Compressibility, 1/kPa	5.5×10^{-7}
Viscosity Compressibility coefficient, 1/ MPa	0.031
Length, cm	95
Inner Diameter, cm	3.8
Volume, ml	1076.86
Cross-sectional Area, cm^2	11.33

4.3 Experimental Procedure

4.3.1 Sand-pack Model Preparation

Since the 1-D cylindrical model used in these experiments is previously used in other experiments, there are leftover sand and crude oil. In order to ensure the accuracy of the experiments, the 1-D cylindrical model must be carefully cleaned before starting the experiments. The model is immersed in toluene, kerosene, and ethanol in sequence until thoroughly cleaned.

In these tests, a kind of liquid electrical tape (Brush-on Electrical Tape) is treated as the coating. This electrical tape is unevenly applied to the inner wall of the model to create a rough and soft surface. This allows sand to be embedded in this surface, thus avoiding the wall effect.

The six ports are welded to a metal filter. The density of the metal filter is 400 mesh, which is large enough to prevent sand production during the experiments. Then the Swagelok fittings are assembled on all ports except the inlet port on the model.

Place the model vertically on the ground and bundle it with the vibrator. This vibrator is driven by an air flow, which is enough to cause the model to vibrate so that the sand is evenly distributed in the model during the sand packing process. Because of pollution and health problems, these experiments used glass beads with a diameter between 90 and 150 μm, instead of real sand, to create the porous media. Pour the glass beads into the model at a very slow rate while adjusting the vibrator to the maximum frequency. When the sand fills the

model evenly and tightly, assemble the Swagelok fitting welded with the filter mesh on the inlet ports on the model. Finally, connect all ports to the pressure transducers. The working range of the pressure transducers is up to 350 bar (35 MPa). Pressure data is read by a computer and automatically recorded. The prepared 1-D cylindrical sand-pack model is shown in Figure 4.2.

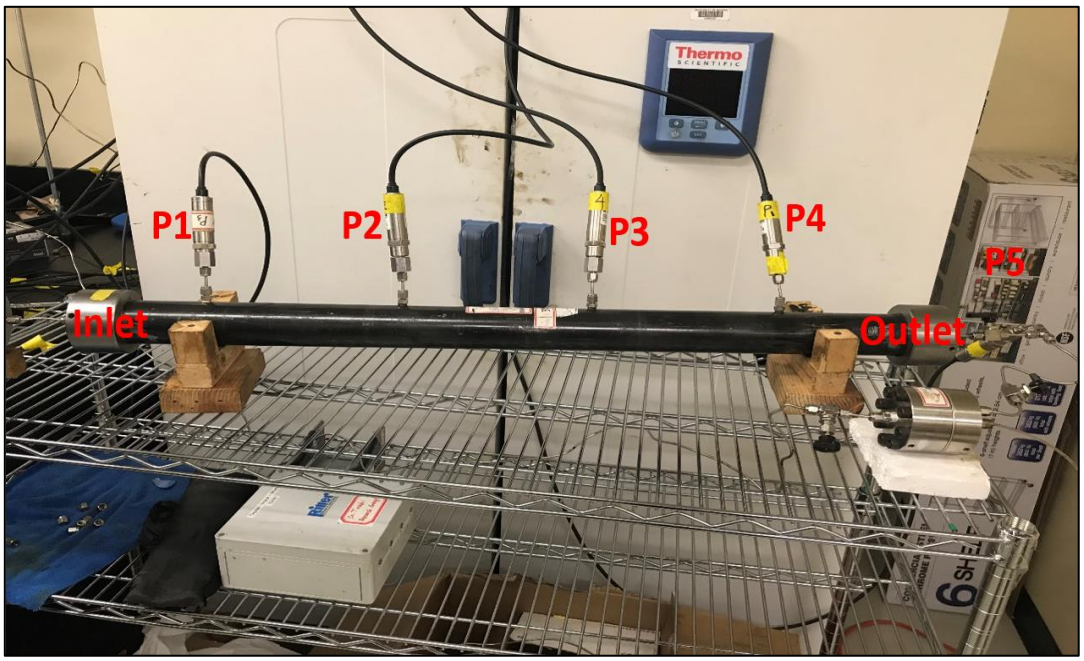

Figure 4.2 Distribution of Inlet/Outlet Port and Pressure Points

4.3.2 Experimental System Setup

The illustration of the experimental device set-up is shown in Figure 4.3. Two transfer cylinders are connected to the inlet end of the model. These two transfer cylinders are filled with gaseous nitrogen and live oil, respectively. The inner pressure or the flow rates of these two cylinders are controlled by a syringe pump. Both of the two transfer cylinders and the 1-D model are placed in an oven. The temperature of the oven is set at 50 ℃ to simulate the high-temperature formation environment. One back pressure regulator is connected to the outlet end of the model, and its role is to control the pressure at the outlet. The syringe pump regulates the pressure of BPR. The outlet end of the BPR is connected to a production system, which consists of a digital scale and a gas flowmeter. This production system is used to measure oil production and gas production. The pressure transducers and the gas flow meter are all directly connected to the computer to record the readings automatically. The digital scale readings are recorded by the camera.

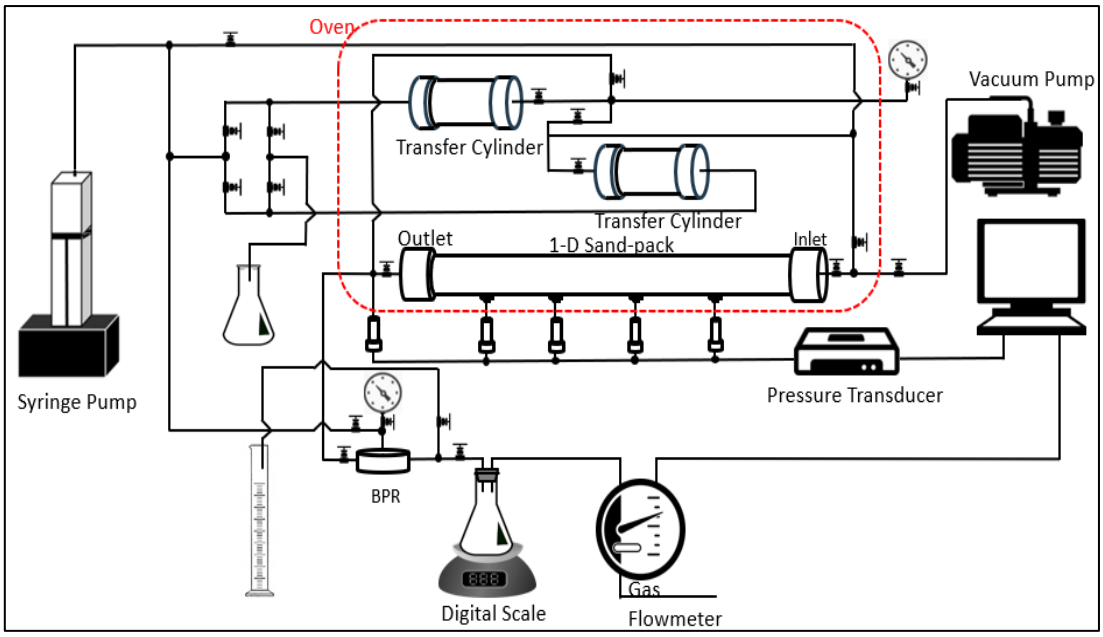

Figure 4.3 Illustration of the Experimental Device System

4.3.3 Leaking Tests

Pressure depletion tests require a high degree of pressure control. The interior of the experimental system needs to be completely isolated from the outside. Therefore, leak tests are required before the start of the experiments to ensure that the entire experimental system is sealed.

After setting up the experimental system, nitrogen is injected into the model from the inlet port, and the model is sealed by BPR at the outlet port. The maximum pressure for the ideal conditions of the experiments is 7 MPa. In order to be safe, the leak pressure needs to be higher than 7 MPa. In these tests, nitrogen is injected into the model to increase the pressure to 7.5 MPa, and the pressure of BPR is set at 8 MPa to seal the model. After the sand-pack model is pressurized, observe the reading on the pressure gauge. If the pressure drop is less than 5 kPa in 24 hours, the whole system is considered to be sealed. Otherwise, apply a soapy liquid leak detector (FORMULA 365) to each of the connectors to check for air bubbles. The connectors where the bubbles are generated need to be reconnected until the pressure drop is less than 5 kPa within 24 hours. After that, the whole experimental system in pressure depletion tests is considered as a leak-free system.

It is worth noting that water and carbon dioxide cannot be injected into the experimental system during the leaking tests process. Water is very sensitive to temperature. If water is used as a leak test fluid, a slight temperature change can cause pressure fluctuations in the model. Carbon dioxide as a corrosive gas also cannot be used for leaking tests. The two caps

at both ends of the model and the pistons in the transfer cylinders are sealed by rubber O-rings, placing them in a carbon dioxide environment will reduce their service life.

4.3.4 Pore Volume Measurement

The pore volume of the model is measured by injecting water into the model, and once the water fills the entire pore space, the amount of water injected is equal to the pore volume. Injecting water directly into the model does not guarantee that the water will fill all the pores. It is necessary to vacuum the model first before drawing water into each pore. Hence, the outlet port of the model is first closed, and then the vacuum pump is connected to the inlet port. The whole leak-free sand-pack model system is vacuumized for 4 hours until all gases are removed from the sand-pack model, and the inner pressure of the model becomes stable. The pressure inside the model after this process will usually remain at around -94 kPa.

A measuring cylinder with water is connected to the inlet port of the model. Water will be sucked into the sand-pack model by the pressure difference between the negative inner pressure of the sand-pack model and the atmospheric pressure. When the pressure in the model reaches atmospheric pressure and the model no longer draws in water, the amount of water drawn in the model is measured by the measuring cylinder.

The outlet port is opened and connected to an empty measuring cylinder. Deionized water is injected into the sand-pack model from the inlet port of the model by a syringe pump until the amount of water injected exceeds 1.5 PV. Record the amount of water injected, and the amount of water discharged in the measuring cylinder. Hence, the amount of water

saturated in the model is equal to the amount of water drawn in plus the amount of water injected then minus the amount of water discharged. Finally, the amount of water saturated in the model is the pore volume of the model. The porosity is calculated as:

$$\emptyset = \frac{V_{water}}{V_{bulk}}$$

where $\emptyset$ is the porosity of the sand-pack model, %; V_{water} is the volume of water saturated in the model, cm^3; V_{bulk} is the bulk volume of the sand-pack model, cm^3.

The details of the porosity measurement are listed in Table 4.2.

Table 4.2 Porosity Measurement

Diameter, cm	3.80
Cross-sectional Area, cm^2	11.34
Length, cm	95.00
Bulk Volume, cm^3	1077.41
Inhaled Water, cm^3	370.50
Injected Water, cm^3	600.00
Discharged Water, cm^3	593.50
Saturated Water, cm^3	377.00
Porosity, %	34.99

4.3.5 Absolute Permeability Measurement

Using Darcy's law, the absolute permeability is calculated as shown in Equation 4.1.

$$K = -\frac{Q\mu}{A}\frac{\triangle L}{\triangle p} \tag{4.1}$$

Where Q is the rate of fluid flowing, cm^3/s; K is the permeability, Darcy's; μ is the viscosity of the flowing fluid, cP; A is the cross-sectional area across which flow occurs, cm^2; dp/dl is the pressure drop per unit length, atm/cm.

The length of the model is 95 cm, and the diameter is 3.8cm. Permeability needs to be calibrated using a fluid with a known viscosity. In these experiments, the accuracy of measuring absolute permeability does not need to be too high. Therefore, using water as a standard can meet the measurement needs.

After the porosity measurement, the model is saturated with water. A fixed flow rate is set to allow water to flow through the model. Once the pressure stabilizes at the inlet and outlet ends (this process usually lasts 10 minutes), the flow rate on the pump and the pressure readings at both ends are recorded. The flow rate is set from 2 to 20 ml/min with 2 ml/min incremental increase.

When flow rates fall below 20 ml per minute, water behaves as a laminar flow through the porous media in the model (Wu, 2018). Therefore, Darcy's law is available in this range. The details of the permeability measurement are shown in Figure 4.4 and Table 4.3, and the results are revealed in Table 4.4

Table 4.3 Permeability Measurement

P1, kPa	P2, kPa	△P, kPa	Q, cm^3/min
4.6	1.2	3.4	2
9.4	1.4	8	4
13.1	1.6	11.5	6
17.1	1.8	15.3	8
21.9	2	19.9	10
25.7	2.3	23.4	12
31.4	2.5	28.9	14
36.5	2.9	33.6	16
41	3	38	18
47	3.4	43.6	20

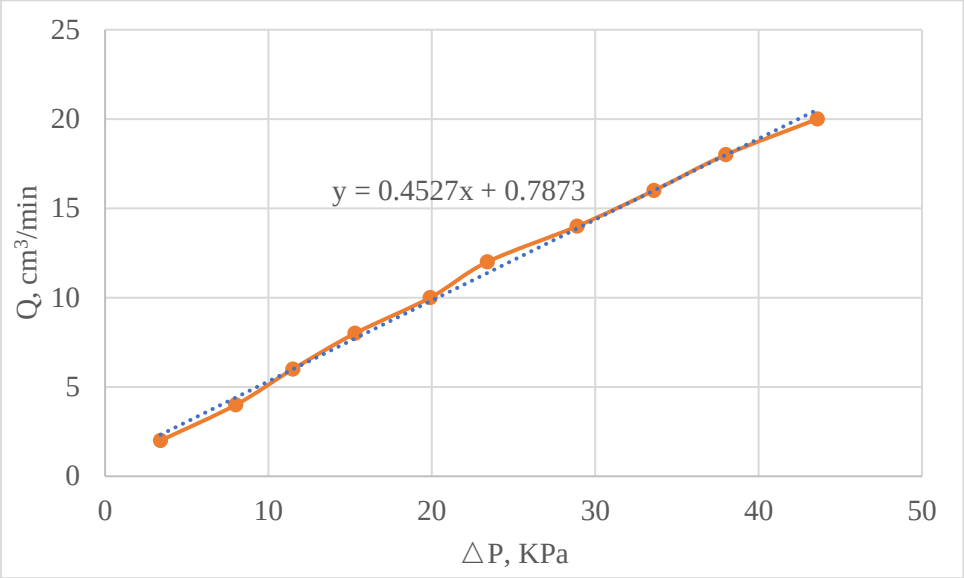

Figure 4.4 Permeability Measurement

Table 4.4 Permeability of the Sand-pack Model

Diameter, cm	3.8
Cross-sectional Area, cm^2	11.34
Length, cm	95
Viscosity, cP	1
$\triangle q/\triangle p$, $cm^3/min \cdot kPa$	0.45
Permeability, Darcy	6.32

4.3.6 Live Oil Preparation

The process of preparing the live oil is to inject a certain proportion of dead oil and nitrogen into the same transfer cylinder while maintaining high pressure. The transfer cylinder is then fixed on a rotating machine for two days. The rotation process is to ensure full contact between nitrogen and the dead oil until nitrogen is completely dissolved in the oil. The rotary is shown in Figure 4.5.

In the pressure depletion experiments, it is assumed that the initial conditions of the reservoir are at 50 °C and 7 MPa. In order to ensure single-phase flow in the first stage of the experiments, the saturation pressure of the prepared live oil must be less than 7 MPa. It is required to prepare a live oil with a saturation pressure of 6 MPa at 50 °C. From the data of the previous experiment, the solubility of nitrogen is 6.9 cm^3/cm^3 at 50 ℃ and 6 MPa. Thus, the live oil with a saturation pressure of 6 MPa at 50 ℃ requires 900 ml of dead oil and 6,750 ml of nitrogen at room temperature and pressure.

Figure 4.5 Live Oil Rotary

4.3.7 Live Oil Saturation and Initial Oil/Water Saturation Measurements

After the above process, the 1-D cylindrical sand-pack model is completely saturated with water. In the live oil saturation process, water is first injected into the 1-D cylindrical sand-pack model. The pressure on the BPR is set at 7.5 MPa, making the pressure in the whole system higher than 7 MPa. This process is to prevent the live oil from releasing nitrogen during the live oil injection process. Then, the outlet of the BPR is connected to an empty measuring cylinder, and live oil is injected into the model with a very slow flow rate. The pressure of BPR is maintained at 7.5 MPa at the beginning and reduced to 7 MPa at the end of the saturation process. The only possible way to saturate the model with live oil is to choose a very low flow rate for live oil injection. In these tests, the flow rate of 0.03 ml/min is selected. The live oil volume needed for injection is 1.5 times of the pore volume (PV) to ensure the model is well saturated with live oil (Zhou, 2015).

After the sand-pack model is saturated with live oil, the discharged water, which is measured by the measuring cylinder, equals the volume of the injected live oil. The residual water is equal to the saturated water minus the amount of discharged water. So that the initial oil saturation and initial water saturation is determined by:

$$s_{oi} = \frac{V_{wd}}{V_{pore}} \tag{4.2}$$

$$s_{wi} = 1 - \frac{V_{wp}}{V_{pore}} \tag{4.3}$$

where s_{oi} is the initial oil saturation of the sand-pack model; s_{wi} is the initial water saturation of the sand-pack model; V_{wd} is the volume of the discharged water; V_{pore} is the pore volume of the sand-pack model.

The initial oil saturation and the initial water saturation of the sand-pack model are 93% and 7%, respectively. Finally, the complete parameters of the 1-D cylindrical sand-pack model in pressure depletion tests are shown in Table 4.5.

Table 4.5 Parameters of the 1-D Cylindrical Sand-pack Model

Diameter, cm	3.80
Cross-sectional Area, cm^2	11.34
Length, cm	95.00
Bulk Volume, cm^3	1077.41
Pore Volume, cm^3	377.00
Porosity, %	34.99
Permeability, Darcy	6.32
Initial Oil Saturation, %	93
Initial Water Saturation, %	7

4.3.8 Live Oil Viscosity Measurement

Maintain BPR pressure at 7.5 MPa, live oil is continuously injected into the model. A fixed flow rate is set to allow live oil to flow through the model. Once the pressure at the inlet and outlet ends stabilizes (this process usually lasts for about 10 minutes), the flow rate on the pump and the pressure readings at both ends are recorded. The flow rate is set from 2 to 20 ml/min with 2 ml/min incremental increase.

Finally, the viscosity of this live oil at 50 ℃ and 7 MPa is calculated by Darcy's equation, as shown in Equation 4.1. Since the subsequent experiments are conducted at 50 ℃, the viscosity of the live oil measured in these experiments is only at 50 ℃. The viscosity of dead oil and live oil at 50 ℃ is 598 cP and 575 cP, respectively. This shows that there is no noticeable viscosity reduction after the nitrogen is dissolved in the heavy oil. Since the solubility of nitrogen has been previously demonstrated to be low, the small amount of nitrogen dissolved in the heavy oil is not sufficient to make a significant change in the viscosity of the heavy oil.

4.3.9 Pressure Depletion Tests

After completing all preparations, the experiments may begin. In this step, except for the inlet port, all other ports are opened. The initial pressure inside the model is set to 7 MPa, and so is the pressure of the BPR. Oil is produced with depletion back pressure under different constant pressure decline rates, which is controlled by the syringe pump. The outlet end of

the BPR is connected to a production system, which consists of a digital scale and a gas flowmeter. This production system is used to measure oil production and gas production.

In Zhou's study (Zhou, 2015), the best pressure decline rate in terms of oil recovery factor and gas recovery for heavy oil-methane, heavy oil-propane and heavy oil-mixture gas system is 2 kPa/min. Therefore, the pressure decline rates in these tests start from 2 kPa/min to verify whether the heavy oil-nitrogen system can form foamy oil or not. Then the pressure decline rate is changed to find the best condition to form the foamy oil.

4.4 Results and Discussion

4.4.1 Overview

The oil recovery factor of the four experiments in these tests is listed in Table 4.6. Figure 4.6 shows the cumulative oil production of the four pressure decline rate as a function of the dimensionless time, which is defined as T/Tt. Tt is the total experimental production time of each pressure decline rate. Based on the oil recovery and gas recovery data, it can be concluded that the higher the pressure decline rate, the greater the oil recovery factor.

Table 4.6 Oil/Gas Recovery Factor

Pressure Decline Rate, kPa/min	Cumulative Oil Production, g	Cumulative Gas Production, cm^3	Oil Recovery Factor, %	Gas Recovery Factor, %	Cumulative Gas/Oil Ratio, m^3/m^3
2	46.8	2042.5	12.88	91.97	42.84
8	61.4	1915	16.9	86.23	30.62
16	90.6	1665	24.94	74.97	18.04
32	117.6	1465	32.37	65.97	12.23

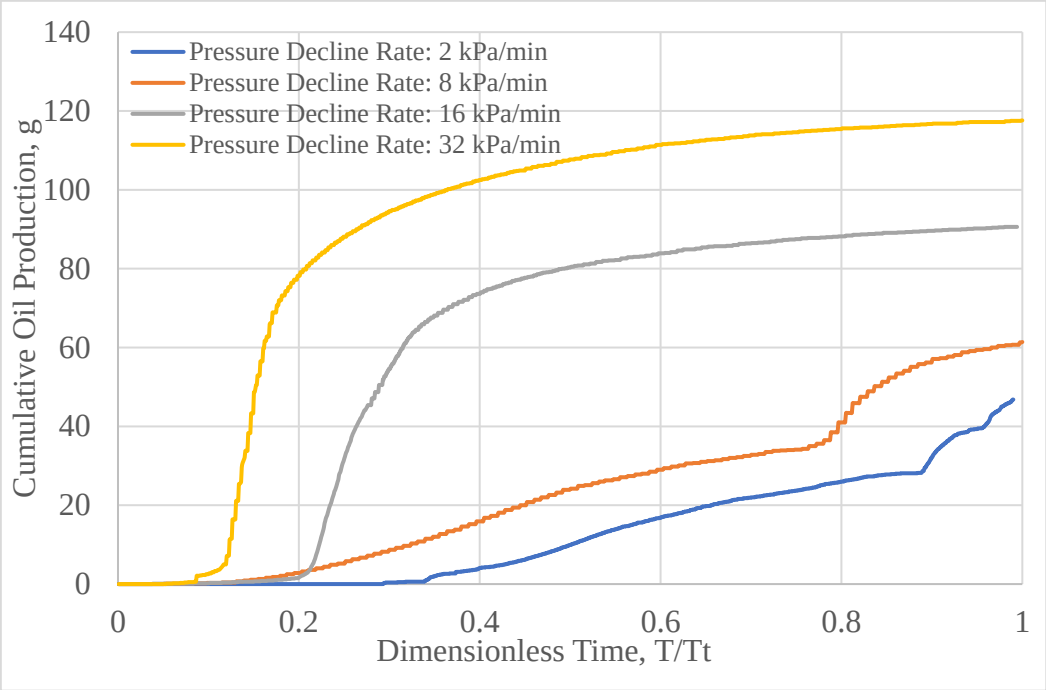

Figure 4.6 Cumulative Oil Production

4.4.2 Oil/Gas Production

The oil production performance behaves differently in all four experiments. Based on the shapes of the oil production curves in Figure 4.6, the four sets of experiments can be divided into two groups. Pressure decline rates of 2 and 8 kPa/min are grouped together, and pressure decline rate of 16 and 32 kPa/min are grouped together. In the experiments of 2 and 8 kPa/min, there is no oil production at the beginning of the experiments, and oil production stays as low as zero. Then, the oil production rates start to increase at the end of the beginning period. During this period, the oil recovery curves show straight lines, which means the oil production rates are constant. After these regions, there is a rapid increase in oil production until the end of these two experiments. In the latter two experiments with pressure decline rates of 16 and 32 kPa/min, there is also no oil production at the beginning. However, this is followed by a period of high-rate production. In this production period, oil production performs like foamy oil flow behavior where the oil production rate is maintained at a very high speed. After that, the oil production rate slowly decreases with time until approaching zero at the end of the experiments.

Pressure decline rate: 2 kPa/min

Figure 4.7 is the cumulative oil production curve and the inner pressure curves as a function of time elapsed in the experiment with the pressure decline rate of 2 kPa/min. In the first 1,000 minutes, no oil is produced in this region. The reason for this phenomenon is that during this period, the inner pressure of the model is high than bubble point pressure (6000 kPa). Since nitrogen has not been released from the crude oil during this process, the fluid in

the model remains as a single-phase flow. The driven force of the fluid is mainly derived from the elastic expansion of the saturated live oil. However, the volume expansion of crude oil is very small. The volumetric expansion of crude oil is negligible compared to the internal volume of the 1-D sand-pack model and the empty volume in the production tube. Therefore, in the first period of this region, no oil is produced from the sand-pack model. This production stage is considered as oil single-phase flow region (Zhou, 2015). Then, gas starts to produce, but there is still no oil production. In this period, the pressure in the model is lower than the bubble point pressure, and nitrogen begins to be released from the oil. However, because of the slow pressure decline rate, the solution gas drive is not enough to displace the oil. At this stage, there is only gas production and no oil production. So, this stage is considered to be a gas single-phase flow region. These two stages together are considered as the single-phase flow region.

When the outlet port pressure is less than 5,500 kPa, oil begins to be produced from the model. For a long time after this, the rate of oil production remains at a relatively stable level. The cumulative oil production curve of this stage is like a straight line. This production curve is very similar to the curve from the conventional solution gas drive flow (Wu, 2018). Since the experiment is conducted at a high temperature of 50 ℃, the viscosity of the live oil is only 575 cP, and the pressure decline rate is very slow, the small bubbles released from the crude oil are separated from the oil when they are too late to gather and form a weak two-phase flow. Consequently, this stage is considered as a weak two-phase flow region. But it is

worth noting that although at this stage, conventional solution gas drive is dominant, foamy oil flow also exists.

When this experiment runs to 53 hours, and the pressure drops to about 400 kPa, there is a sudden increase in oil production rate. In this region, small bubbles begin to aggregate toward the nucleated bubbles and form a slightly larger bubble before they are separated from the oil. Since there is large capillary force due to the high viscosity of the heavy oil, these bubbles are trapped in the heavy oil. Because of the large volume of gas bubbles, oil-gas foamy flow volume is expanded rapidly. Foamy oil flow is a dynamic process. When the foam is large enough, it will separate from the crude oil and form a conventional solution gas drive flow. Since oil production is mainly derived from foamy oil flow, the oil production rate at this stage is very high, and it is considered to be the foamy oil flow region or active two-phase flow region. Many researchers found similar curve feature in their studies(Wu, 2018; Y. Zhang, 1999). Zhang didn't explain the reason, and Ming believes that this is due to the fact that after the gas is released from the oil, the viscosity of the oil rises sharply, causing the gas to be trapped in the oil to form a foamy oil. However, it was determined that the viscosity of the nitrogen-saturated live oil is only 25 cP lower than the viscosity of the dead oil at 50 ℃. Therefore, it is unreasonable to attribute the increase in foamy oil to the increase in viscosity of crude oil. Rather, the most likely reason is that the bubbles trapped in the oil become larger and larger as the pressure decreases. After reaching a certain level, the flow of foamy oil suddenly increased.

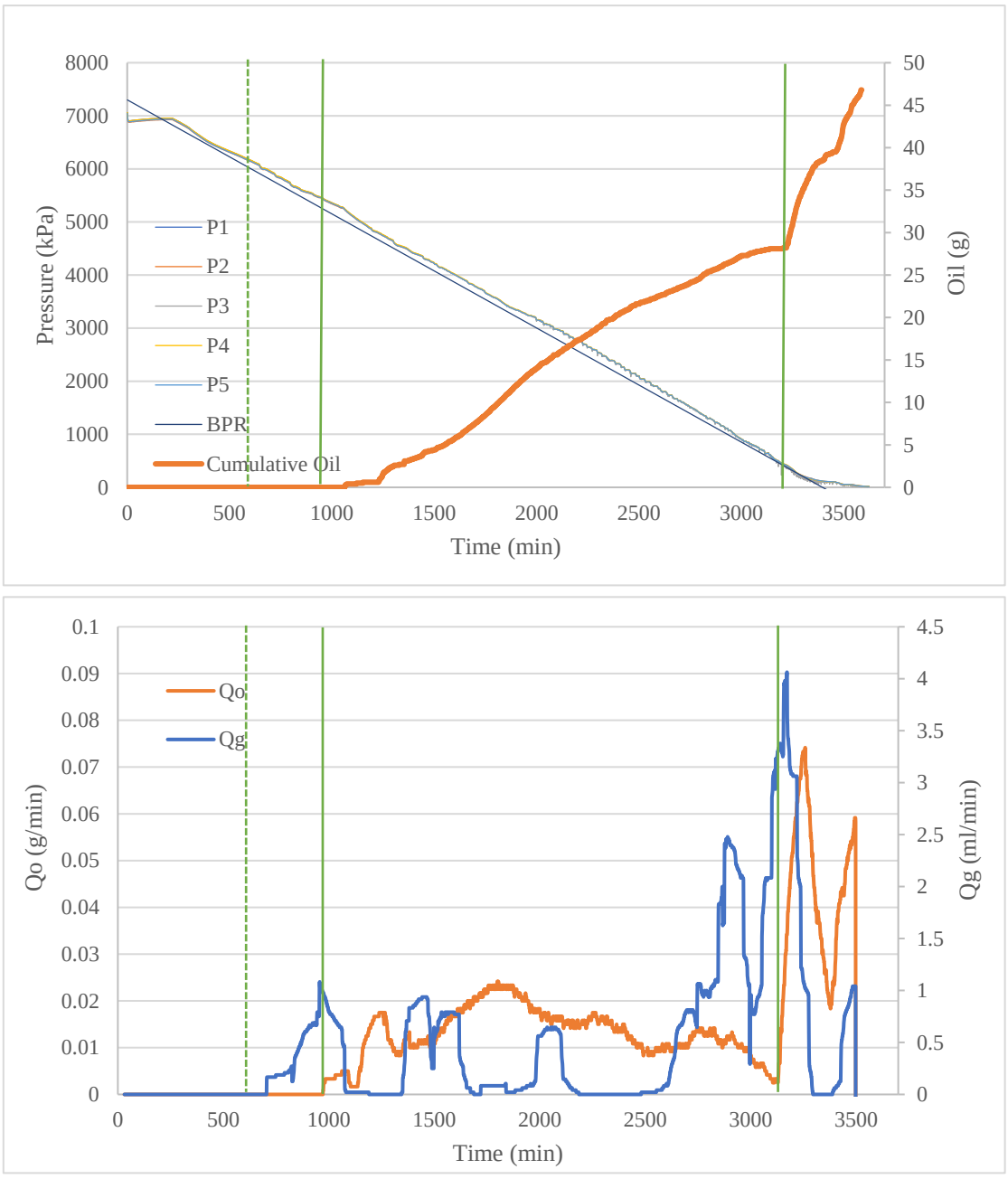

Figure 4.7 Cumulative oil production, Oil/Gas Production Rate, and the Inner Pressure Curves with Pressure Decline Rater of 2 kPa/min

Pressure decline rate: 8 kPa/min

When the pressure decline rate is 8 kPa/min, the single-phase flow region becomes narrower. Under this pressure decline rate, gas single-phase flow stage does not exist. The release rate of nitrogen is fast enough that the solution gas drive is sufficient to displace the oil. This pressure decline rate allows the weak two-phase flow region to begin directly after the oil single-phase flow region.

In the weak two-phase flow region, the oil production rate first rises slowly, and then drops slowly after reaching the apex, as shown in Figure 4.8. The gas production rate has been rising steadily. This form of oil production and gas production is the same as the trend when the pressure decline rate is 2 kPa/min. The weak two-phase flow region of the two experiments with pressure decline rates of 2 and 8 kPa/min have the same slope in Figure 4.6. Since the abscissa is dimensionless time, the same slope indicates that the average oil production per unit pressure depletion is the same which is approximately 0.00625 g/kPa (6.25 kg/ MPa). In other words, even if the pressure decline rate is increased by 4 times, the oil production per unit pressure depletion will not increase, but the gas production will increase significantly. This shows that there is an upper limit to the ability of conventional solution gas drive to displace heavy oil. After reaching the upper limit, the increase in pressure decline rate will only increase gas production. Thus, in the stage of the weak two-phase flow, the maximum oil production per unit pressure depletion is about 0.0625 g/kPa. (10 kg/ MPa). At this weak two-phase flow stage, experiments with pressure decline rates of 2 and 8 kPa/min produced 28.8 g and 32.8 g of oil, respectively. For the test with the pressure

decline rate of 2 kPa/min, since there is a gas single-phase flow region in the early stage of the weak two-phase flow, and if the effect of the foamy oil is removed, there would be minimal production difference in the weak two-phase flow region. From this, the limit of oil production from conventional solution gas drive is approximately 30 g.

When this experiment runs to 13 hours, and the pressure drops to about 600 kPa, a sudden increase in oil production rate exists. The characteristics of this active two-phase flow region are similar to those of the pressure decline rate of 2 kPa/min. In the experiment with a pressure decline rate of 2 kPa/min, the oil production curve fluctuates, indicating that the foamy oil produced is unstable. The oil production in the active two-phase flow region is 18.6 g. However, in the experiment with a pressure decline rate of 8 kPa/min, the oil production curve is very smooth, indicating that the foamy oil produced is stable. Here the oil production in the active two-phase flow region is 27.5 g. This shows that compared to the pressure decline rate of 2 kPa/min, the pressure decline rate of 8 kPa/min can produce a more stable foamy oil flow.

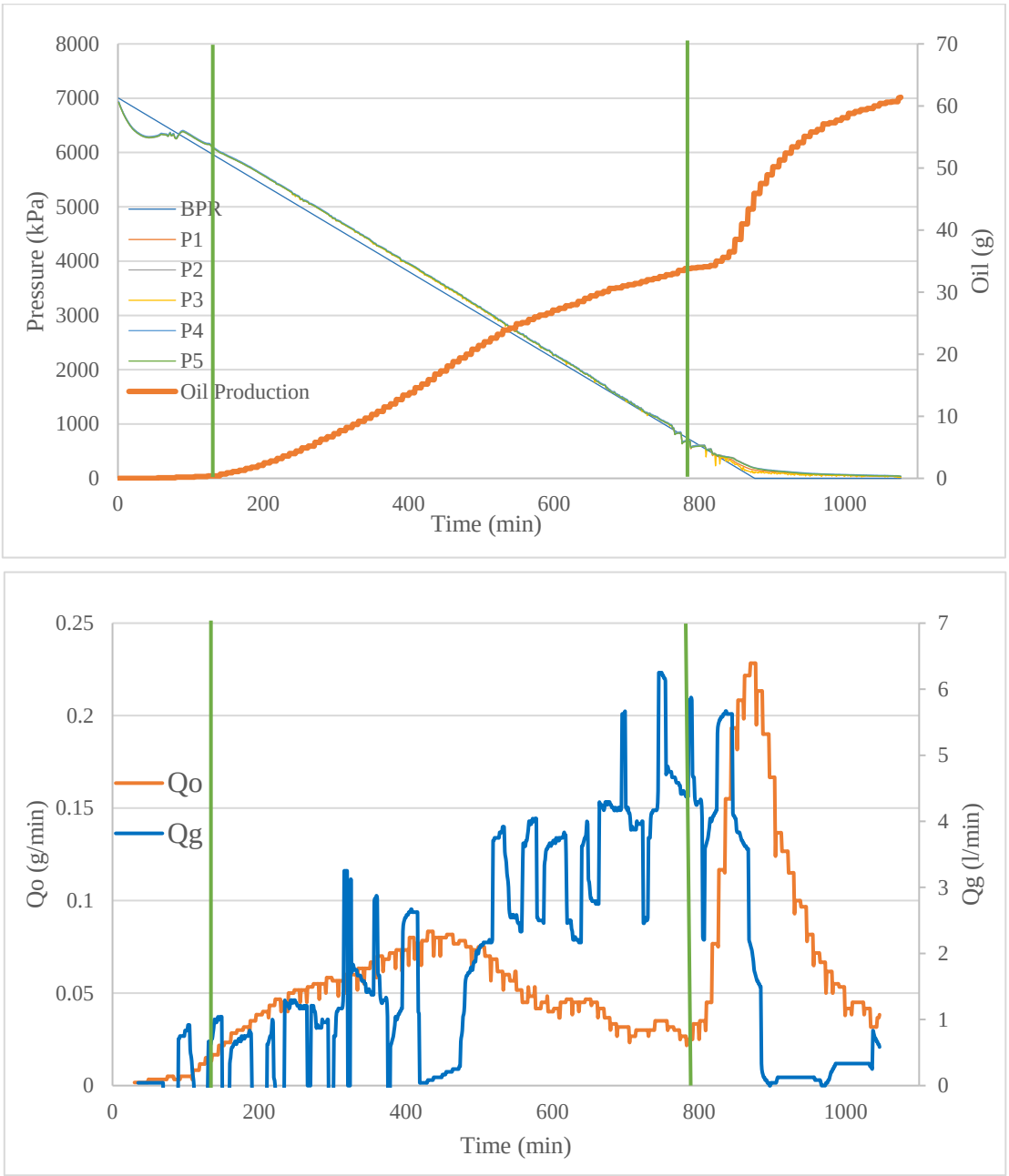

Figure 4.8 Cumulative oil production, Oil/Gas Production Rate, and the Inner Pressure Curves with Pressure Decline Rater of 8 kPa/min

Pressure decline rate: 16 kPa/min

Figure 4.9 shows the cumulative oil production curve and the inner pressure curves as a function of time elapsed in the experiment with a pressure decline rate of 16 kPa/min. When the pressure is higher than the bubble point, the oil production and gas production characteristics are the same as the experiment with a pressure decline rate of 8 kPa/min. However, when the pressure drops below the bubble point pressure, nitrogen begins to be released from the oil. In this stage, the oil and gas production rate are very low since the nitrogen bubbles are trapped in the high viscosity oil and the bubble size is so small that it is negligible. Despite of this low production rate, the gas molecules start to nucleate in this flow region.

When this experiment runs to 4.6 hours, and the pressure drops to about 2,600 kPa, there is a sudden increase in oil production rate. From here on, foamy oil begins to produce. In this region, small bubbles begin to aggregate toward the nucleated bubbles and form a slightly larger bubble before they are separated from the oil. In this active two-phase region, a total of 66.2 g of oil is produced. It can be seen from Figure 4.9 that the gas production characteristics at this stage are very consistent with the production characteristics of the foamy oil. This stage is maintained until the pressure at the outlet port of the sand-pack model drops to atmospheric pressure.

When the pressure at the outlet of the model drops to atmospheric pressure, there is still some pressure inside the model. This shows that the previously dissolved nitrogen has not been completely released from the oil, and the remaining small amount of nitrogen is still

being released slowly. However, since only a small amount of nitrogen remains, and the gas release rate is very slow, it is insufficient to form foamy oil flow. This stage is mainly dominated by conventional solution gas drive, and it lasts nearly two-thirds of the total production time with a total production of 23 g of oil.

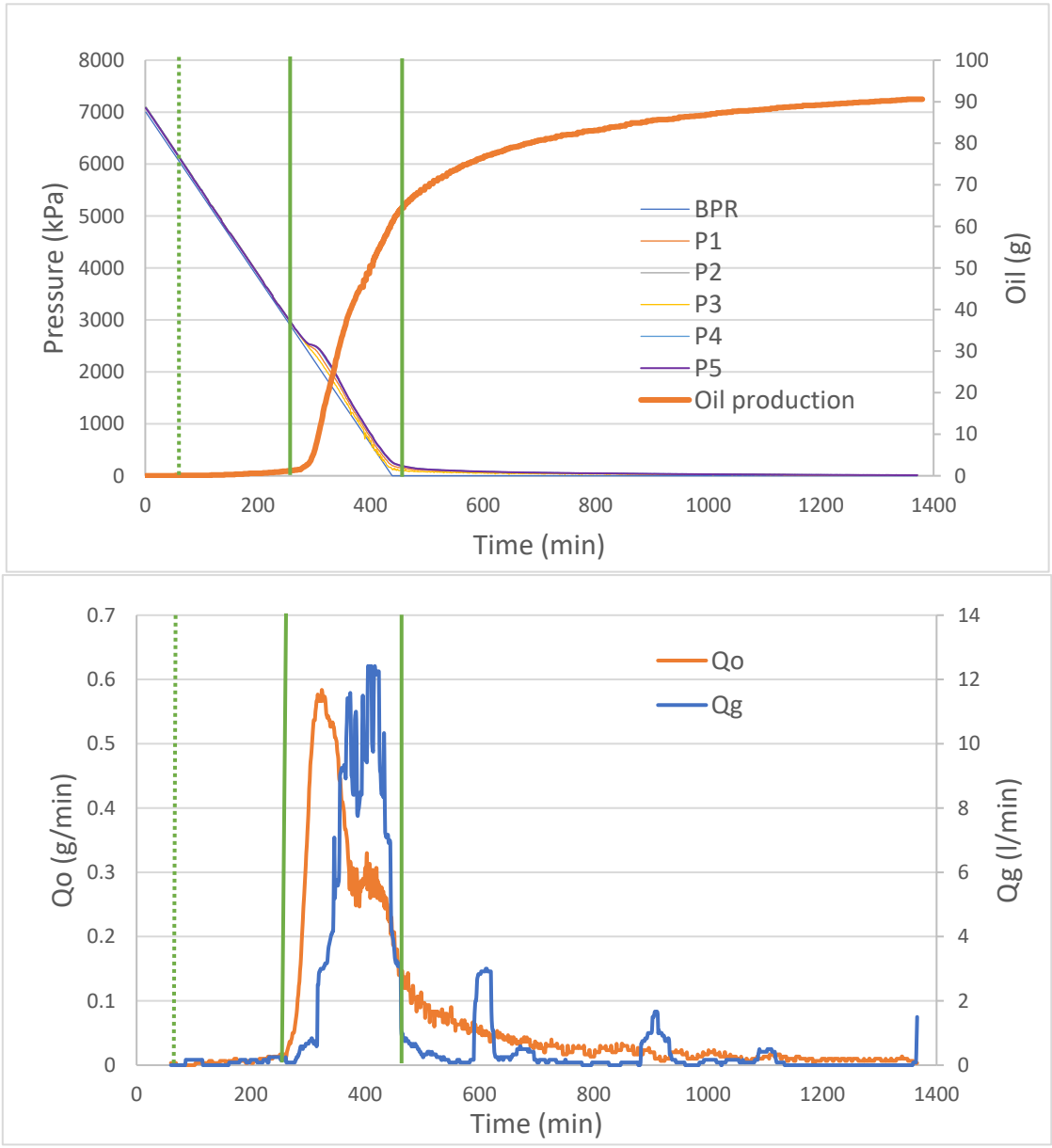

Figure 4.9 Cumulative oil production, Oil/Gas Production Rate, and the Inner Pressure Curves with Pressure Decline Rater of 16 kPa/min

Pressure decline rate: 32 kPa/min

The production curve characteristic of the experiment with a pressure decline rate of 32 kPa/min is very similar to the pressure decline rate of 16 kPa/min. The difference being more oil is produced during the active two-phase flow region (71.6 g). As the pressure decline rate increases, more nitrogen remains in the oil after the end of the active two-phase flow region. This allows the weak two-phase flow to be maintained for a longer period of time and produces more oil (45.6 g).

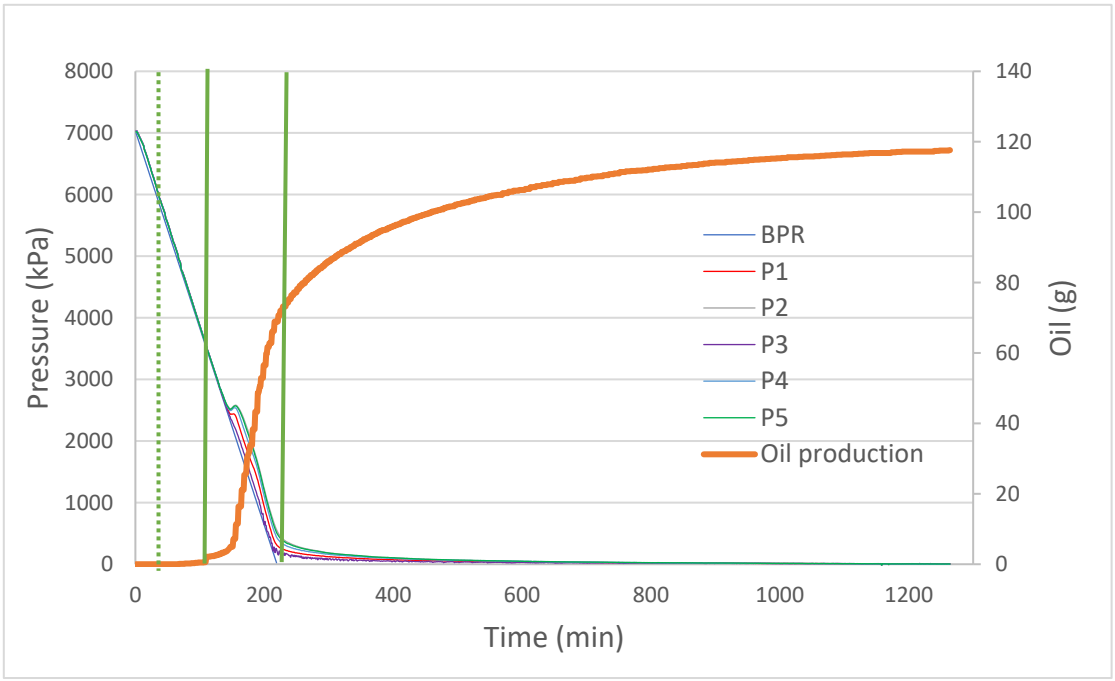

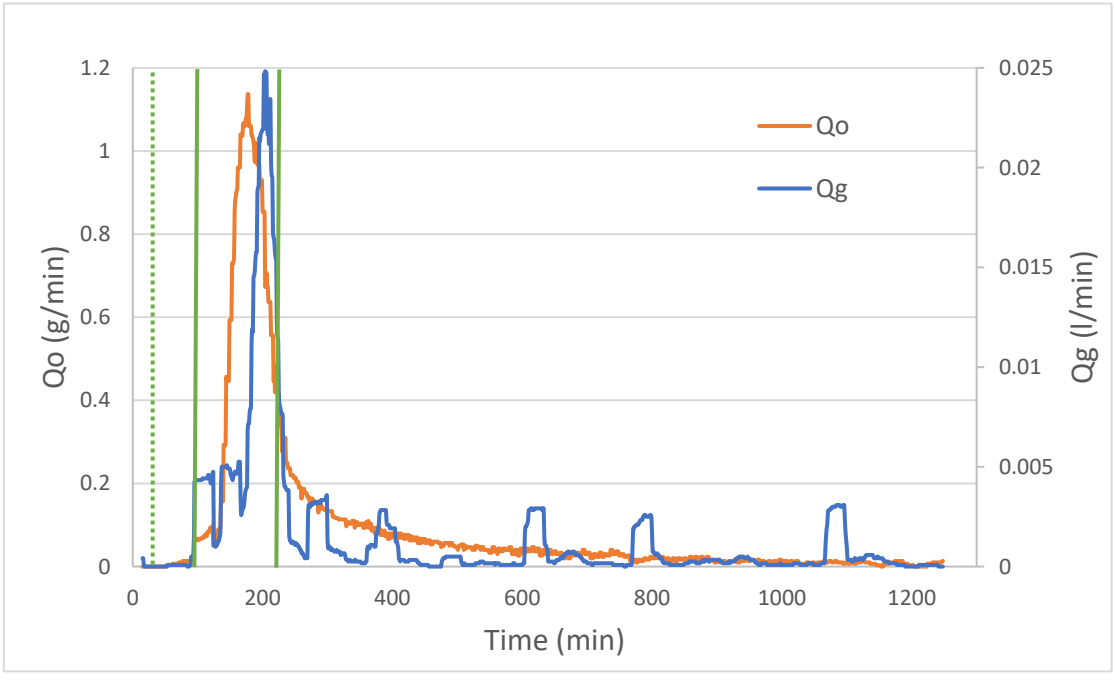

Figure 4.10 Cumulative oil production, Oil/Gas Production Rate, and the Inner Pressure Curves with Pressure Decline Rater of 32 kPa/min

Table 4.7 shows the oil recovery factor of each part of the flow region in each of the four experiments. The oil production of single-phase flow is too small to discover any trends. The causes of weak two-phase flow in the low pressure decline rates differ from the causes of conventional solution gas drive in the high pressure decline rates. In the weak two-phase flow region, there is a tendency for the recovery factor to increase as the pressure decline rate increases. In the active two-phase flow region, as the pressure decline rate increases, the oil recovery rate increases significantly. This shows that the higher the pressure decline rate, the stronger the foamy oil can be formed.

Table 4.7 Oil Recovery Factor of Each Experiment.

Pressure Decline Rate, kPa/min	Oil Recovery Factor, %			
	Single-Phase Flow	Weak Two-phase Flow	Active Two-phase Flow	Total
2	0.00	7.76	5.12	12.88
8	0.11	9.22	7.57	16.90
16	0.39	6.33	18.22	24.94
32	0.11	12.55	19.71	32.37

4.4.3 Pressure Analysis

In this study, the pressure data is more reflective for the characteristics of the flow state. The distribution of pressure points is shown in Figure 4.11. This section will include four experiments that compare the difference in pressure between P5-P1, P5-P2, P5-P3, and P5-P4, and analyze the pressure changes in the various flow regions. The pressure transducer at P1 shows the pressure at the outlet port outside the model, which is also the pressure of the BPR. The pressure transducers from P2 to P5 shows the pressure of the four ports in the model, which are evenly distributed from the outlet port to the inlet port.

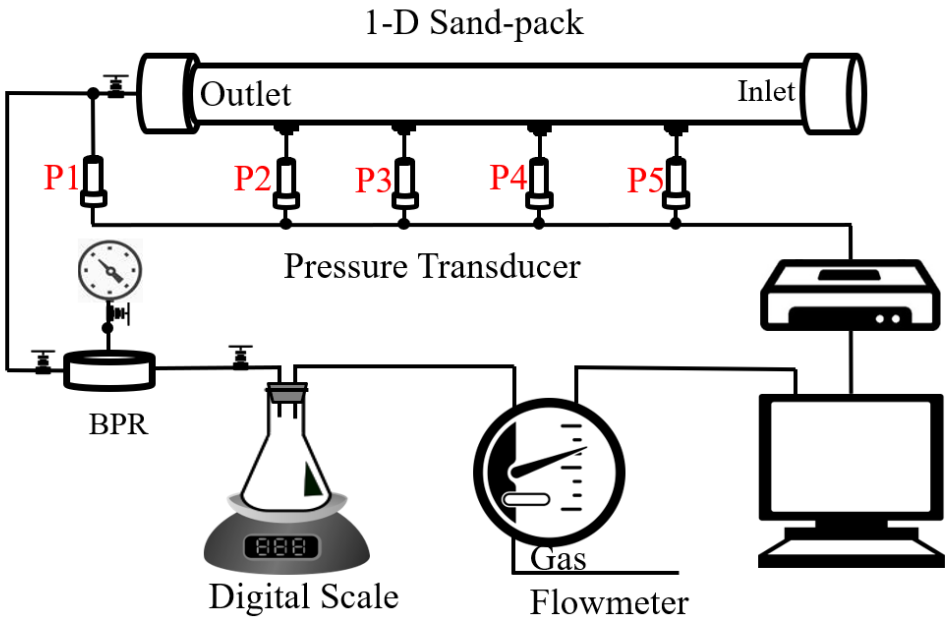

Figure 4.11 The Distribution of Pressure Points

Pressure decline rate: 2 kPa/min

The change in pressure difference with time is shown in Figure 4.12. In the single-phase flow region, whether it is the oil single-phase flow of the former part or the gas single-phase flow of the latter part, the pressure difference of the five pressure points is less than 15 kPa. The error of the pressure transducers are ± 5 kPa, so the pressure differences between five pressure points are very small. Since there is no pressure difference in the entire one-dimensional model, there is no oil production at this stage.

When the weak two-phase flow region starts, the pressure difference inside the model begins to rise gradually. There has been a significant increase in pressure difference starting from the middle of this region. From the curves of oil and gas production, the oil production rate is slowly reduced after this point, while the gas production rate is suddenly increased. This shows that the change in pressure difference after the mid stage is caused by a large amount of gas production.

When the pressure difference rises to a certain extent, or when the volume of the bubble trapped in the oil is increased to a certain extent, it enters the stage of foamy oil production. At the start of the active two-phase flow stage, the pressure difference begins to rise sharply, indicating that the model fluid volume changes significantly and continue to increase.

Combined with changes in pressure and changes in previous oil/gas production trends, a reasonable explanation can be given for the foamy oil generation at this stage. The gas release rate of nitrogen from the oil is defined as the following formula;

$$v_{release} = \frac{dV}{dP} \times \frac{dP}{dt} \times \frac{ZTP_{sc}}{z_{sc}T_{sc}P} \tag{4.4}$$

$$\frac{dV}{dP} = A \times \frac{dS}{dP} \tag{4.5}$$

where $v_{release}$ is the gas release rate of nitrogen from the oil; V is the gas volume under standard condition; P is the pressure; t is the time; Z is the compressibility factor; T is the temperature; A is a coefficient that determines how much gas is actually released from the oil, which is mainly related to the diffusion coefficient; S is the solubility.

The solubility of nitrogen in this oil sample is determined in Chapter 3. Since the solubility of nitrogen as a function of pressure approximates a straight line, it is assumed that the amount of gas released from the unit volume of oil under the per unit pressure drop is also constant. In theory, when the time is long enough, $\frac{dV}{dP}$ equals $\frac{dS}{dP}$. In this experiment, the pressure decline rate is 2 kPa/min, and the amount of gas released from the unit volume of oil under per unit pressure drop is 0.0008 $m^3/m^3 \cdot kPa$. Therefore, the gas nitrogen released per unit oil volume per unit time is 0.0016 m^3 where 0.0016 m^3 is the gas volume under standard conditions. Assuming that the values of A does not change at the same pressure decline rate, the mass rate of the gas released is constant at the same pressure decline rate, but the volumetric release rate is different at different pressure stages. Due to the significant gas compression coefficient, the volumetric rate at low pressure is greater than the volumetric rate at high pressure. At the pressure decline rate of 2 kPa/min, the pressure at the beginning of the weak two-phase flow and at the beginning of the active two-phase flow are 5241 kPa and 303 kPa, respectively. The gas release rate of nitrogen at these two points is 0.031×A $l/m^3 \cdot min$ and 0.528×A $l/m^3 \cdot min$, respectively. For that reason, when the gas release rate of

nitrogen exceeds $0.031 \times A$ l/m^3·min, weak two-phase flow occurs, and when the gas release rate of nitrogen exceeds $0.528 \times A$ l/m^3·min, foamy oil flow is dominant.

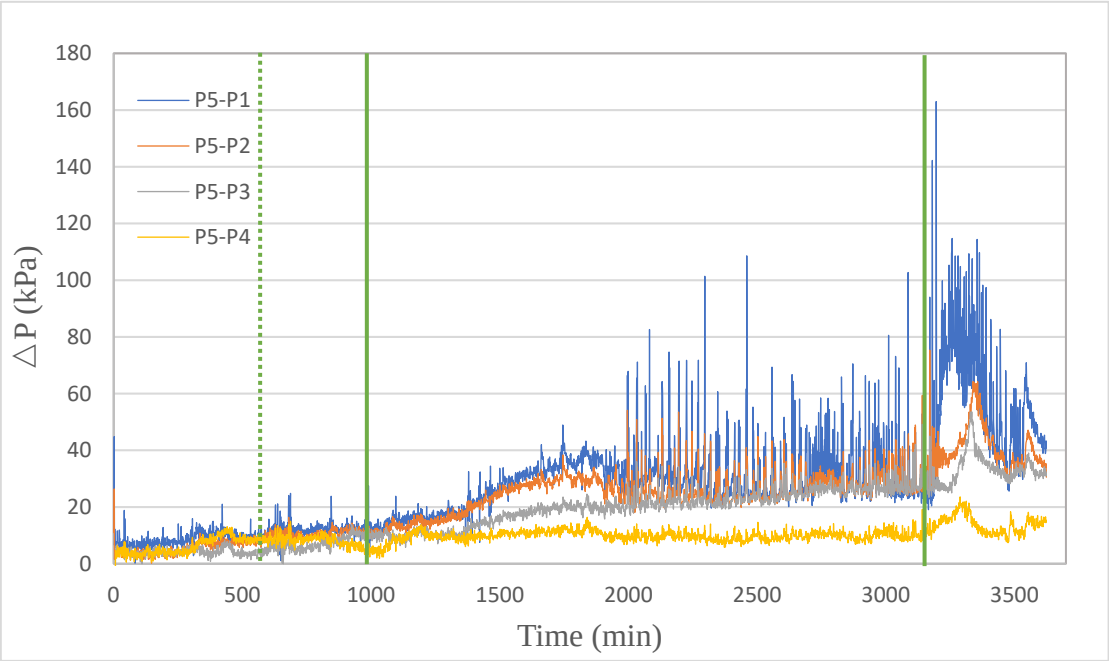

Figure 4.12 Pressure Difference in the Test with Pressure Decline Rate of 2 kPa/min

Pressure decline rate: 8 kPa/min

The pressure differences curves with a pressure decline rate of 8 kPa/min are very similar to the curves of the previous experiment. The difference is that the curves at 8 kPa/min are more stable during both the weak two-phase flow region and the active two-phase flow region. The same method is used to calculate the volumetric rate of nitrogen released per unit volume of oil. At the pressure decline rate of 8 kPa/min, the pressure at the beginning of the weak two-phase flow and at the beginning of the active two-phase flow is 6,000 kPa and 695 kPa, respectively. The volumetric rate of nitrogen released at these two points is $0.107 \times A$ l/m^3·min and $0.920 \times A$ l/m^3·min, respectively. This shows that a higher volumetric rate of nitrogen released (or a higher pressure decline rate) results in a more stable conventional solution gas drive and foamy oil flow.

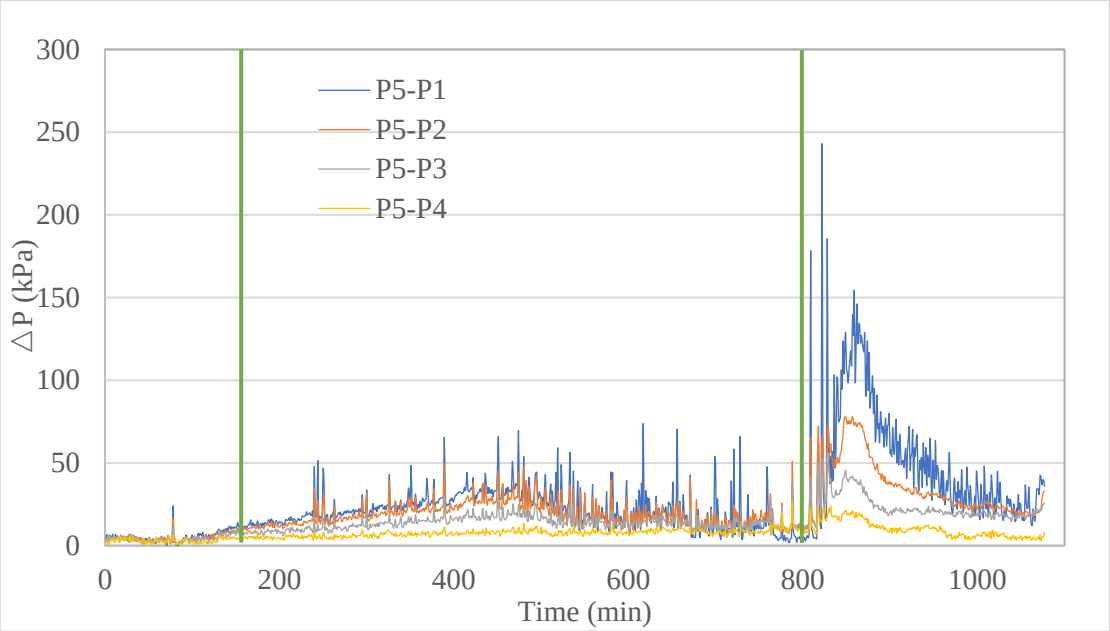

Figure 4.13 Pressure Difference in the Test with Pressure Decline Rate of 8 kPa/min

Pressure decline rate: 16 kPa/min and 32 kPa/min

In these experiments, the active two-phase flow region follows the single-phase flow region. The pressure at the starting point of the active two-phase flow region for these two experiments is 2,525 kPa and 3,720 kPa, respectively. The corresponding volumetric rate of nitrogen released is $0.507 \times A$ l/m^3·min and $0.698 \times A$ l/m^3·min, respectively. Higher volumetric rate results in a more stable foamy oil flow for the experiment with the pressure decline rate of 32 kPa/min (as shown in Figure 4.14). Since the starting point of the weak two-phase flow region is after the BPR pressure drops to atmospheric pressure, the actual pressure decline rate in the model starts to differ and cannot be measured. The pressure decline rate at each point in the model also begins to differ and cannot be measured. Therefore, the gas release rate at the beginning of the active two-phase flow region of these two experiments cannot be calculated.

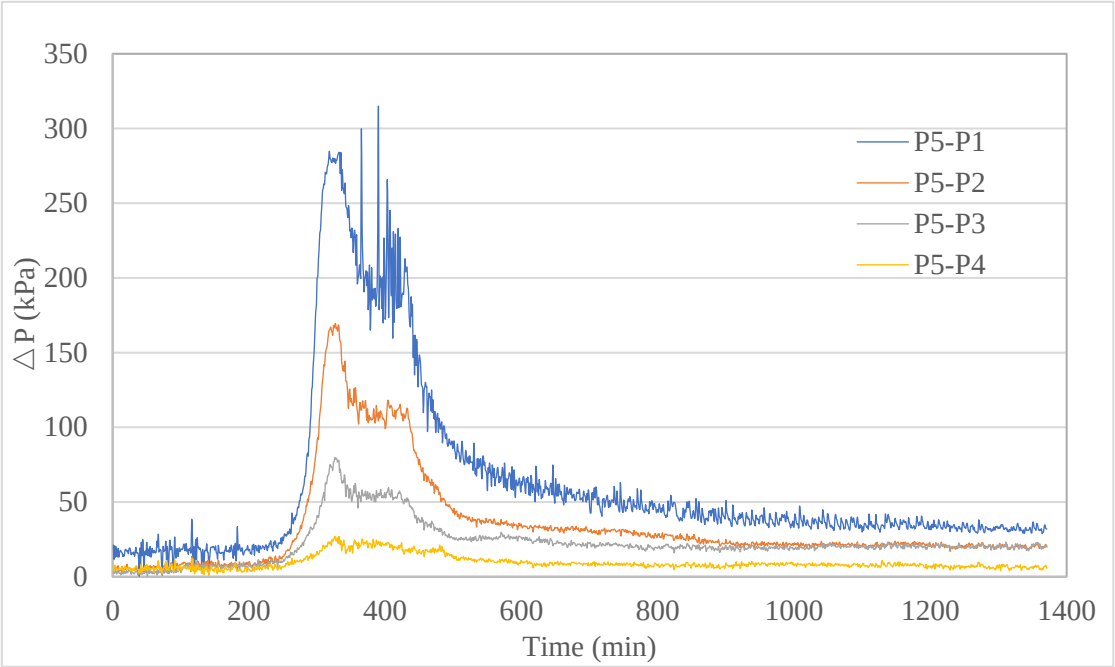

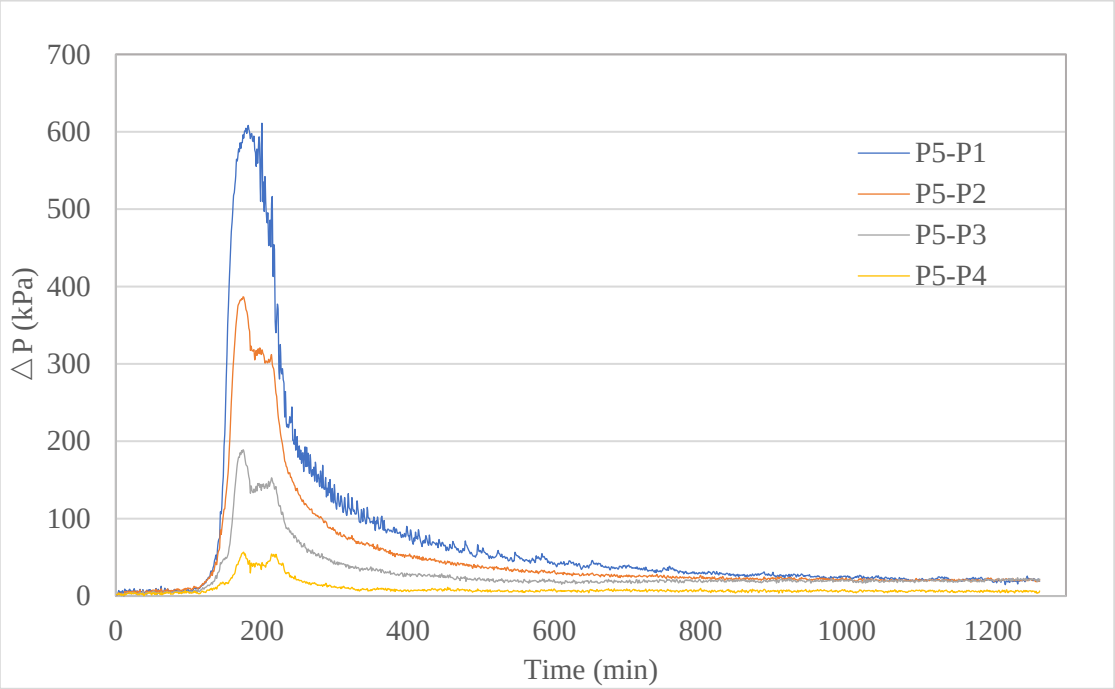

Figure 4.14 Pressure Difference in the Test with Pressure Decline Rate of 16 and 32 kPa/min

Table 4.8 shows the volumetric rate of nitrogen released per unit volume of oil at the beginning of each flow region in these four experiments. The condition at which the weak two-phase flow started is $0.031 \times A$ l/m 3 ·min, which is determined by experiment under pressure decline rate of 2 kPa/min, because the experiment with the pressure decline rate of 2 kPa/min experiences a period between gas single-phase flow and weak two-phase flow. In the experiment with the pressure decline rate of 8 kPa/min, the pressure decline rate is faster than the start limits of weak two-phase flow. When the pressure drops to the bubble point pressure, weak two-phase flow begins immediately. Moreover, the condition at which the active two-phase flow started is around $0.52 \times A$ l/m 3 ·min, which is determined by experiments under pressure decline rate of 2 and 16 kPa/min. In the experiment with a pressure decline rate of 32 kPa/min, the calculated result is too large due to the rapid pressure decline rate which exceeds the fastest release rate of nitrogen.

Table 4.8 Nitrogen Release Rate at Each Stage

Pressure decline rate, kPa/min	Pressure at Starting Point, kPa		Gas Release Rate at Starting Point, l/m3·min	
	Weak Two-phase Flow	Active Two-phase Flow	Weak Two-phase Flow	Active Two-phase Flow
2	5242	303	0.031A	0.528A
8	6000	695	0.107A	0.920A
16		2525		0.507A
32		3670		0.698A

4.4.4 Comparison with Other Solvent

The four sets of curves in Figure 4.15 are the production curves for the pressure depletion tests in the same 1-D sand-pack model for carbon dioxide, methane, methane-propane mixture, and propane, respectively. These curves are from Xiang's and Mingyi's studies (Wu, 2018; Zhou, 2014)

The production curves of the experiments for carbon dioxide, methane and methane-propane mixture are very similar to those of nitrogen experiments. Moreover, each inflection point in the curves of the two groups of experiments can be clearly explained by the viewpoint of the gas release rate.

In these three experiments, only the test of carbon dioxide had a significant weak two-phase flow region at 50 ℃, and the oil production of carbon dioxide in the weak two-phase flow region at 40 ℃ is approximately zero. In the other experiments, there is no apparent weak two-phase flow region, but as the temperature decreases, the production in the active two-phase flow region increases. In this 1-D sand-pack model, the temperature directly affects the viscosity of the oil. Therefore, the higher the oil viscosity, the weaker the conventional solution gas drive and the stronger the foamy oil flow(Wu, 2018).

In the experiments of propane, since the solubility of propane too large, the initial pressure is low, and there is a large gas release rate at the start of the experiments, the active two-phase flow occurs at the beginning of the pressure depletion. However, for a highly soluble gas, when the volumetric rate of the gas released is increased to a certain extent, the stability of the foamy oil is reduced.

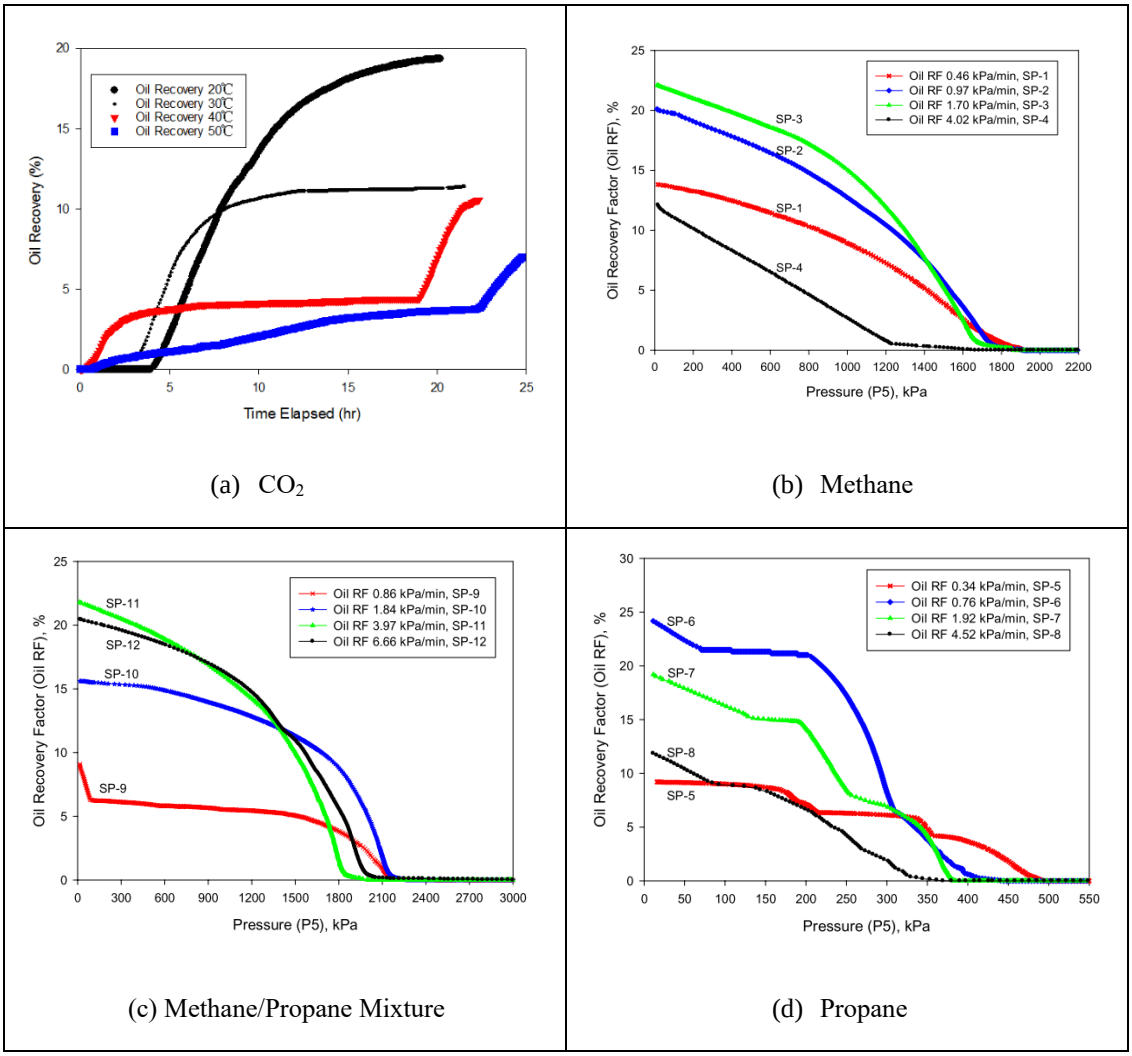

Figure 4.15 Production Curves for Other Solvents

Table 4.9 summarizes the experimental oil recovery of different solvents under different conditions. The comparison of oil recovery factors from nitrogen and carbon dioxide pressure depletion tests at 50 ℃ shows that there is a stronger conventional solution gas drive in the nitrogen tests. Compared to the pressure decline tests of methane, nitrogen has a similar solubility with methane, but production of methane tests is much higher than that of nitrogen under same pressure decline rate, due to the higher viscosity of oil sample in methane tests. This shows that nitrogen still has great application potential in a high-viscosity heavy oil.

Table 4.9 Oil Recovery of Other Solvents

Solvent	Temperature, ℃	Decline Rate, kPa/min	Initial GOR, Sm^3/m^3	Oil Recovery, %	Gas recovery, %
CO_2	20	2	21.80	19.35	82.12
Methane	20	1.7	6.62	22.13	94.86
Propane	20	1.92	74.70	19.19	36.82
C1/C3 Mixture	20	1.84	25.30	15.61	69.91
CO_2	50	2	21.80	6.96	94.91
N_2	50	2	6.67	12.88	91.97

4.5 Chapter Summary

Since foamy oil is a very significant production mechanism in Huff-n-Puff, especially in Cyclic Solvent Injection, the objective of this chapter is to experimentally determine whether or not the oil saturated with nitrogen can form foamy oil during the pressure depletion process. This chapter has reached the following conclusions in the experiments of nitrogen live oil pressure depletion tests.

1. The solubility of nitrogen is low and does not have much effect on viscosity reduction. A decrease in viscosity is not significant, which is advantageous for the production of foamy oil flow.
2. The higher the pressure decline rate, the greater the oil recovery factor and the smaller the gas recovery factor.
3. In the weak two-phase flow region, the two groups of experiments (one with low pressure decline rates and the other with high pressure decline rates) have different causes of weak two-phase flow. Under low pressure decline rate, the pressure decline rate does not affect the oil recovery factor of the weak two-phase flow stage. The maximum oil production per unit pressure depletion is about 0.01 g/kPa.
4. Under high-pressure decline rate, due to the difference in the amount of residual gas in the oil from the previous active two-phase flow stage, the faster the pressure decline rate, the higher the oil recovery factor in the weak two-phase flow region.
5. In the active two-phase flow region, as the pressure decline rate increases, the oil recovery rate also increases significantly. This shows that the higher the pressure decline rate, the

stronger the foamy oil can be formed. However, in experiments with high solubility solvents, when the pressure decline rate is too high, the stability of the foamy oil will be destroyed.

6. Under the premise that the viscosity of the oil remains unchanged, the change of the flow state mainly depends on the volumetric rate of the gas release. With the increase of gas release rate, the flow state is followed by gas single-phase flow, conventional solution gas drive, unstable solution gas drive, unstable foamy oil flow, and stable foamy oil flow.
7. It is finally confirmed that in the high-pressure reservoir at 50 ℃, the nitrogen-heavy oil live oil in pressure decline tests can form foamy oil.

CHAPTER 5 HUFF-N-PUFF TESTS IN 2-D SAND-PACK

5.1 Overview

It has been confirmed that nitrogen can form foamy oil in live oil pressure depletion tests. Since foamy oil is only one of the key factors in the Huff-n-Puff, to determine whether or not nitrogen Huff-n-Puff can be used in the heavy oil, this method must be tested by the complete process. The objective of this chapter is to experimentally determine the feasibility of nitrogen Huff-n-Puff in deep heavy oil reservoirs. Some researchers have previously observed the effect of Huff-n-Puff or Cyclic Solvent Injection (CSI) by conducting Huff-n-Puff tests in the 2-D planar sand-pack model (K. Zhang, 2018; K. Zhang, Zhou, Peng, & Zeng, 2019; X. Zhang, Du, Deimbacher, Crick, & Harikesavanallur, 2009). They have demonstrated that this method of studying the Huff-n-Puff process by using a 2-D planar sand-pack model is reliable. This study is aimed at high temperature deep heavy oil reservoirs and assumes a condition of 7 MPa and 50 ℃. The purpose of the study is to discuss the feasibility of nitrogen Huff-n-Puff under these conditions, so the temperature and viscosity of the crude oil are no longer changing. The experiments in this chapter will be conducted at four different constant pressure decline rates(Du, Zeng, Peng, & Chan, 2016). Oil samples, oil's viscosity, sand-pack properties, and other parameters are set to be the same.

5.2 Experimental Material and Apparatuses

5.2.1 Oil sample

The oil sample used in this chapter is the same as in Chapter 3. This heavy oil sample is first settled to centrifuge at 3000 rpm for 90 minutes. This process is to make sure the dead oil sample is free of water. After the dehydration process, the viscosity of the dead oil is 4810 cP at 25 ℃, and 598 cP at 50 ℃.

5.2.2 2-D Planar Sand-pack Model

The experiments in this part are conducted in a 2-D planar sand-pack model, as shown in Figure 5.1. The bottom of the model is a 5 cm stainless steel plate, and the upper part of the model is an 8 cm thick acrylic plate. The upper-pressure limit of both plates is 10 MPa, which meets the experimental conditions. However, the hardness of acrylic is not high enough, and the disassembly and assembly of the model will cause the acrylic surface to wear. Tiny wear scars can undermine the seal of the model under high pressure. In order to reduce the contact between the acrylic plate and the stainless steel plate, the model is separated by a polycarbonate plate, which is a harder material. The upper and lower parts of the model are fixed with 12 bolts.

The length, width, and height of the internal cavity of the model are 40 cm, 10 cm, and 2 cm, respectively. The internal height is small enough to identify the model as a 2-dimensional planar model. The bulk volume of the internal cavity is 800 cm^3. Since the interior of the model will be coated, the actual total volume in the experiments will be slightly smaller than 800 cm^3.

There are 12 fitting ports on the sand-pack. One inlet port and one outlet port are at the two ends of the sand-pack with five ports evenly distributed on both sides of the model. The six intermediate ports are used to measure temperature and are sealed by the thermal coupler. The six ports at both ends of the model are open ports that are used to inject and produce fluid into the model and sometimes to connect to the pressure transducers. The fittings

assembled on the six ports are welded to prevent fluid from carrying sand as it flows out of the model. The stand of the model can adjust the angle of the model.

This model has two undeniable flaws (Du, Zeng, & Chan, 2015). The first is the wall effect. The inner wall of the model is a hard, smooth stainless steel and polycarbonate material. The sand does not conform to the inner wall which results in a high permeability gap between the two. This problem can be alleviated by using a coating. Another flaw is the boundary effect. The boundary effect causes the fluid flow direction in the model to be different from the actual formation. Other researchers tried to conduct Huff-n-Puff tests in multiple-scale models to study the effects of the boundary (Du et al., 2015; M. Zhang, Du, Zeng, Hong, & Xu, 2016). However, the boundary effect is beyond the scope of this research. This study will use a model of a predetermined size to study the performance of nitrogen in the Huff-n-Puff process. Then, the results are compared with other solvents Huff-n-Puff tests in models of a similar size.

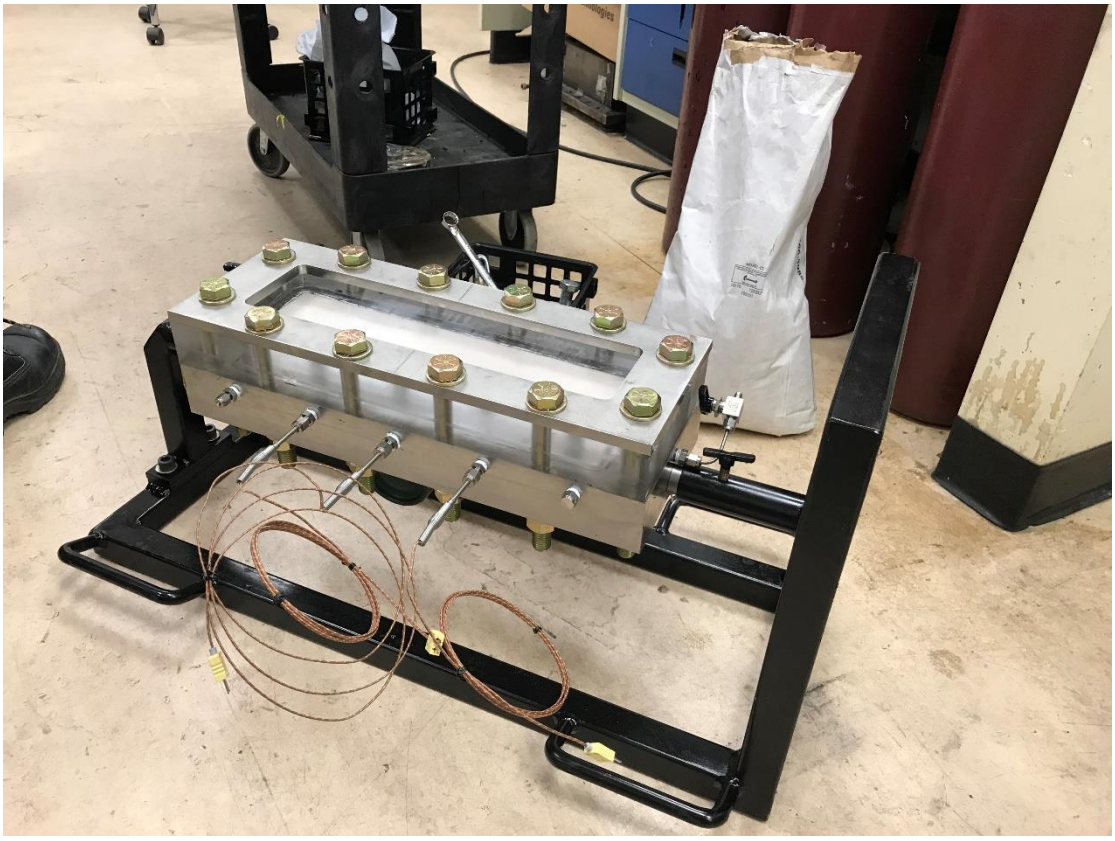

Figure 5.1 2-D Planar Sand-pack Model

5.3 Experimental Procedure

5.3.1 Sand-pack Model Preparation

Since the 2-D model used in the experiments is previously used in other experiments, there are leftover sand and crude oil. In order to ensure the accuracy of the experiments, the 2-D model must be cleaned before experimenting. The Swagelok fittings and tubing assembled on the model must be removed first, and be immersed in toluene, kerosene, and ethanol in sequence until thoroughly cleaned. Then, the inner wall of the model and each contact surface are sequentially wiped with toluene, kerosene, and ethanol.

In these tests, a kind of liquid electrical tape (Brush-on Electrical Tape) is treated as the coating. This electrical tape is unevenly applied to the inner wall of the model to create a rough and soft surface. Sprinkling a thin layer of sand before the coating solidifies, this allows sand to be embedded in the surface, thus avoiding the wall effect. After applying the electrical tape, the actual length, width, and height of the cavity inside the model are 39.34 cm, 9.40 cm, and 1.89 cm, respectively. The actual bulk volume becomes 700.11 m^3.

Except for the ports with the thermocouple assembled and the inlet ports, the rest of the three outlet ports are glued to the metal filter with a strong resin adhesive. Figure 5.2 shows the distribution of inlet ports, outlet ports, and thermocouples on the model. The density of the metal filter is 400 mesh, which is large enough to prevent sand production during the experiments. Then, assemble Swagelok fittings on all the ports except the inlet port on the model. These fittings are welded to the metal mesh. This allows each fluid outlet ports to

have two layers of filter to prevent sand leaking due to workmanship problems. The model is then sealed with an O-ring and 12 bolts.

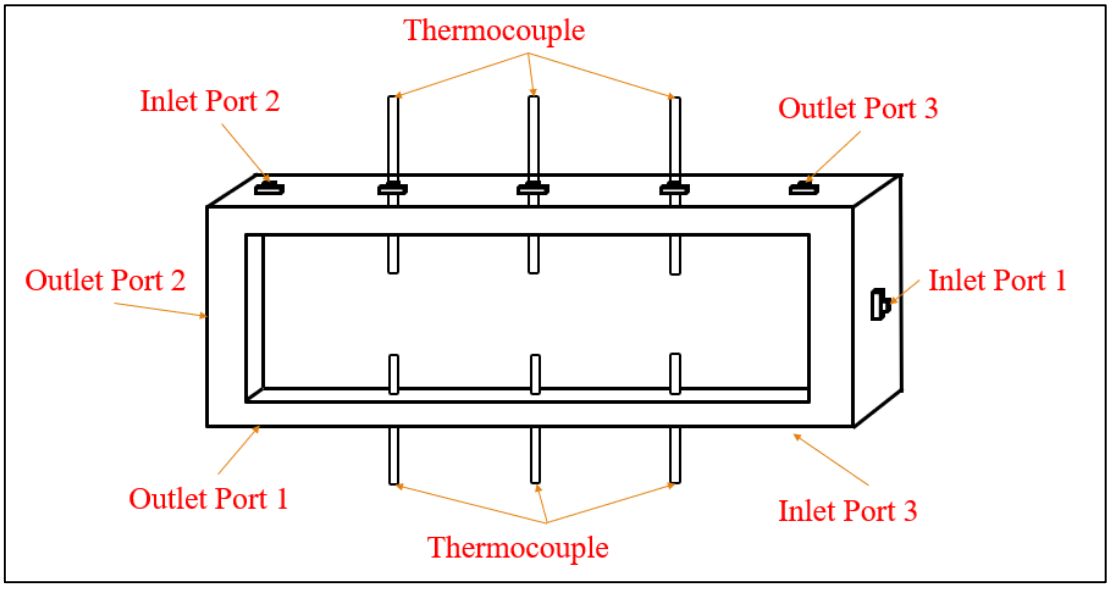

Figure 5.2 Distribution of Inlet ports, Outlet ports, and Thermocouples

5.3.2 Sand Packing

Assemble the vibrator on the bottom of the model (as shown in Figure 5.3). This vibrator is driven by an air flow that is strong enough to cause the model to vibrate so that the sand can be evenly distributed during the packing process. Because of potential pollution and healthcare problems, the experiments used glass beads with a diameter between 90 and 150 μm, instead of real sand, to create the porous media.

Figure 5.3 Vibrator on the 2-D Model

The model is placed perpendicular to the ground so that the inlet port 1 is at the top. Pour the glass beads into the model from the inlet port 1 at a very slow rate while adjusting the vibrator to maximum frequency. Since there are many corners in the 2-D model, packing sand only in one direction does not guarantee that the sand is tightly packed. When it is not possible to fill more sand from the inlet port 1, place the model horizontally on the ground. Then sand is poured from the inlet port 2 and inlet port 3. Put the model vertically on the ground again and continue packing sand from the inlet port 1. This process needs to be repeated at least three times, and it will only end when no more sand can be packed in any of the inlet ports. When the sand fills the model evenly and tightly, assemble the Swagelok fitting welded with the filter mesh on the inlet ports of the model.

5.3.3 Experimental System Setup

The illustration of the experimental device system set-up is shown in Figure 5.4. Two transfer cylinders are connected to the model. These two transfer cylinders are filled with gaseous nitrogen and dead oil, respectively. The inner pressure or the flow rates of these two cylinders are controlled by a syringe pump. Both of these two transfer cylinders and the model are placed in an oven. When the experiments are carried out, the temperature of the oven is set at 50 ℃ to simulate the high-temperature formation environment. One back pressure regulator is connected to the outlet port 1 of the model. Its role is to control the pressure at the outlet. The pressure of the BPR is regulated by the syringe pump. The outlet end of the BPR is connected to a production system, which consists of a digital scale and a

gas flow meter. This production system is used to measure oil production and gas production. In this case, the pressure transducers and the gas flow meter are directly connected to the computer to record the readings automatically. The digital scale readings are recorded by the camera, and the video file is processed by WRead (an ORC software), which can generate a data file for the balance reading. There are two pressure points in the model, one is at the inlet port 1, and the other one is at the outlet port 1. They measure the pressure at the far end of the model and the bottom-hole pressure.

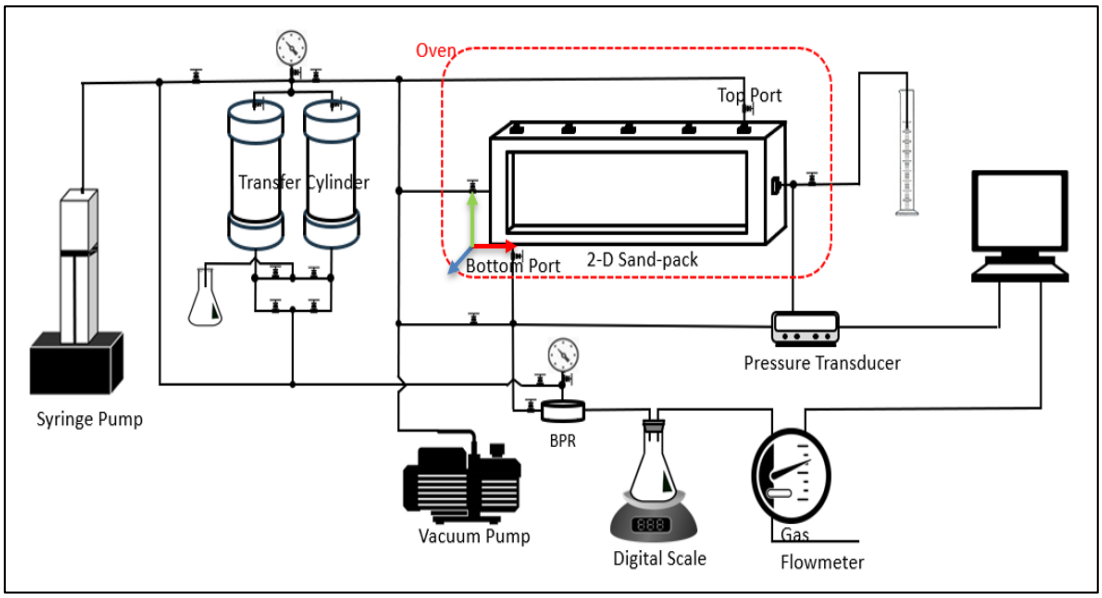

Figure 5.4 The Illustration of the Experimental Device System

5.3.4 Leaking Tests

The Huff-n-Puff tests require a high degree of pressure control and the interior of the experimental system needs to be completely isolated from the outside. Therefore, leak tests are required before the start of the experiments to ensure that the entire experimental system is sealed.

After setting up the experimental system, nitrogen is injected into the model from the inlet port, and the model is sealed by BPR at the outlet port. The maximum pressure for the ideal conditions of the experiments is 7 MPa. In order to be safe, the leak pressure needs to be higher than 7 MPa, so in these tests, nitrogen is injected into the model to increase the pressure to 7.5 MPa, and the pressure of BPR is set at 8 MPa to seal the model. After the sand-pack model is pressurized, observe the reading on the pressure gauge. If the pressure drop is less than 5 kPa in 24 hours, the whole system is considered to be sealed. Otherwise, apply a soapy liquid leak detector (FORMULA 365) to each of the connectors to check for air bubbles. The connectors where the bubbles are generated need to be reconnected until the pressure drop is less than 5 kPa within 24 hours. After that, the whole experimental system in Huff-n-Puff tests is considered as a leak-free system.

It is worth noting that water and carbon dioxide cannot be injected into the experimental system during the leaking tests. Water is very sensitive to temperature. If water is used as a leak tests fluid, a slight temperature change can cause pressure fluctuations in the model. Carbon dioxide as a corrosive gas also cannot be used for leaking tests. The two caps at both

ends of the model and the pistons in the transfer cylinders are sealed by rubber O-rings, placing them in a carbon dioxide environment will reduce their service life.

5.3.5 Pore Volume Measurement

The pore volume of the model is measured by injecting water into the model, and once the water fills the entire pore space, the amount of water injected is equal to the pore volume. Injecting water directly into the model does not guarantee that the water will fill all the pores. It is necessary to vacuum the model first before drawing water into each pore. Hence, the outlet port of the model is first closed, and then the vacuum pump is connected to the inlet port. The whole leak-free sand-pack model system is vacuumized for 4 hours until all gases are removed from the sand-pack model, and the inner pressure of the model becomes stable. The pressure inside the model after this process will usually remain at around -94 kPa.

A measuring cylinder with water is connected to the inlet port 1 of the model. Water will be sucked into the sand-pack model system by the pressure difference between the negative inner pressure of the model and the atmospheric pressure. When the pressure in the model reaches atmospheric pressure, and the model no longer draws in water, the amount of water drawn in the model is measured by the measuring cylinder.

Then the outlet port 2 is opened and connected to an empty measuring cylinder. Deionized water is injected into the sand-pack model from the inlet port 1 by a syringe pump until the amount of water injected exceeds 1.5 PV. Record the amount of water injected, and the amount of water discharged in the measuring cylinder. Thus, the amount of water

saturated in the model is equal to the amount of water drawn in plus the amount of water injected then minus the amount of water discharged.

Finally, the amount of water saturated in the model is the pore volume of the model. The porosity is calculated as:

$$\emptyset = \frac{V_{water}}{V_{bulk}} \tag{5.1}$$

where $\emptyset$ is the porosity of the sand-pack model, %. V_{water} is the volume of water saturated in the model, cm^3. V_{bulk} is the bulk volume of the sand-pack model, cm^3.

The details of the porosity measurement are listed in Table 5.1

Table 5.1 Porosity Measurement

Length, cm	39.34
Width, cm	9.40
Thickness, cm	1.89
Bulk Volume, cm^3	700.11
Inhaled Water, cm^3	260
Injected Water, cm^3	400
Discharged Water, cm^3	393
Saturated Water, cm^3	267.00
Porosity, %	38.13

5.3.6 Absolute Permeability Measurement

Using Darcy's law, as shown in Equation 3.1, to calculate the absolute permeability.

$$K = -\frac{Q\mu}{A}\frac{\triangle L}{\triangle p} \tag{5.2}$$

where Q is the rate of fluid flowing, cm^3/s; K is the permeability, Darcy's; μ is the viscosity of the flowing fluid, cP; A is the cross-sectional area across which flow occurs, cm^2; dp/dl is the pressure drop per unit length, atm/cm.

The length of the model is 39.34 cm, and the cross-sectional area is 17.79 cm^2. Permeability needs to be calibrated using a fluid with a known viscosity. In these experiments, the accuracy of measuring absolute permeability does not need to be too high. Therefore, using water as a standard can meet the measurement needs.

After the porosity measurement, the model is saturated with water. A fixed flow rate is set to allow water to flow through the model. Once the pressure at the inlet and outlet ends stabilizes (this process usually lasts 10 minutes), the flow rate on the pump and the pressure readings at both ends are recorded. The flow rate is set from 2 to 16 ml/min with 2 ml/min incremental increase.

When the range of flow rates fall below 16 ml/min, water behaves in a laminar flow through the porous media\(Wu, 2018). Therefore, Darcy's law is suitable in this range. The details of the permeability measurement are shown in Figure 5.5, Table 5.2, and the results are shown in Table 5.3.

Table 5.2 Permeability Measurement

P1, kPa	P2, kPa	△P, kPa	Q, cm^3/min
4.9	1.2	3.7	2
13.1	1.4	11.7	4
21.4	1.6	19.8	6
29.5	1.8	27.7	8
37.3	2	35.3	10
45.8	2.3	43.5	12
53.2	2.5	50.7	14
61.5	2.9	58.6	16

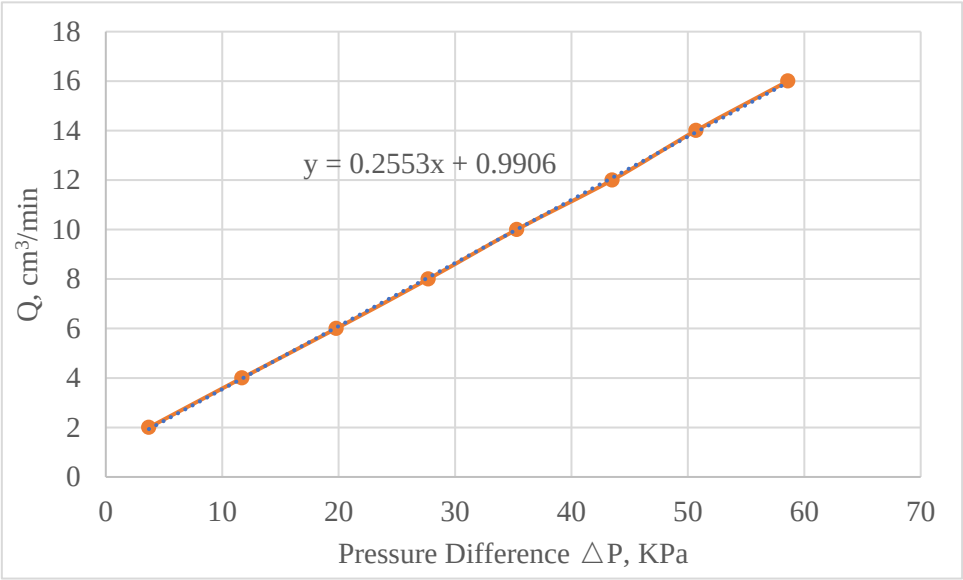

Figure 5.5 Permeability Measurement

Table 5.3 Permeability of the 2-D Sand-Pack Model

Cross-sectional Area, cm^2	17.79
Length, cm	39.34
Viscosity, cP	1
$\triangle q/\triangle p$, $cm^3/min \cdot KPa$	0.2553
Permeability, Darcy	0.918

5.3.7 Oil Saturation and Initial Oil/Water Saturation Measurements

Before the following tests, the 2-D planar sand-pack model is entirely saturated with water. In the oil saturation process, outlet port 1 is connected to an empty measuring cylinder, and dead oil is injected into the model with a very slow flow rate from inlet port 1. In these tests, the flow rate of 0.03 ml/min is selected. If the sand in the model is tight enough and the injection flow rate is appropriate, then the oil-water interface should approximate a straight line, as shown in Figure 5.6.

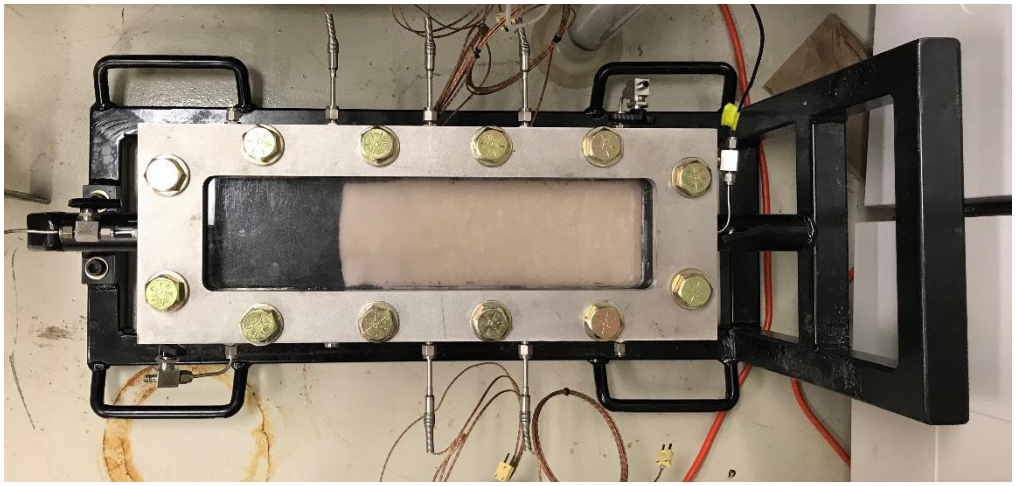

Figure 5.6 Oil Saturation Process

The oil volume needed for injection is 1.5 times that of the pore volume (PV) to ensure the model is fully saturated with live oil (Zhou, 2015). After the sand-pack model is saturated with live oil, the discharged water, which is measured by a measuring cylinder, equals to the amount of dead oil present in the model. The residual water is equal to the saturated water minus the amount of discharged water. From that, the initial oil saturation and initial water saturation are determined by:

$$s_{oi} = \frac{V_{wd}}{V_{pore}} \tag{5.3}$$

$$s_{wi} = 1 - \frac{V_{wp}}{V_{pore}} \tag{5.4}$$

where s_{oi} is the initial oil saturation of the sand-pack model; s_{wi} is the initial water saturation of the sand-pack model; V_{wd} is the volume of the discharged water; V_{pore} is the pore volume of the sand-pack model.

The initial oil saturation and the initial water saturation of the sand-pack model are 91.76% and 8.24%, respectively.

Finally, the complete parameters of the 2-D planar sand-pack model in Huff-n-Puff tests are shown in Table 5.4.

Table 5.4 Parameters of the 2-D Planar Sand-pack Model

Length, cm	39.34
Width, cm	9.40
Thickness, cm	1.89
Bulk Volume, cm^3	700.11
Pore Volume, cm^3	267.00
Porosity, %	38.18
Permeability, Darcy	0.934
Initial Oil Saturation, %	91.76
Initial Water Saturation, %	8.24

5.3.8 Single-Well Huff-n-Puff Tests

After completing all preparations, the experiments may begin. The first step is to set the temperature in the oven to 50 ℃. Nitrogen gas is injected into the model after the internal pressure of the model is raised to 50 ℃. One transfer cylinder filled with nitrogen is connected at the outlet port 1. Gas nitrogen is injected by the syringe pump at a constant flow rate of 80 ml/min. When the pressure at the inlet port 1 of the model rises to 6,500 KPa, the injection mode is changed to constant pressure injection while the pressure is set at 7,000 KPa. When the pressure rises to 7 MPa, the outlet port of the model is closed. The soaking time is set at 30 minutes, and the model pressure will drop significantly during the soaking process, indicating that some nitrogen is dissolved into the oil.

After the soaking process, the outlet port 1 is treated as a production well. The bottom-hole pressure (BHP) drops from the initial reservoir pressure to the ambient atmospheric pressure. The initial pressure will be slightly lower than 7 MPa, and will continue to decrease during the cycle. The pressure decline rates used in these tests are the same as in Chapter 3, which is convenient for comparison.

When a cycle is over, restart a new cycle and repeat the above steps from the gas injection process. The entire production procedure will continue until the oil production for three consecutive cycles is less than 1 g.

5.3.9 2-Well Huff-n-Puff Tests

After the single-well Huff-n-Puff tests, in order to increase oil recovery, the production model is changed to 2-well Huff-n-Puff tests. During the gas injection process, nitrogen is injected from the outlet port 3 while all other processes are unchanged. Similarly, the entire production process will continue until the oil production for three consecutive cycles is less than 1 g.

5.4 Results and Discussions

5.4.1 Overview

Table 5.5 shows the ultimate oil recovery factor at four pressure decline rates in these tests. In general, the oil recovery factor does not rise with the increase of the pressure decline rate. The optimal pressure decline rate is around 16 kPa/min. This shows that in the 2-D Huff-n-Puff experiments, the final recovery factor is not only affected by the strength of the foamy oil but also related to many other factors.

Table 5.5 Oil Recovery Factor of the Tests.

Pressure Decline Rate	Oil Recovery Factor		
	1-Well Huff-n-Puff Tests	2-Well Huff-n-Puff Tests	SUM
2 kPa/min	17.59%		17.59%
8 kPa/min	30.38%	1.73%	32.11%
16 kPa/min	34.52%	1.21%	35.73%
32 kPa/min	27.95%	0.00%	27.95%

5.4.2 Oil/Gas Production

Pressure decline rate: 2kPa/min

The oil recovery for this experiment is the lowest of the four experiments under different pressure decline rates. Moreover, its oil production is concentrated in the first two cycles, as shown in Figure 5.7. The oil production becomes negligible starting from the third cycle.

Figure 5.8 is the pressure depletion curve and the oil production curve of the first cycle. It is obvious to find that oil production curve is a straight line. Since there is almost no pressure difference between bottom-hole pressure and model pressure during this cycle, it implies that oil production mainly depends on gravity force. The pressure decline rate is so slow that the solution gas drive is not enough to displace the oil. Therefore, after the second cycle, the gravity-dependent oil production in the model reached its limit and no longer produced oil.

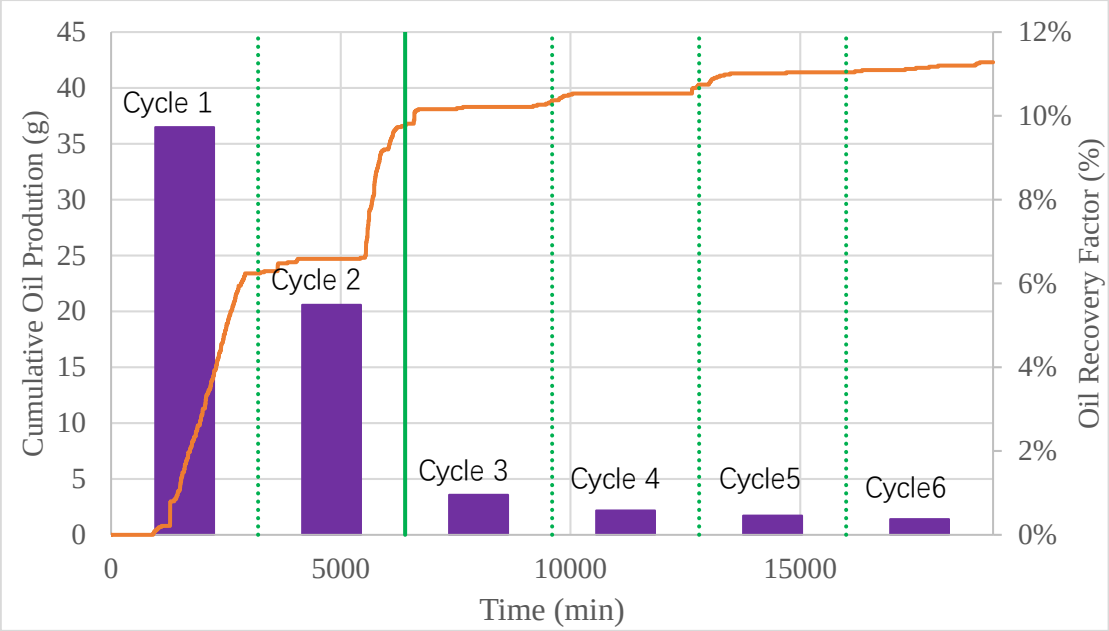

Figure 5.7 Cumulative Oil Production with Pressure Decline Rate of 2 kPa/min

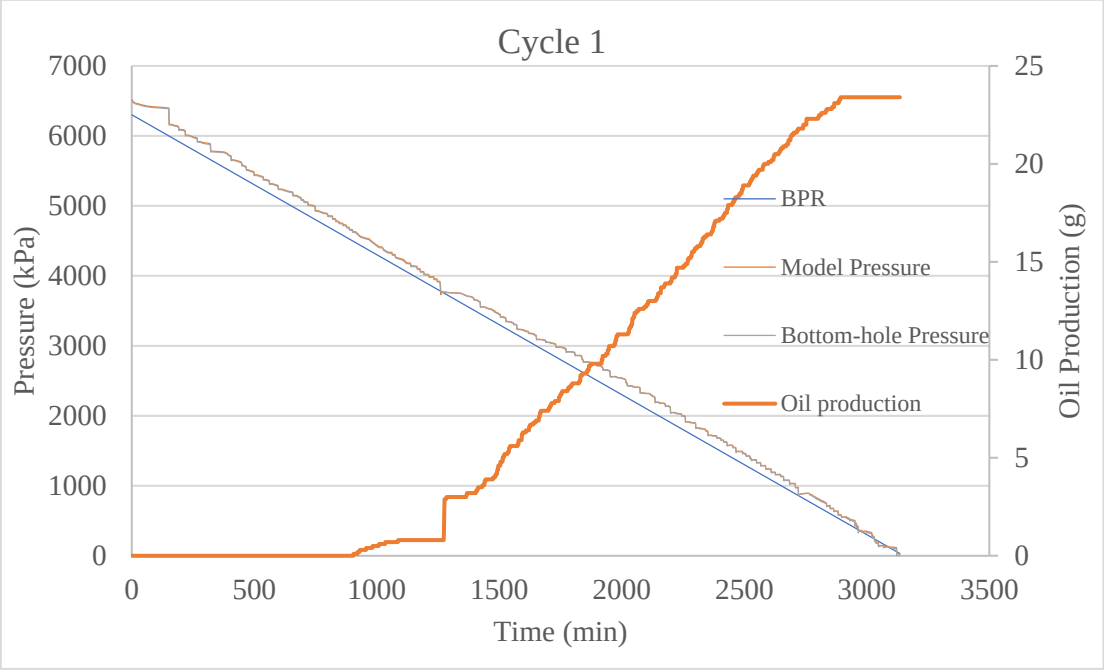

Figure 5.8 Pressure Depletion Curve and the Oil Production Curve of the First Cycle

Pressure decline rate: 8 kPa/min

From this experiment, the oil recovery factor of the nitrogen huff-n-puff process increased significantly. Take the first cycle as an example. The oil production curve is no longer a straight line, as shown in Figure 5.10. As time goes by, the oil production rate is getting faster and faster. And when the pressure drops to 2,000 kPa, a significant pressure difference between the model's pressure and the bottom-hole pressure begin to appear. It is also from this time that the oil production rate has increased significantly. The change in pressure differences indicates that there is a two-phase flow at the later-stage of this cycle. Therefore, when the pressure decline rate is higher than 8 kPa/min, the solution gas drive begins to function. Due to the action of solution gas drive, the number of cycles of the Huff-n-Puff process also increases. From two cycles, under a pressure decline rate of 2 kPa/min, increased to 9 cycles at a pressure decline rate of 8 kPa/min.

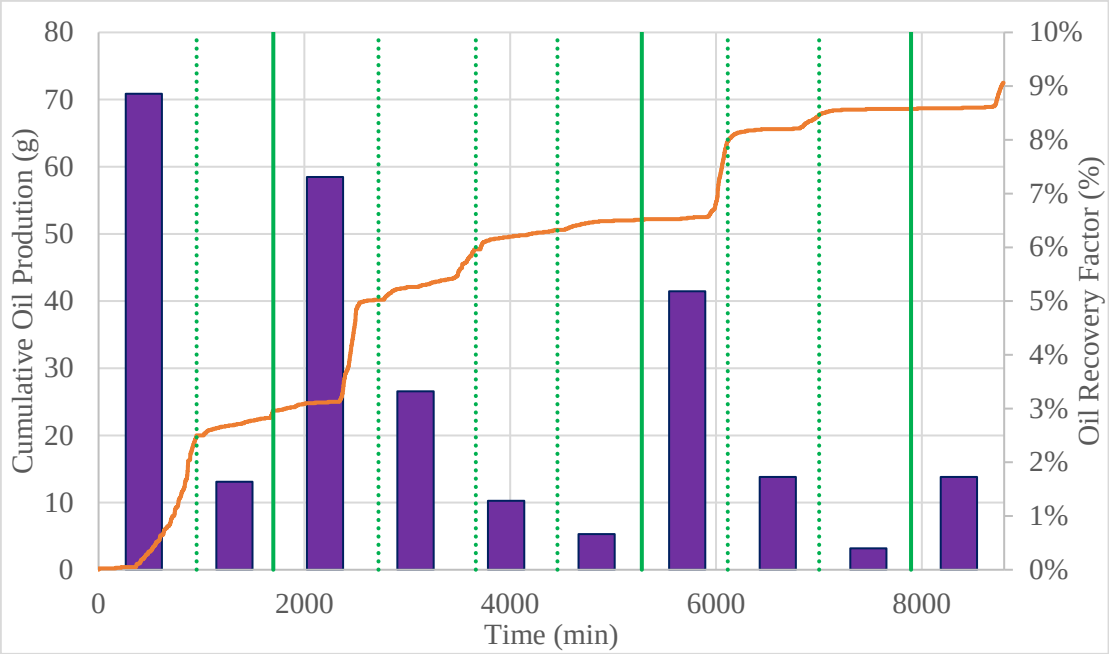

Figure 5.9 Cumulative Oil Production with Pressure Decline Rate of 8 kPa/min

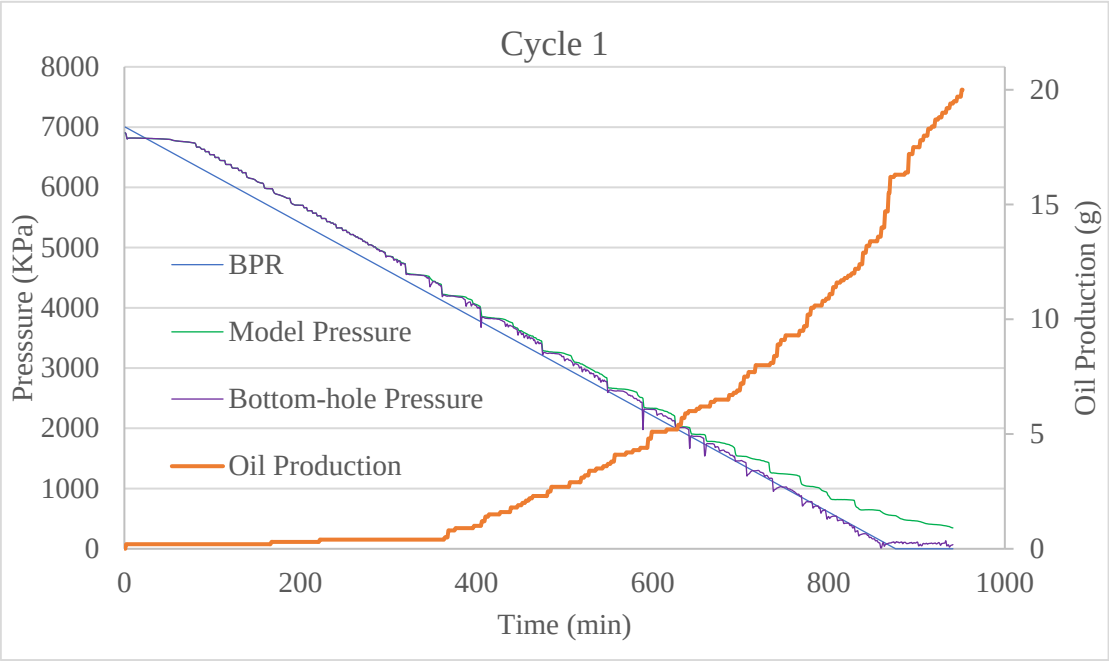

Figure 5.10 Pressure Depletion Curve and the Oil Production Curve of the First Cycle

From the third cycle, the oil production curve behavior begins to differ. In the first seven-eighth of the production period (650 min), there is essentially no oil production for each cycle. Oil production is concentrated in the production period of the latter part. Figure 5.11 is the pressure and oil production curve in cycle 7. Compared with the experiment under the same pressure decline rate in the pressure depletion tests, they have similar production characteristics except for the difference in the intermediate production stage. The reason for this difference can be explained from the perspective of the distribution of remaining oil. Oil that can be recovered from the near-well-bore zone has been produced in the previous stage. Moreover, during the gas injection stage at the beginning of each cycle, a large amount of high-velocity gas will displace the oil away from the wellbore. These two effects cause many gas chambers to form in the near-well-bore zone before the beginning of each production phase. In the production stage, the driven oil preferentially resaturate a portion of the gas chambers and is then recovered from the well. This stage of production is called the re-saturation region. This is why there is barely any oil production at the beginning of the production stage for each cycle. Due to the insufficient dissolved gas in the Huff-n-Puff process, there is no oil production in the later stages of each cycle.

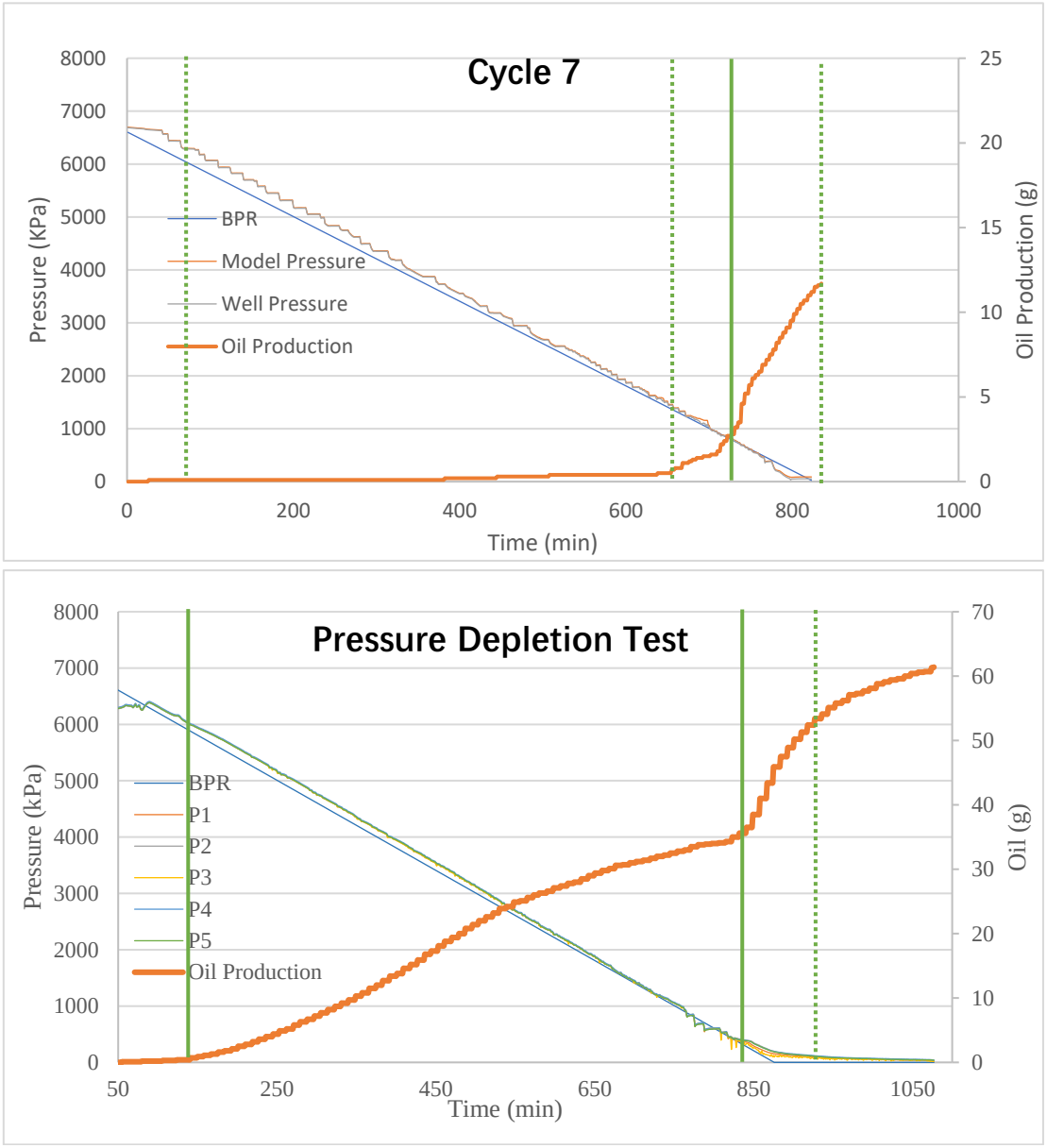

Figure 5.11 Pressure Depletion Curve and the Oil Production Curve in the 7th Cycle and in the Pressure Depletion Test

Pressure decline rate: 16 and 32 kPa/min

In the experiment with a pressure decline rate of 16 kPa/min, the oil recovery rate reached the highest value, which is 35.75%. However, the main source of production is in the first two cycles with a recovery factor of 17 % and 13 %, respectively. There is approximately no production after the third cycle. Similarly, the same phenomenon is observed in the experiment with a pressure decline rate of 32 kPa/min. The oil production of the first three cycles is relatively high, and suddenly there is no production from the fourth cycle. The reason for this is that low solubility nitrogen forms some large gas chambers in the model. When the volume of the gas chamber is large enough, the volume of the driven oil becomes relatively small, so that the driven oil will only flow back and forth in the gas chamber. Since the oil production of the first few cycles of the two experiments is very high, the growth rate of the gas chamber is too fast, and the number of cycles capable of maintaining a higher production is reduced. The specific content of the gas chamber growth will be discussed later.

In these two Huff-n-Puff tests, the single cycle oil production curves are similar to those under pressure decline rate of 8 kPa/min. However, due to the larger pressure decline rate, the time spent in the re-saturation region is shorter.

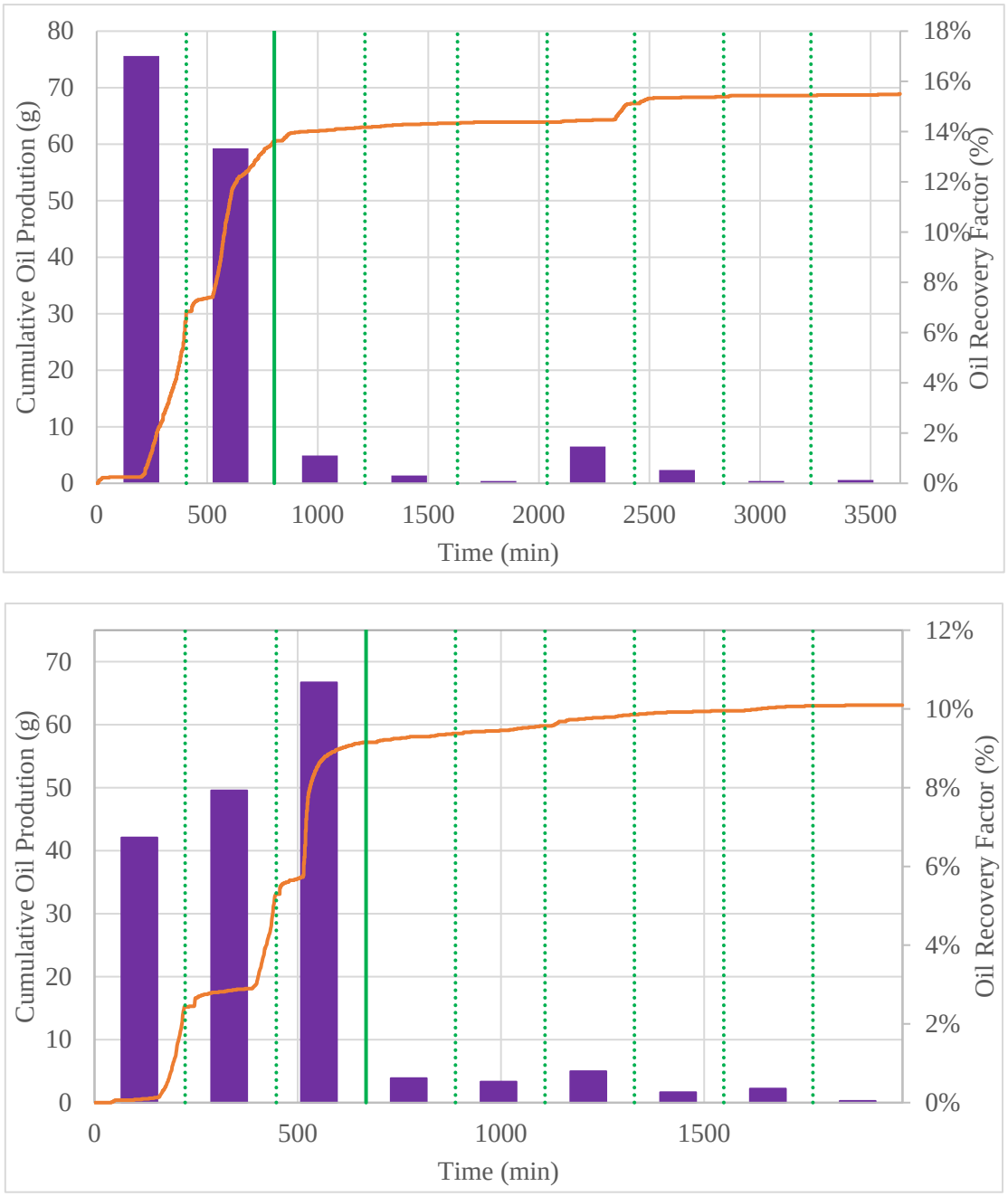

Figure 5.12 Cumulative Oil Production with Pressure Decline Rate of 16 and 32 kPa/min

5.4.3 Production Phase Analysis

According to the analysis method of the previous studies (Du, 2017; K. Zhang, 2018), the cumulative oil production curves of the Huff-n-Puff tests are divided into two phases. Phase 1 is the high-production stage, and Phase 2 is the low-production stage. In this study, the experiments with a pressure decline rate of 16 kPa/min and 32 kPa/min followed this law of Du and Zhang's research.

Table 5.6 summarizes the oil production characteristics of Phase 1 and Phase 2 of previous similar experiments (Du, 2017; Du, Peng, & Zeng, 2018b; K. Zhang, 2018). For the high solubility pure solvent-based Huff-n-Puff process, there are more cycles in Phase 1. However, the oil recovery efficiency in the first stage is low. Among them, the solubility of propane at normal temperature is higher than the solubility of propane after heating. Comparing these two experiments, it is found that the higher the solubility, the more cycles in the first stage. In Phase 2, the production rate of all experiments is similar. However, the number of cycles of pure propane is higher, so that the recovery factor of oil in Phase 2 propane experiments is higher than that of other experiments.

For low solubility nitrogen, although the number of cycles in Phase 1 is small, the oil recovery efficiency is very high. However, after the rapid oil recovery in phase 1, the recovery rate of Phase 2 is dropped abruptly. This phenomenon is also reflected in the mixture gas-based (CO_2/C3) Huff-n-Puff tests. Because of the diffusion boundary effect, the mixture gas of carbon dioxide and propane is also considered as a solvent with low solubility.

Table 5.6 Oil Production Characteristics of Phase 1 and Phase 2 in Previous Studies

Solvent	Pressure Decline Rate	Cycle range of each phase		Average production rate		Recovery %		
		Phase 1	Phase 2	Phase 1	Phase 2	Phase 1	Phase 2	Total
CO_2/C3	12.5 kPa/min	1-4	5-11	0.134, g/min	0.017, g/min	24.5	4.4	28.9
C3 (CHSI)	12.5 kPa/min	1-12	13-19	0.052, g/min	0.009, g/min	47.5	5.3	52.8
C3	12.5 kPa/min	1-35	36-END	0.014, %/min	0.004, %/min	52	15	67
C3	8 kPa/min	1-26	27-END	0.011, %/min	0.005, %/min	26	13	39
C3	5 kPa/min	1-8	9-END	0.024, %/min	0.004, %/min	40	10	50
C3	3 kPa/min	1-12	13-END	0.013, %/min	0.006, %/min	48	18	56
N_2	32 kPa/min	1-3	4-9	0.086, g/min	0.004, g/min	25	3	28
N_2	16 kPa/min	1-2	3-9	0.085, g/min	0.003, g/min	30	4	34

Du believes that the difference between Phase 1 and Phase 2 is due to the direction in which the gas chambers grow (Du, 2017). In Zhang's point of view, Phase 1 is mainly affected by foamy oil flow and conventional solution gas drive, while Phase 2 is dominated by the pressure gradient (K. Zhang, 2018). However, these views do not explain why the oil production rate of Phase 1 in the low solubility solvent-based Huff-n-Puff tests is much higher than that in the high solubility solvent-based Huff-n-Puff tests. It is also impossible to explain why the experiments with pressure decline rates of 2 kPa/min and 8 kPa/min in the nitrogen-based Huff-n-Puff tests do not have a division of the oil production phase.

It has previously been mentioned that the oil being driven during a single cycle of production will preferentially resaturate the gas chambers. Combining this point of view, the reason for the existence of Phase 1 and Phase 2 is probably due to the gas chamber's growth rate.

For nitrogen Huff-n-Puff, since the solubility and dissolution rate of nitrogen are too low, a large amount of gas exists in the form of continuous free gas during the injection process. A large amount of free gas is compressed under high pressure, forming some high-pressure gas chambers. Then, in the production process, under the various factors of gas expansion, gravity drainage, foamy oil, conventional solution gas drive, etc., the oil production rate is exceptionally high. Moreover, the high oil recovery rate leads to an increase in the potential volume of free gas during the injection process in the next cycle, thereby accelerating the growth rate of the gas chambers. The faster the growth rate of the gas chamber, the larger the oil-gas contact interface, thereby accelerating the dissolution rate of nitrogen, which in turn

stimulates the oil recovery rate. Therefore, under the mutual stimulation of the recovery rate and the gas chamber growth rate, the recovery rate of Phase 1 will be very high. However, the gas chamber grows too fast causing a small number of cycles to form a large volume of continuous gas chamber. When a continuous gas chamber is formed, the gas chamber is a high permeability channel for undissolved free gas, which weakens the effect of gas expansion, gravity drainage, and conventional solution gas drive. And for low solubility nitrogen, the foamy oil flow is inherently weak. Therefore, for the Huff-n-Puff process of nitrogen or other low solubility gases, their Phase 1 is maintained for a short period of time, and after the end of phase 1, the oil production rate drops drastically. In the experiments under low-pressure decline rate, the gas release rate is not fast enough, resulting in weak foamy oil and dissolved gas drive, and the gas expansion effect is not strong. Rather than forming a sizeable continuous gas chamber at a time, some new gas chambers are formed as the experiment progresses. Consequently, in the experiment under a pressure decline rate of 8 kPa/min, there is a phenomenon that the recovery rate rises every few cycles, as shown in Figure 5.9.

5.4.4 Residual Oil Saturation Profile

At the end of the experiments, sand samples of 8 uniformly distributed points in the model are extracted, the saturation of the residual oil there is measured, and the results are shown in Figure. 5.13.

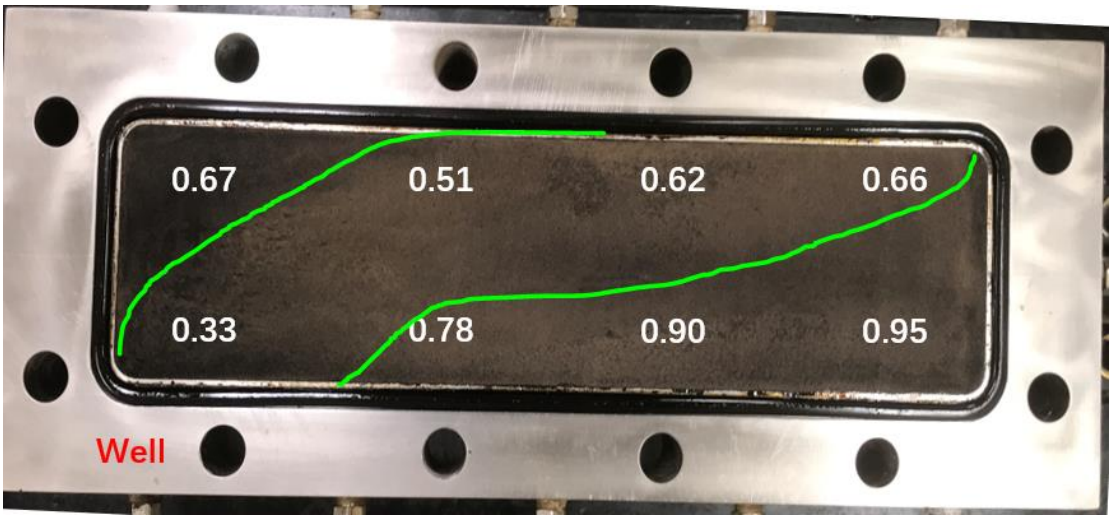

Figure 5.13 Residual Oil Distribution

The residual oil saturation measured near the wellhead is the lowest, and from the cross-section image, the sand near the wellhead is darker. This is due to the extraction of light components from the heavy oil by nitrogen, while the remaining heavy components stayed near the wellhead. This phenomenon is known as asphaltene precipitation in the reservoir.

Due to the light density of nitrogen, in the gas injection process, the compressed nitrogen collects in the upper part of the model through the high-permeability flow channel. Then, in the production process, the expansion of the gas plus the action of gravity causes the upper part of the model to form a secondary gas cap. This results in lower residual oil saturation in the upper part of the model compared to the lower part.

From the perspective of residual oil distribution, the results of this experiment are very consistent with those of Zhang's CHSI tests. However, the distribution of residual oil in this experiment is entirely different from that of Zhang’s Mixture gas CSI test (K. Zhang, 2018), as shown in Figure 5.14. Moreover, a severe wall effect is observed in Figure 5.14.b.

(a) Propane-based CSI

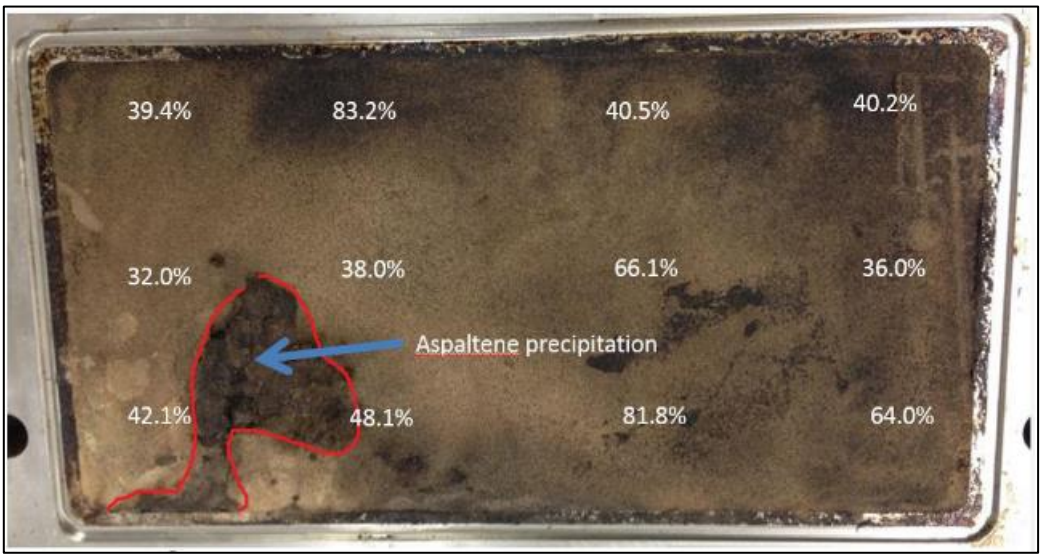

(b) Mixture Solvent CSI

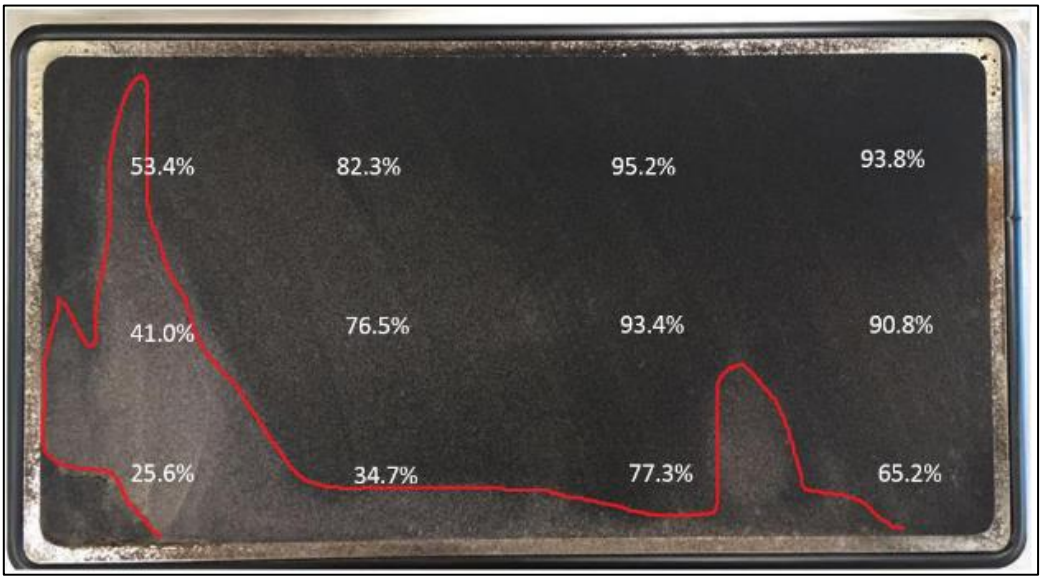

Figure 5.14 Residual Oil Distribution in Propane-based and Mixture Solvent CSI

5.4.5 Solvent chamber growth

Since the model is heated in the oven during the experiments, the direction of the gas chamber growth cannot be observed in real time, but the section taken from the final model can infer the direction of the gas chamber growth.

In the experiment with a pressure decline rate of 2 kPa/min, no apparent traces of the gas chambers are observed (Figure 5.15). This result is consistent with the previous speculation that when the pressure decline rate is too small, effective gas chambers cannot be formed. The oil production is mainly derived from the gas-assisted gravity drainage.

Figure 5.15 Solvent Chambers in the Test with Pressure Decline Rate of 2 kPa/min

The gas chambers formed in the three experiments with faster pressure decline rate are roughly the same. Take the experiment with a pressure decline rate of 16 kPa/min as an example. The section after sampling of the model is shown in Figure 5.16. Two rings with very low oil saturation can be seen in the four sampling pits near the wellhead. In the four sampling pits away from the wellhead, one ring with a very low residual oil saturation can be seen faintly. It can be inferred that two very thin planar gas chambers are formed in the model. One of them extends to the far end of the model and has a larger area, while the other only exists in the near-well zone and has a small area. Figure 5.17 is a representation of the shape of the simulated gas chamber in the model by speculation.

Figure 5.16 Solvent Chambers in the Test with Pressure Decline Rate of 16 kPa/min

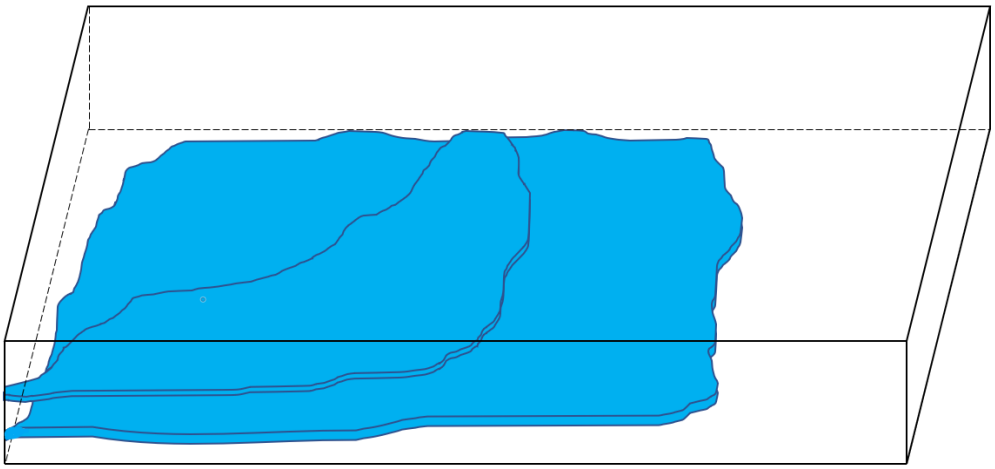

Figure 5.17 The Shape of the Simulated Gas Chambers

Comparing the results of the propane-based CHSI tests, the gas chambers formed by nitrogen and propane are entirely different in shape. In the propane-based CHSI tests, the gas chambers are independently dispersed thin strips, as shown in Figure 5.18. In the experiments of nitrogen Huff-n-Puff tests, the gas chamber is an utterly connected plane. This phenomenon should have appeared in the experiment of mixed gas-based CSI test (K. Zhang, 2018), but due to the severe wall effect in Zhang's experiment, the gas chamber grew along the wall surface instead. This difference may be due to the relationship between the gas injection rate and the gas dissolution rate.

From the perspective of gas chamber growth, the surface area of the gas chamber formed by nitrogen Huff-n-Puff is much larger than that of other gases. This makes the contact area between gas and oil larger, which is more favorable for the gas to be dissolved in the oil.

Figure 5.18 Solvent Chambers in Propane-based CSI

5.5 Chapter Summary

In order to determine whether nitrogen can be used in the heavy oil Huff-n-Puff, it must be tested by the Huff-n-Puff tests. The objective of this chapter is to experimentally determine the feasibility of nitrogen Huff-n-Puff in deep heavy oil reservoirs. In this chapter, not only is the feasibility of nitrogen Huff-n-Puff process proven, but the following conclusions are also obtained.

1. Under the conditions of these experiments, the optimal pressure decline rate is 16 kPa/min, which leads to a recovery rate of 35.73%.
2. No oil production is found at the beginning of the production stage for each cycle. This stage of production is called the re-saturation region.
3. The advantage of nitrogen Huff-n-Puff is that the high early production (Phase 1), the application of nitrogen Huff-n-Puff in the early stage of exploitation is not only low in cost but also highly efficient in production.
4. In the later stage of the Huff-n-Puff process (Phase 2), the gas chambers have been formed. The production at this stage mainly depends on the viscosity reduction effect of the solvent and foamy oil flow, which are extremely poor at this stage in the nitrogen Huff-n-Puff process. Therefore, oil production in Phase 2 is reduced.
5. The surface area of the gas chambers formed during nitrogen gas Huff-n-Puff process is larger, which is more favorable for solvent-oil contact.
6. Nitrogen is more suitable for the early application of the Huff-n-Puff process. It not only has low cost, good recovery efficiency, but also forms some large contact surface area

gas chambers which can enhance the effect of using other high-cost solvents in the later stage.

CHAPTER 6 CONCLUSIONS AND RECOMMENDATIONS

6.1 Conclusion

In this research, two series of experiments are conducted to determine whether or not nitrogen can form foamy oil in nitrogen-heavy oil system and to experimentally determine the feasibility of nitrogen Huff-n-Puff in deep heavy oil reservoirs. Significant conclusions can be drawn as follows:

Foamy Oil Flow Experiments

1. The solubility of nitrogen is low and does not have much effect on viscosity reduction. A decrease in viscosity is not significant, which is advantageous for the production of foamy oil flow.
2. The higher the pressure decline rate, the greater the oil recovery factor and the smaller the gas recovery factor.
3. In the weak two-phase flow region, the two groups of experiments (one with low pressure decline rates and the other with high pressure decline rates) have different causes of weak two-phase flow. Under low pressure decline rate, the pressure decline rate does not affect the oil recovery factor of the weak two-phase flow stage. The maximum oil production per unit pressure depletion is about 0.01 g/kPa.

4. Under high-pressure decline rate, due to the difference in the amount of residual gas in the oil from the previous active two-phase flow stage, the faster the pressure decline rate, the higher the oil recovery factor in the weak two-phase flow region.
5. In the active two-phase flow region, as the pressure decline rate increases, the oil recovery rate also increases significantly. This shows that the higher the pressure decline rate, the stronger the foamy oil can be formed. However, in experiments with high solubility solvents, when the pressure decline rate is too high, the stability of the foamy oil will be destroyed.
6. Under the premise that the viscosity of the oil remains unchanged, the change of the flow state mainly depends on the volumetric rate of the gas release. With the increase of gas release rate, the flow state is followed by gas single-phase flow, conventional solution gas drive, unstable solution gas drive, unstable foamy oil flow, and stable foamy oil flow.
7. It is finally confirmed that in the high-pressure reservoir at 50 ℃, the nitrogen-heavy oil live oil in pressure decline tests can form foamy oil.

Huff-n-Puff Tests

8. The optimal pressure decline rate is 16 kPa/min, which leads to a recovery rate of about 35.73%.
9. No oil production is observed at the beginning of the production stage for each cycle. This stage of production is called the re-saturation region.

10. The advantage of nitrogen Huff-n-Puff is high early production (Phase 1), the application of nitrogen Huff-n-Puff in the early stage of exploit is not only low in cost but also highly efficient in production.
11. In the later stage of the Huff-n-Puff process (Phase 2), the gas chambers have been formed. The production at this stage mainly depends on the viscosity reduction effect of the solvent and the foamy oil flow, which are extremely poor at this stage in the nitrogen Huff-n-Puff process. Therefore, oil production in Phase 2 is reduced.
12. The surface area of the gas chambers formed during nitrogen gas Huff-n-Puff process is larger, which is more favorable for solvent-oil contact.
13. Nitrogen is more suitable for the early application of the Huff-n-Puff process. It not only has low cost, good recovery efficiency, but also forms some large contact surface area gas chambers which can enhance the effect of using other high-cost solvents in the later stage.

6.2 Recommendation

Based on this study, several recommendations are listed for future work.

1. Since the decisive factor in determining the flow pattern in heavy oil is the size of the bubbles trapped in the oil and not the pressure decline rate, in future experiments, high production periods can be extended by using different pressure decline rates at different pressure ranges.

2. The reason for the planar gas chambers created in the 2-D experiments may be that the shape of the model limits the growth of the gas cavity in any other directions. In order to better simulate the environment in the actual formation, Huff-n-Puff tests in the 3D model are required.
3. Foamy oil is not the only production mechanism for nitrogen Huff-n-Puff process. Other production mechanisms need to be studied in future research.
4. A scale-up analysis is needed to fit and guide oil field production.
5. The preferences of nitrogen Huff-n-Puff to other high-solubility solvents Huff-n-Puff in the early period requires specific experimental verification.

Reference

Aghabarati, H., Dumitrescu, C. C., Lines, L., & Settari, A. (2008). Combined Reservoir Simulation And Seismic Technology, A New Approach For Modeling CHOPS, (1957). https://doi.org/10.2118/117581-ms

Bayestehparvin, B., Ali, S. M. F., & Abedi, J. (2016). Use of Solvents With Steam - State-of-the-Art and Limitations. *SPE EOR Conference at Oil and Gas West Asia*, (March), 21–23. https://doi.org/10.2118/179829-MS

Boyle, T. B., Gittins, S. D., & Chakrabarty, C. (2003). The evolution of SAGD technology at East Senlac. *Journal of Canadian Petroleum Technology*, *42*(1), 58–61.

Chang, S., Grigg, R. B., & Recovery, P. (1996). Displacement Modeling in CO2 Flooding Processes, (1), 575–583.

Crandall, G. R., & Wise, T. H. (1984). Market Outlook for Canadian Heavy Crude. *Journal of Canadian Petroleum Technology*, *23*(3), 67–71.

Das, S. K. (1998). Vapex : An Efficient Process for the Recovery of Heavy Oil and Bitumen. *SPE Journal*, (September), 232–237.

Ding, L. Y., Mehra, R. K., & Donnelly, J. K. (2007). Stochastic Modeling in Reservoir Simulation. *SPE Reservoir Engineering*, *7*(01), 98–106. https://doi.org/10.2118/18431-pa

Doe, S. P. E., & Doe, S. P. E. (1990). Mathematical Modeling of Foam Flooding.

Dong, M., & Huang, S. (2002). Flue gas injection for heavy oil recovery. *Journal of Canadian*

Petroleum Technology, *41*(9), 44–50.

Du, Z. (2017). Experimental and Mathematical Studies of Cyclic Solvent Injection To Enhance Heavy Oil Recovery.

Du, Z., Peng, X., & Zeng, F. (2018a). Comparison analyses between the linear and non-linear pressure-decline methods in cyclic solvent injection (CSI) process for heavy oil recovery. *Fuel*, *224*(December 2017), 442–450. https://doi.org/10.1016/j.fuel.2018.03.092

Du, Z., Peng, X., & Zeng, F. (2018b). Experimental investigation of cyclic solvent injection based on mixture solvent of carbon dioxide and propane. *Fuel*, *225*(January), 646–654. https://doi.org/10.1016/j.fuel.2018.03.187

Du, Z., Zeng, F., & Chan, C. (2015). An Experimental Study of the Post-CHOPS Cyclic Solvent Injection Process. *Journal of Energy Resources Technology*, *137*(4), 042901. https://doi.org/10.1115/1.4029972

Du, Z., Zeng, F., Peng, X., & Chan, C. (2016). Optimizing the pressure decline rate on the cyclic solvent injection process for enhanced heavy oil recovery. *Journal of Petroleum Science and Engineering*, *145*, 629–639. https://doi.org/10.1016/j.petrol.2016.06.028

Du, Z., Zeng, F., Peng, X., & Chan, C. (2018). Experimental and material balance equations analyses of cyclic solvent injection based on a large 3D physical model. *Fuel*, *215*(November 2017), 915–927. https://doi.org/10.1016/j.fuel.2017.10.076

Falk-Pedersen, O., & Dannstrom, H. (1997). Separation of Carbon Dioxide from Offshore Gas Turbine Exhaust, 81–86.

Firoozabadi, A. (2001). Mechanisms of solution gas drive in heavy oil reservoirs. *Journal of*

Canadian Petroleum Technology, *40*(3), 15–20. https://doi.org/10.2118/01-03-DAS

Freitag, N. P. (2014). Chemical Reaction Mechanisms That Govern Oxidation Rates During In-Situ Combustion and High-Pressure Air Injection. *SPE Heavy Oil Conference-Canada*, (November). https://doi.org/10.2118/170162-MS

Holden, L. (1998). Modeling of fluvial reservoirs with object models. *Mathematical Geology*, *30*(5), 473–496. https://doi.org/10.1023/A:1021769526425

Huang, T., Zhou, X., Yang, H., Liao, G., & Zeng, F. (2017). CO 2 flooding strategy to enhance heavy oil recovery. *Petroleum*, *3*(1), 68–78. https://doi.org/10.1016/j.petlm.2016.11.005

Ingham, J. P., Law, D. H.-S., Coskuner, G., Asghari, K., Rivero, J. A., Pearce, A., … Newman, R. (2011). Modeling CHOPS Using a Coupled Flow-Geomechanics Simulator With Nonequilibrium Foamy-Oil Reactions: A Multiwell History Matching Study, (Dusseault 2007), 1–21. https://doi.org/10.2118/135490-ms

Isaacs, E. E., Green, M. K., Jossy, W. E., & Maunder, J. D. (2007). Conformance Improvement by Using High Temperature Foams and Gels, 345–351. https://doi.org/10.2118/23754-ms

Izquierdo, A., Kamp, A., & Vallejos, C. (2000). Heavy oil production: Foamy oil and in-situ upgrading. *World Petroleum Congress Proceedings*, *2*, 242–244.

Jia, X. (2014). ENHANCED SOLVENT VAPOUR EXTRACTION PROCESSES IN THIN HEAVY OIL RESERVOIRS. *Master Thesis*, *8*(33), 44.

Jia, X., Zeng, F., & Gu, Y. (2015). Dynamic solvent process (DSP) for enhancing heavy oil recovery. *Canadian Journal of Chemical Engineering*, *93*(5), 832–841.

https://doi.org/10.1002/cjce.22178

Jiang, T. (2013). An Improved Vapour Solvent Injection Technique for Enhanced Heavy Oil Recovery.

Jin, F.-Y., Gao, H., Chen, Y.-F., Wei, B., Li, Y.-B., Dong, H., & Pu, W.-F. (2017). Low temperature oxidation characteristics analysis of ultra-heavy oil by thermal methods. *Journal of Industrial and Engineering Chemistry*, *48*, 249–258. https://doi.org/10.1016/j.jiec.2017.01.017

Knorr, K. D., & Imran, M. (2012). Solvent-chamber development in 3D-physical-model experiments of solvent- Vapour extraction (SVX) processes with various permeabilities and solvent-vapour qualities. *Journal of Canadian Petroleum Technology*, *51*(6), 425–436. https://doi.org/10.2118/149190-PA

Leung, Y. T., Gadelle, F., Kovscek, A. R., Kumar, M., Sahni, A., Castanier, L. M., & Tang, G.-Q. (2006). An Investigation of the Effect of Oil Composition on Heavy Oil Solution-Gas Drive. *SPE Journal*, *11*(01), 58–70. https://doi.org/10.2118/84197-pa

Liu, P., Wu, Y., & Li, X. (2013). Experimental study on the stability of the foamy oil in developing heavy oil reservoirs. *Fuel*, *111*, 12–19. https://doi.org/10.1016/j.fuel.2013.03.021

Maini, B. (2007). Effect of Depletion Rate on Performance of Solution Gas Drive in Heavy Oil Systems. https://doi.org/10.2523/81114-ms

Maini, B. B., Sarma, H. K., & George, A. E. (2010). Significance of Foamy-oil Behaviour In Primary Production of Heavy Oils. *Journal of Canadian Petroleum Technology*, *32*(09).

https://doi.org/10.2118/93-09-07

Mansourizadeh, A., & Ismail, A. F. (2009). Hollow fiber gas-liquid membrane contactors for acid gas capture: A review. *Journal of Hazardous Materials*, *171*(1–3), 38–53. https://doi.org/10.1016/j.jhazmat.2009.06.026

Mastmann, M., Moustakis, M. L., & Bennion, D. B. (2001). Predicting Foamy Oil Recovery. *SPE Western Regional Meeting*. https://doi.org/10.2118/68860-MS

Mehrotra, A. K., & Svrcek, W. Y. (1982). Correlations for properties of bitumen with CO2, CH4 and N2 and experiments with combustion gas mixtures. *Journal of Canadian Petroleum Technology*, *21*(6), 95–104.

Merotra, A. K., & Svrcek, W. Y. (1982). Gas Solubility , Viscosity and Density Measurements for Athabasca Bitumen. *Journal of Canadian Petroleum Technology*, (August).

Muijs, H. M., Keijzer, P. P. M., & Wiersma, R. J. (1988). Surfactants for Mobility Control in High-Temperature Steam-Foam Applications (pp. 905–914). https://doi.org/10.2118/17361-ms

Nelson, D. G., Sheehy, P., O'Donnell, J., & Heisler, M. A. (2016). Saving Heavy Oil Reserve Value in a Carbon Constrained Market, *32*(Ab 32). https://doi.org/10.2118/180447-ms

Peng, X. (2016). Experimental Study on Improving the Waterflooding Potential in Different Heavy Oil- Solvent Systems.

Peng, X., Zeng, F., Du, Z., & Yang, H. (2017). Experimental study on pressure control strategies for improving waterflooding potentials in a heavy oil-methane system. *Journal of Petroleum Science and Engineering*, *149*(October), 126–137.

https://doi.org/10.1016/j.petrol.2016.10.040

Ransohoff, T. C., & Radke, C. J. (2007). Mechanisms of Foam Generation in Glass-Bead Packs. *SPE Reservoir Engineering*, *3*(02), 573–585. https://doi.org/10.2118/15441-pa

Sadykova, Y. V. (2014). Geothermal regime in the subsurface of the southern areas of the Ob-Irtysh interfluve. *Oil and Gas Business*, *8*(1), 48–64. https://doi.org/10.17122/ogbus-2014-1-48-64

Sheng, J. J. J., Maini, B. B. B., Hayes, R. E. E., & Tortike, W. S. S. (1999). Critical Review of Foamy Oil Flow, Transport in Porous Media. *Transport in Porous Media*, *35*(4), 157–187.

Sheng, J. J., Maini, B. B., Hayes, R. E., & Tortike, W. S. (1997). Experimental study of foamy oil stability. *Journal of Canadian Petroleum Technology*, *36*(4), 31–37.

Smith, G. E. (1988). Fluid Flow and Sand Production in Heavy-Oil Reservoirs Under Solution-Gas Drive. *SPE Production Engineering*, *3*(02), 169–180. https://doi.org/10.2118/15094-PA

Sobocinski, D. P., & Cornelius, A. J. (2007). A Correlation for Predicting Water Coning Time. *Journal of Petroleum Technology*, *17*(05), 594–600. https://doi.org/10.2118/894-pa

Sun, X., Zhang, Y., Cui, G., Duan, X., & Zhao, C. (2014). Feasibility study of enhanced foamy oil recovery of the Orinoco Belt using natural gas. *Journal of Petroleum Science and Engineering*, *122*, 94–107. https://doi.org/10.1016/j.petrol.2014.06.022

Tang, G. Q., & Firoozabadi, A. (2006). Effect of GOR, Temperature, and Initial Water Saturation on Solution-Gas Drive in Heavy-Oil Reservoirs. *SPE Journal*, *10*(01), 34–

43. https://doi.org/10.2118/71499-pa

Trevisan, O. V., Laboissiere, P., & Monte-Mor, L. S. (2013). Laboratory Study on Steam and Flue Gas Co-injection for Heavy Oil Recovery. https://doi.org/10.2118/165523-ms

Wang, R., Liu, S. ., Lin, T. ., & Chung, T. . (2002). Characterization of hollow fiber membranes in a permeator using binary gas mixtures. *Chemical Engineering Science*, *57*(6), 967–976. https://doi.org/10.1016/S0009-2509(01)00435-3

Wang, X., Peng, X., Zhang, S., Du, Z., & Zeng, F. (2018). Characteristics of oil distributions in forced and spontaneous imbibition of tight oil reservoir. *Fuel*, *224*(December 2017), 280–288. https://doi.org/10.1016/j.fuel.2018.03.104

Wang, Y. (1999). SPE-37553-MS.pdf. *Spe*.

Wang, Y., Du, Y., Ge, J., Jiang, P., & Zhang, G. (2013). Mechanism and Feasibility Study of Nitrogen Assisted Cyclic Steam Stimulation for Ultra-Heavy Oil Reservoir, 1–10. https://doi.org/10.2118/165212-ms

Wu, M. (2018). EFFECTS OF TEMPERATURE AND HEAVY OIL VISCOSITY ON FOAMY OIL FLOW IN POROUS MEDIA. *Master Thesis*. https://doi.org/10.1109/ROMAN.1994.365947

Yadali Jamaloei, B., Dong, M., Yang, P., Yang, D., & Mahinpey, N. (2013). Impact of solvent type and injection sequence on Enhanced Cyclic Solvent Process (ECSP) for thin heavy oil reservoirs. *Journal of Petroleum Science and Engineering*, *110*, 169–183. https://doi.org/10.1016/j.petrol.2013.08.028

Yanbin, Z., Guanghuan, W., Qiuying, C., Long, J., Jianfang, S., & Yang, Y. (2012). Research

and Application on Nitrogen and Dissolver Assisted Horizontal Well Steam-injection to Develop Shallow Thin Super Heavy Oil Reservoirs. https://doi.org/10.2118/154010-ms

Yazdani, A., & Maini, B. B. (2006). Effect of Height and Grain Size on the Production Rates in the Vapex Process: Experimental Study. *SPE Reservoir Evaluation & Engineering*, *8*(03), 205–213. https://doi.org/10.2118/89409-pa

Yuan, C., & Jin, L. (2008). The compositional simulation and seismic monitoring of CO2 EOR and sequestration in new gas condensate reservoir.

Zhang, K. (2018). CYCLIC HOT SOLVENT INJECTION METHOD TO ENHANCE HEAVY OIL RECOVERY BASED ON EXPERIMENTAL STUDY. *Master Thesis*.

Zhang, K., Zhou, X., Peng, X., & Zeng, F. (2019). A comparison study between N-Solv method and cyclic hot solvent injection (CHSI) method. *Journal of Petroleum Science and Engineering*, *173*(June 2018), 258–268. https://doi.org/10.1016/j.petrol.2018.09.061

Zhang, M., Du, Z., Zeng, F., Hong, S. Y., & Xu, S. (2016). Upscaling study of the cyclic solvent injection process for post-chops reservoirs through numerical simulation. *Canadian Journal of Chemical Engineering*, *94*(7), 1402–1412. https://doi.org/10.1002/cjce.22508

Zhang, X., Du, C., Deimbacher, F., Crick, M., & Harikesavanallur, A. (2009). IPTC 13338 Sensitivity Studies of Horizontal Wells with Hydraulic Fractures in Shale Gas Reservoirs.

Zhang, Y. (1999). Effects of temperature on Foamy Solution Gas-Drive, (10).

https://doi.org/10.1007/s10973-014-3688-4

Zhao, L., Anderson, D. B., & O' Rourke, C. (2005). Understanding SAGD Producer Wellbore/Reservoir Damage Using Numerical Simulation. *Canadian International Petroleum Conference*, (1), 1–14. https://doi.org/10.2118/2005-067

Zhao, L., Nasr, T. N., Golbeck, H., Beaulieu, G., Coates, R., Law, D. H. S., & Heck, G. (2010). SAGD Wind-Down: Lab Test and Simulation. *Journal of Canadian Petroleum Technology*, *44*(01). https://doi.org/10.2118/05-01-04

Zhao, Y. long, Xie, S. chang, Peng, X. long, & Zhang, L. hui. (2016). Transient pressure response of fractured horizontal wells in tight gas reservoirs with arbitrary shapes by the boundary element method. *Environmental Earth Sciences*, *75*(17), 1–14. https://doi.org/10.1007/s12665-016-6013-7

Zhou, X. (2014). EXPERIMENTAL STUDY ON FOAMY OIL FLOW BY USING DIFFERENT HEAVY OIL-SOLVENT SYSTEMS.

Zhou, X. (2015). Experiemental Study on Foamy Oil Flow by Using Different Heavy Oil-Solvent, 173.

Zhou, X., Yuan, Q., Zeng, F., Zhang, L., & Jiang, S. (2017). Experimental study on foamy oil behavior using a heavy oil–methane system in the bulk phase. *Journal of Petroleum Science and Engineering*, *158*(July), 309–321. https://doi.org/10.1016/j.petrol.2017.07.070

Zhou, X., & Zeng, F. (2014). Feasibility Study of Using Polymer to Improve SAGD Performance in Oil Sands with Top Water. *SPE Heavy Oil Conference-Canada*, 1–22.

https://doi.org/10.2118/170164-MS

Zhu, W., Hrabanek, P., Gora, L., Kapteijn, F., & Moulijn, J. A. (2006). Role of adsorption in the permeation of CH4 and CO2 through a silicalite-1 membrane. *Industrial and Engineering Chemistry Research*, *45*(2), 767–776. https://doi.org/10.1021/ie0507427